Modeling and Analysis of The Chemical Milling Process

by

Narintr Narisaranukul

B.S. Mechanical Engineering
Carnegie Mellon University (1995).

Submitted to the Department of Mechanical Engineering
in partial fulfillment of the requirements for the degree of

Master of Science in Mechanical Engineering

at the

MASSACHUSETTS INSTITUTE OF TECHNOLOGY

May 9, 1997

Author .....
Department of Mechanical Engineering
May 9, 1997

Certified by .....
Mary C. Boyce
Associate Professor of Mechanical Engineering
Thesis Supervisor

Accepted by .....
Ain A. Sonin
Chairman, Department Committee on Graduate Students
Department of Mechanical Engineering

Modeling and Analysis of The Chemical Milling Process

by

Narintr Narisaranukul

Submitted to the Department of Mechanical Engineering on
May 9, 1997, in partial fulfillment of the requirements for the
Degree of Master of Science in Mechanical Engineering

Abstract

In the manufacturing of aircraft components, the chemical milling process is often used after forming a part to selectively thin the sheet material and thus reduce weight while maintaining needed structural integrity. Chemical milling usually results in part distortion due to the re-equilibration of the residual stress in the part. In order to improve the manufacturing capability of aircraft components, a finite element analysis is used to model the stretch forming and the chemical milling process. The results from simulations of the chemical milling process, in particular, are analyzed to study the effects on the final part configuration.

The simulations of both the stretch forming and the chemical milling process utilize shell elements to model the sheet. In the chemical milling simulation an algorithm is developed whereby the "initial" residual stress is imposed to the chemical milled part, after which the part is allowed to re-equilibrate. The comparison between the experimental and simulation results of the forming and the chemical milling of a set of parts with simple geometry shows an excellent predictive capability of the forming and chemical milling simulations. The chemical milling of a part with more complex geometry, such as a saddle shape, is simulated to study the effects of the chemical milling process on the part shape as well as to demonstrate the capability of the developed chemical milling simulation to model complex shapes. The simulation results show a significant part distortion at the perimeter of the part and the chemical milled regions in the part. By using the springforward die design algorithm developed by Karafillis and Boyce to incorporate the effects of the chemical milling process to the die design, the accuracy of the manufacturing of the aircraft components can be significantly improved.

Thesis Supervisor: Mary C. Boyce
Title: Associate Professor of Mechanical Engineering

Acknowledgments

There are a number of people who made it possible for me to complete this thesis. First, I would like to thank both my parents for all of their love and support for me over the years. Thanks so much for believing in me and I love you both very much. I would also like to give a very special thank to Prof. Mary Boyce, who has provided a tremendous guidance and advice for me during this past couple of years at MIT. I learned so much from you and I am very grateful for all your help and wisdom. Also, Big thanks to Simona for all the help and advice she gave me with this project. It has been a lot of fun working with you and I will always remember the all-nighters we pulled the nights before each Quarterly meeting.

I would like to thank Northrop Grumman Corporation, particularly John Papazian, for giving me the support and the opportunity to work on this project. It has been a tremendous learning experience for me. I would like to thank Prof. David Hardt for all of his suggestions and wonderful stories. Also, thanks to Joe Boivin for helping me with the experimental part of this project. Without your help, I wouldn't be able to complete that portion of my work. Marko and David, thanks for all your help this past year.

Also, I would like to thank both my sisters, Sarah and May, who always care about me, even though we don't get to see each other very much. I would like to thank all of my friends in the Mechanics and Materials Group. Oscar for being my buddy on and off the court. You are a great friend (and an excellent basketball player, I finally admit). Jorgen for all the interesting ideas you gave me and for making me laugh. Clarence, Hong and Ganti...you guys have made my life so much easier. Thanks for all your help and wonderful advice. (Hong, congratulations on your new baby!) Kevin, thanks for being such a terrific colleague and friend and best wishes on your marriage. Srihari, Manish, Brian Gally, Gu, Mike (and the rest of the lab, you know who you are) ... thanks for the support over the years.

In addition, all of my friends at TSMIT and in Boston have made me feel like I have a big loving family in a big city. Gon, (5 years and counting, pal) thanks for putting up with me for so long. Chalee (Tha Main Man), thanks for all the adventurous nightlife in Boston. P'Joh, P'Nong, P'Yoy, P'Kruak...you all made one hell of a basketball team. Thanks for treating me so well. P'Lena and P'Eauy for being such a good role model. And thanks to nong nong TSMIT who gave me so much respect I don't really deserve. Boy (a sports fanatic just like me, but too bad you're a Cowboy fan), Meaw (you always make me laugh, thanks), Paeng, Yai, Pirote, Jeab, Bee, Kate (for all the strawberries). Ya, Teng, Kung, Itsra ... glad to get to know y'all. Jump (one of the trios), you have to try to get away from me and Gon, huh? P'Boy (the Boston man) thanks for everything. Noon and Kwan..my two cool friends. Last, but not least, thanks to all other friends I've left out 'cause I'm tired.

Thank you Everyone, from the bottom of my heart, for making the past couple of years of my life so memorable!!!

Table of Contents

List of Figures

List of Tables

Chapter 1

Introduction

1.1 Overview of The Reconfigurable Tooling for Flexible Fabrication (RTFF) Project

In 1995, a collaborative effort between MIT, Northrop Grumman Corporation and Cyril Bath was formed in order to improve the efficiency and productivity of the stretch forming process used in manufacturing aircraft parts and components. This project, entitled Reconfigurable Tooling for Flexible Fabrication (RTFF), is aimed at utilizing feedback control and finite element modeling capabilities, combined with new adaptive tooling design, to allow for a low-cost, real-time and flexible fabrication of any specified part shape. By implementing the technology developed from this research effort, the productivity of the manufacturing of the aircraft sheet metal components can be greatly increased while significantly reducing the manufacturing costs in terms of both time and money. Essentially, the RTFF technology would improve the stretch forming process by increasing the flexibility in making new parts and reducing the number of design iterations for the die shape. The design and production of dies is a major cost in forming aircraft structures because of the low volume production.

The fundamental concept and methodology of the RTFF technology is depicted in Figure 1.1. It shows the major components of the die design methodology which includes the finite element simulation for modeling the process and predicting the first die shape, the forming machine with adaptive tooling with a feedback control capability, and the CMM machine for part shape measurement. The main concept of this technology is quite simple. Using finite element methods, the forming process and other post-forming processes, such as the chemical milling process, are simulated. Numerical simulations are coupled with the springforward die design algorithm developed by Karafillis and Boyce [1] and [2], thus allowing the designer to predict the initial die shape. This initial die shape is then transferred to the stretch forming machine, which consists of a set of square pins (see Figure 1.2). The pins are positioned such that they form the specified die shape. Because the position of each pin can be controlled and adjusted, the overall shape of the die is easily

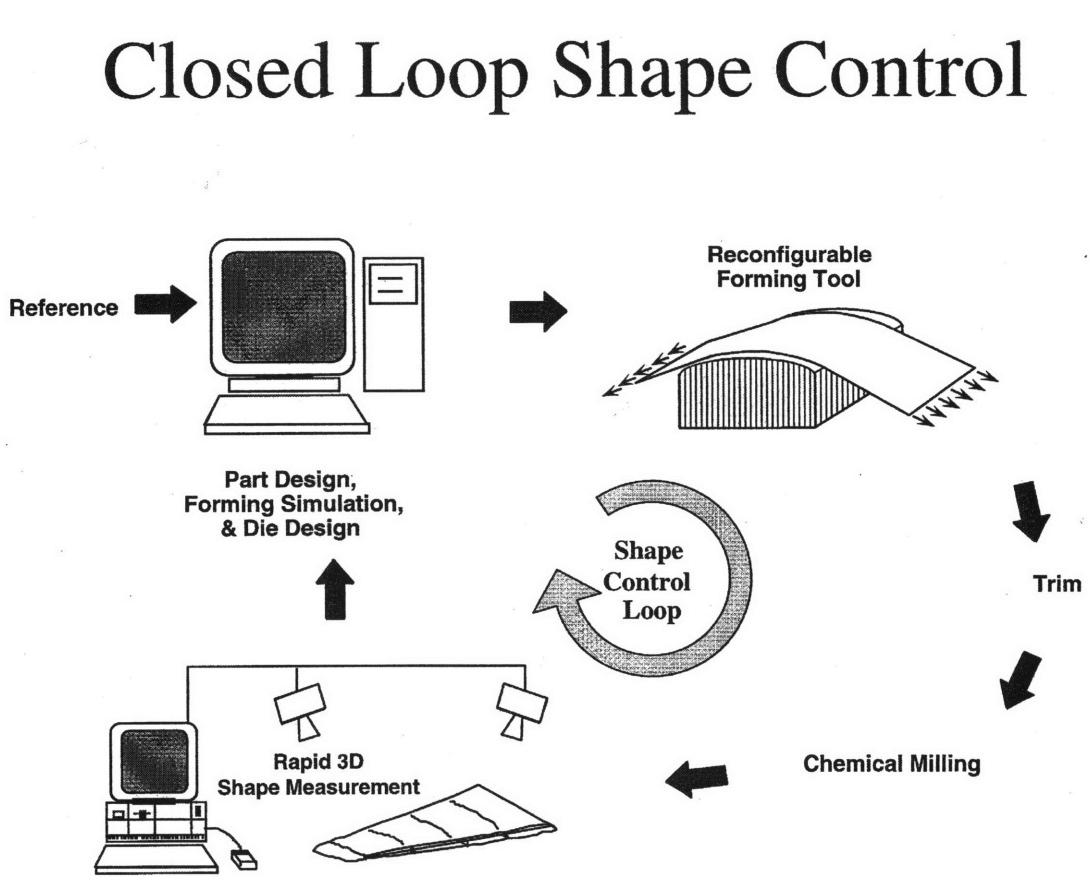

Figure 1.1: Die Design Methodology with Reconfigurable Tooling for Flexible Fabrication.

changed. This concept of adaptive tooling greatly enhances the flexibility of the process because it allows for the feedback control to be implemented in the overall process. In the feedback loop, the errors of the formed part with respect to the reference part shape are measured and fed back to the control algorithm, which will give a new die shape. The design of a die shape is then completed after a few iterations when the formed part meets the design specifications.

A number of post-forming processes are also required to complete the overall manufacturing of the sheet metal part. The processes of chemical milling and trimming are of particular interest because of the potential in causing distortion in the final part configuration. The chemical milling process is essentially a material removal process through a chemical reaction with the sheet material. The objective of chemical milling is mainly to reduce the weight of the part while selectively maintaining the structural strength and integrity of the part. The sheet is also trimmed to specified dimensions after formed.

Because of the presence of residual stresses in the part, trimming and chemical milling can sometimes cause the part to distort. With this in mind, it is rather convincing that the manufacturing of the sheet metal components with the RTFF technology could be further improved if the design of the die takes into account the effects of these post-forming processes.

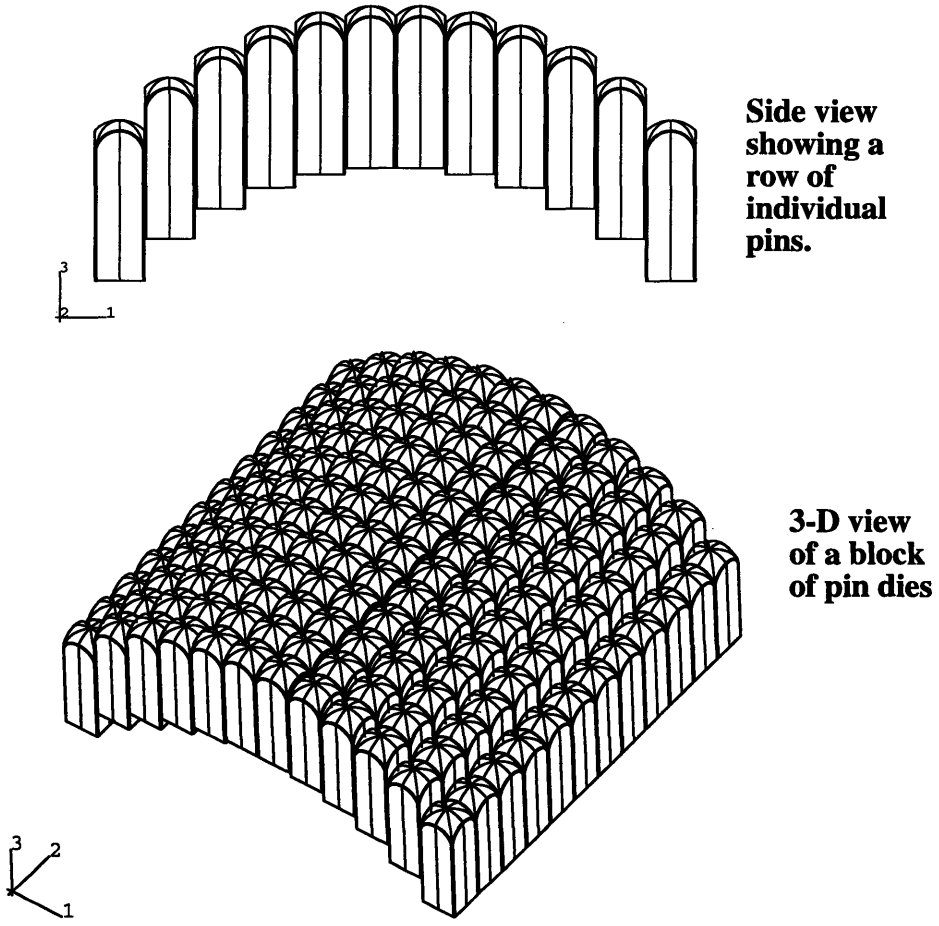

Figure 1.2: A set of square pins making up a block of die.

The ultimate goal of this research work is, therefore, to study the effects of the chemical milling process on the change of part shape and to incorporate any changes due to these effects into the final design of the die. The idea is to incorporate the simulation of chemical milling after the stretch forming simulation is completed. Finite element analysis will also be used as a tool to model and analyze the chemical milling process. The distortion of the part due to the chemical milling and the trimming processes will be studied.

When these effects are included in the algorithm of the die design, after going through all of these processes, the part will be of the desired configuration as conformed to the design specifications.

In order to effectively simulate the stretch forming process as well as subsequent chemical milling, several modeling related issues will first be identified and investigated. These issues include (1) simulations of the effect of friction at the sheet-die interface, (2) selection of the most appropriate and most effective finite element formulation and mesh configuration to model the sheet metal, and (3) development of a simulation methodology for modeling the chemical milling process. The next chapter is devoted to the discussion of these issues. The methodology of the simulations and corresponding predictive capabilities will be described in Chapters 3, 4, and 5. The results from simulations, followed by the analysis of the effects of chemical milling, will be provided.

1.2 Overview and History of The Chemical Milling Process

Chemical milling is a process in which layers of material are removed from a structure by a liquid chemical. It is commonly used in the aerospace industry to remove shallow layers of material from large aircraft, missile skin panels, and extruded parts for airframes, where chemical milling acts to remove material from regions where it is not structurally required in the final part, thereby reducing weight. Chemical milling is also used in the semiconductor industry for fabrication of microelectronic devices and printed-circuit boards. To aid in the understanding of the process and its applications, the history of the chemical milling process will be presented in this section, after which a brief overview of the process will be outlined.

1.2.1 The History of The Chemical Milling Process

The history of the chemical milling process can be dated as far back as the late fourteenth and early fifteenth centuries. The earliest evidence of chemical milling was, however, in a form of armour etching, in which the acid was applied in small amounts to the areas requiring etching. During this time period, the use of etching on armour became more widespread. The engraving method for weapons, helmets, and breastplates with hand tools was soon replaced by the more powerful acid-based process. Because of the

corrosive nature of the process due to a chemical reaction, many of the significant steps in the history of chemical milling were a direct result from the development of the etching solution and the maskant coating. Organic acids such as vinegar, citric acid from lemons, and lactic acid from sour milk, undoubtedly became the first liquids used in the etching of various kinds of materials, while wax was found to be the first material used as a maskant coating in armour etching. A fifteenth-century English manuscript described the use of a wax maskant in a selective etching of required patterns, signifying the origin of step-milling or contour etching as it is known today [3].

During the sixteenth century, the process of armour etching became increasingly popular. The decorating patterns and embellishments were more complex and required a number of different stages before completion. The process of making a suit of armour would consist of weeks or months of etchers mixing wax maskant, applying it by brush, and, after it had hardened, working with a needle or scraper to produce patterns before slowly and carefully applying acid to those etched areas. It was not until the seventeenth century when the use of etching to decorate arms and armours finally became a completely established process. Even though the use of armour in the battle field had declined in this period, parade and ceremonial armours were still ordered by the royals and the nobles. An example of a superb work of craftsmanship produced by the etching process is illustrated in Figure 1.3. This finely decorated gauntlet was made for Henry, Prince of Wales, in 1612 by a master workman by the name of William Pickering. One should note the accurate matching of the decorative designs on the individual pieces as it shows the capability and accuracy of this process.

In the eighteenth and nineteenth centuries, most of the advancements in the etching process was due to the better understanding of the chemical reactions and its applications to photography. There was, however, a considerable increase in the number of developments and applications of chemical milling to various other products in the twentieth century. During the Second World War, the use of chemical milling to improve the structural efficiency of aircraft components was introduced. The consideration of using chemical milling to increase the strength-to-weight performance in aircraft structure was due to two important factors: first, since the production of sheet metal allows only a certain range of gauge thickness, some material would have to be removed from certain areas if the sheet

metal is to have a maximum strength-to-weight ratio; second, due to the aerodynamic requirements of the aircraft design, the shape of most aircraft components has one or more curved surfaces, making it difficult or impossible for conventional machining methods. In the chemical milling process, the cutting tool is liquid and, thus, poses no geometric constraints on the shape of its cut. This very nature of the chemical milling process allows the manufacturer to remove material in areas which would be most difficult, and extremely expensive, to work upon by other manufacturing processes.

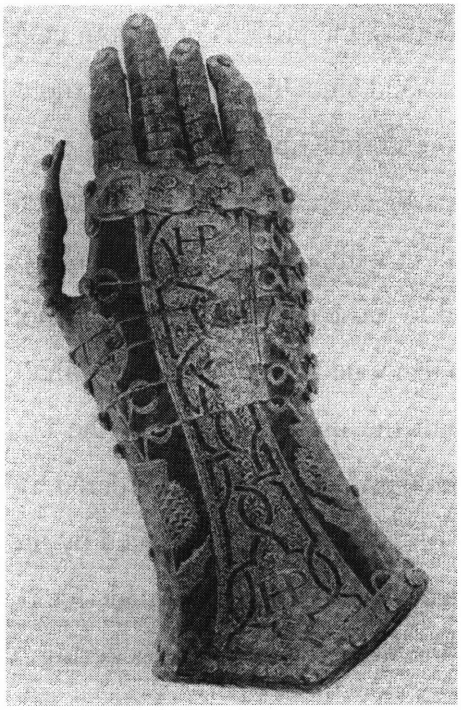

Figure 1.3: Gaunlet of Henry, Prince of Wales. (Courtesy the Trustees of the Wallace Collection, No. A 276.)

During the twentieth century, most of the significant developments of chemical milling came from applications in the aerospace industry. Most of the early research was directed towards producing a consistent etching action at the surface of the component being cut. A number of patents were issued for methods to overcome the problems of scale formation, which, as a result of reaction products adhering to the workpiece or the heating elements and tank interiors, prevented high etch rates or large volumes of metal being removed in a regular and controllable manner. In 1953, a patent, issued to Manual C. Sanz and his team at North American Aviation, described all the essential techniques in chemical milling of

formed aluminum sheets so that pockets can be consistently removed with accurate depths and good surface finish. This patent, in essence, outlines the fundamental approach and technique that were to be used for many thousands of aircraft components in the following two decades. By the late 1950s, the development of the process was extended to being used to the chemical milling of other materials considered to be difficult to process, such as steel, magnesium, titanium, and nickel alloys. In addition, the range of application of the process to other complex components was grown considerably. By the mid 1960s, the development of the chemical milling process and its applications had proved to be a reliable and valuable manufacturing process. It enables many parts to be produced more easily and cheaply than by other means and also provides a means of design and manufacturing of part configurations not previously possible.

In sofar as the history of the chemical milling process is concerned, one can see that the process has evolved from being entirely artistic to being a means to an improvement in the manufacturing and design of aircraft components. In the next section, the basic principles of the process and some of the engineering and design benefits will be discussed.

1.2.2 The Overview of The Chemical Milling Process

In using a finite element method to predict the effect of the chemical milling process, one of the basic rules of thumb is to understand, as much as possible, the physics and the procedure of the process before any simulations can be completed. This section outlines a general overview of the chemical milling process commonly used in the aerospace industry. A more complete detail of the techniques of the process can be found in a book titled ***Chemical Milling: The Technology of Cutting Materials By Etching*** by William T. Harris.[3] Generally, the chemical milling process consists of five basic steps: cleaning, masking, scribing, etching, and demasking.

1. *Cleaning.* In order to ensure uniform adhesion of the maskant and a uniform etch rate, it is essential that the surfaces of the sheet are effectively cleaned. Even though the sheet is to be chemical milled only on one side, both surfaces of the sheet have to cleaned to be free from oil, primer coating, grease, marking or identification inks, and other foreign matters. The standard cleaning procedures include the use of a clean rag with cleaner solutions or vapor degrease, an immersion in alkaline cleaners, and a combination of dip-

spray tank. In addition, after the part or material is cleaned, it must be dried thoroughly and transferred to the next stage as soon as possible in order to avoid contamination by atmospheric dust and moisture. The handling of the parts following the completion of cleaning should also be done with clean cotton gloves to prevent any re-contamination by natural oil present on hands.

2. *Masking.* The masking step in chemical milling, in essence, provides a protective coating over the areas which are not to be cut. The application of maskant onto a part can be accomplished through various techniques, ranging from the dipping operation in an open-topped tank of the maskant to an application of maskant by flow-coating and to the use of electrostatic spraying equipments. Most of the maskant used in industrial chemical milling work is based upon neoprene elastomers or isobutylene-isoprene copolymers. The chemical milling maskant must have sufficient adhesion and inherent strengths to stick to the part and to protect the edges of the etched areas when it is immersed in the etchant solution. Nonetheless, the adhesiveness of the maskant should not be too high as to provide an ease in removing it from the areas to be etched and from the part during the demasking step.

3. *Scribing.* This operation is the critical step in chemical milling which depends entirely on the skills and experiences of the operator for successful results. The scribing stage also tends to be the most expensive part of chemical milling in terms of labor hours. In general, a thin-bladed knife is used to cut the maskant along the lines defining the areas to be etched, after which the unwanted maskant is peeled away by hand. In most cases, the template is used for an accurate positioning of the etched pockets on formed parts.

Accurate positioning of the cuts with respect to the template is not the only requirement in a proper scribing operation. The manner in which the operator scribes the component also affects the etched geometry. For examples, excessive blade pressure during scribing would result in scratching or penetrating of the component material, which produces an undesired fillet notch in the part after etching. This is extremely difficult to do on soft materials such as aluminum alloys. Figure 1.4 illustrates the effect of using excessive scribing pressure.

On the other hand, inadequate scribing pressure or a dull knife would cause the edge of the maskant to be lifted when the maskant is peeled off. This loss of local adhesion would cause unacceptable etching on the chemical milled component. In addition, tilting the knife during scribing with a template could alter the pocket geometry, as shown in Figure 1.5. This can be especially damaging when the lateral tolerances of the etched pocket are to be maintained. Due to the complexity of today's design of aircraft components, a majority of the parts and components require multi-step scribing and chemical milling processes.

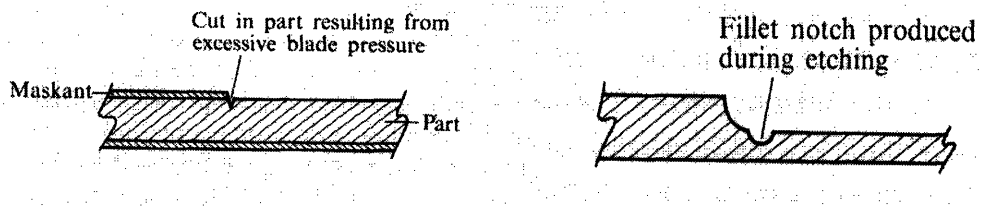

Figure 1.4: Effect of excessive blade pressure during scribing.

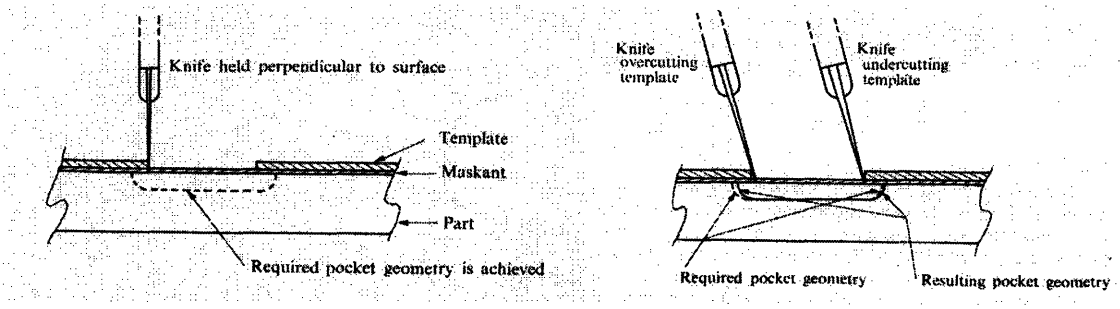

Figure 1.5: The effect of tilting the knife during scribing the maskant from a template.

4. *Etching.* The most critical part in the chemical milling process is the etching stage, at which the material is removed as required by immersion in an etchant solution. Sodium hydroxide is one of the many common chemical solutions used in the chemical milling process of aluminum alloys. Three basic parameters associated with the physics of the process are the depth of cut required, an immersion time or cutting time, and the rate of etching of the chemical solution. The relationship for the three variables used in the industry standard to predict the required immersion time is

$$t = \frac{s}{E} \tag{1.1}$$

where t is time in minutes; s is the depth of material removed per surface, measured in micrometers; and E is the etch rate with a unit of micrometers per minute. The etch rate of a chemical solution largely depends on the concentrations of each chemical constituent, the temperature of the solution during chemical milling, and the specifications and heat treatment conditions of the material.

One important principle of the etching operation is the concept of eat-back, which is illustrated in Figure 1.6. The undercut is caused by a sideways removal of material as the material underneath the maskant is exposed to the etching solution. Because of the eat-back condition, the corners of an etched pocket will have a rounding or fillet radius characteristic, which, in essence, affects the geometry of the section at the edge of the different cuts in multi-step chemical milling. This effect is exemplified in a profile shown in Figure 1.6; one should notice a larger fillet radius, as the depth of cut increases. As a matter of fact, this characteristic of etching turns out to be an advantage in most highly stressed components because a larger fillet radius provides a smoother blend from one thickness to another. Interestingly, most of the aircraft components are chemically milled in multiple steps to help increase the stiffness in a part.

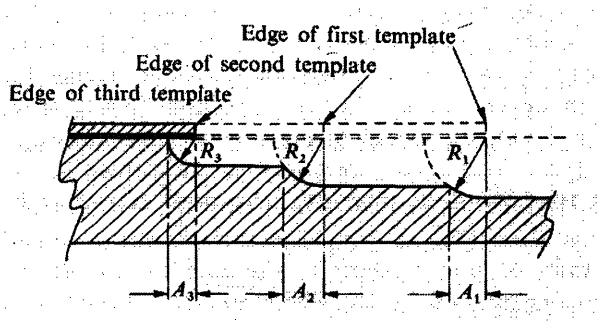

Figure 1.6: Illustration of the concept of eat-back in a multi-step chemical milling process.

5. *Demasking.* The final step in the chemical milling process is the final rinsing and demasking of the residual maskant. After the completion of the etching stage, parts will be rinsed by clean cold water to rid of any remaining chemical solutions. The etching process often leaves an oxide film and smut deposits on the etched surfaces of the part. A de-oxidizing bath, followed by another rinse of clean water, is necessary to remove these deposits. When the part is completely clean, the maskant is then removed by hand or with the

help of a chemical demasking solution. It is important to realize that many sheet metal components, after they were fully etched, will be flimsy and prone to buckling or further deformation upon the removal of the maskant at full adhesion. As a result, a chemical demasking solution is sometimes used to reduce the maskant adhesion or to soften the maskant so that the maskant can be easily removed.

The principal objective of chemical milling of aircraft components is to remove excess material in a part, in order to save weight and to achieve the maximum strength-to-weight performance through increasing the flexible rigidity in the part. Since liquid chemical is essentially the only cutting tool of the process, there are no geometric constraints on the shape of the cuts. The cutting forces are zero and the work-piece only needs to be in contact with a liquid chemical. Parts can be formed first, after which unwanted material is chemically removed. This is a major advantage of the chemical milling process; it is the process capabilities in removing material from the areas on a work-piece, which would be extremely difficult and very expensive to do with other manufacturing methods.

1.3 Basic Mechanics of The Stretch Forming Process and The Chemical Milling Process

1.3.1 The Forming Process

To aid in the understanding of the forming and the chemical milling process, closed form calculations for the problem of elastic-plastic bending and chemical milling of a sheet are provided in this section. It includes a discussion on the stress and strain distribution in the sheet, the resulting moment-curvature relationship, and the change of curvature upon unloading. First, consider the sheet with a rectangular cross section of width b and height or thickness t and length l, as shown in Figure 1.7. Therefore, the moment of inertia of the sheet I is $\frac{bt^3}{12}$. In order to simplify the algebra in the calculations, the material properties of the sheet are assumed to be elastic-perfectly plastic, with the Young's Modulus E and the yield stress σ_y. The moment M is applied to the sheet in the direction as illustrated in Figure 1.7. The moment M bends the sheet to a certain radius of curvature ρ until the sheet becomes fully plastic. From geometry, a corresponding curvature κ is the reciprocal of the radius of curvature:

$$\kappa = \frac{1}{\rho} \tag{1.2}$$

In the elastic region of bending, from the basic mechanics of beam bending, the relationship between the normal stresses σ_{xx} in a beam, the curvature κ,and the applied moment M is found to be

$$\sigma_{xx} = -E\kappa y = \frac{My}{I} \tag{1.3}$$

where I is the moment of inertia of the cross-sectional area with respect to the neutral axis of the sheet and y is distance from the neutral axis.

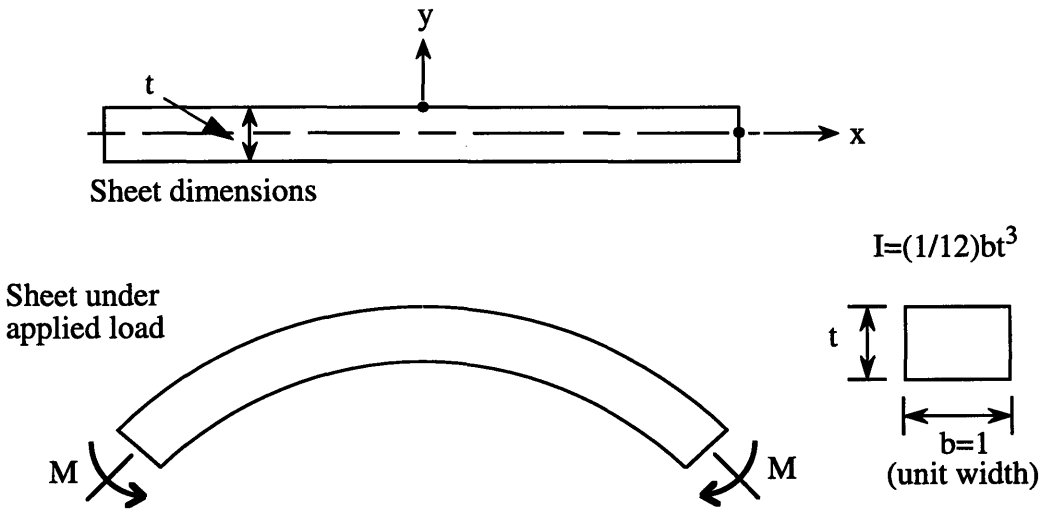

Figure 1.7: Sheet dimensions and the applied moment M.

Figure 1.8 shows the stress distribution through the sheet thickness during pure bending. Figure 1.8 (a) is the case of elastic bending, in which the stress σ_x varies linearly in y through the thickness of the sheet. In addition, this figure corresponds to the initial yielding of the sheet as the stress level on the top and bottom surface of the sheet reaches the yield stress σ_y. The moment at first yield can be calculated from equation 1.3 and is found to be

$$M_y = \frac{\sigma_{xx} I}{y} = \frac{2\sigma_y I}{t} = \frac{\sigma_y b t^2}{6} \tag{1.4}$$

The corresponding curvature at first yield is

$$\kappa_y = \frac{1}{\rho_y} = \frac{M_y}{EI} = \frac{2\sigma_y}{Et} \tag{1.5}$$

When the bending moment exceeds the yield moment M_y, the strains at the extreme points of the cross section will continue to increase, exceeding the yield strain. As a result, the curvature of the sheet increases, ρ becomes smaller and plasticity spreads through the cross section of the sheet. Due to the elastic-perfectly plastic characteristics of the material, the maximum stress will remain constant and equal to σ_y. Eventually, when the whole sheet becomes fully plastic, the resulting stress distribution in the sheet corresponds to the one shown in Figure 1.8 (b). The assumption taken at this point is to neglect the presence of the elastic core in the sheet because the strain in the extreme fibers at this stage are about 10 or 15 times the yield strain. As a result, the stress distribution can be idealized to consist of two rectangular parts shown in Figure 1.8 (b). It should also be noted that the moment obtained from this stress distribution represents the maximum moment that can be sustained in a sheet of elastic-perfectly plastic material.

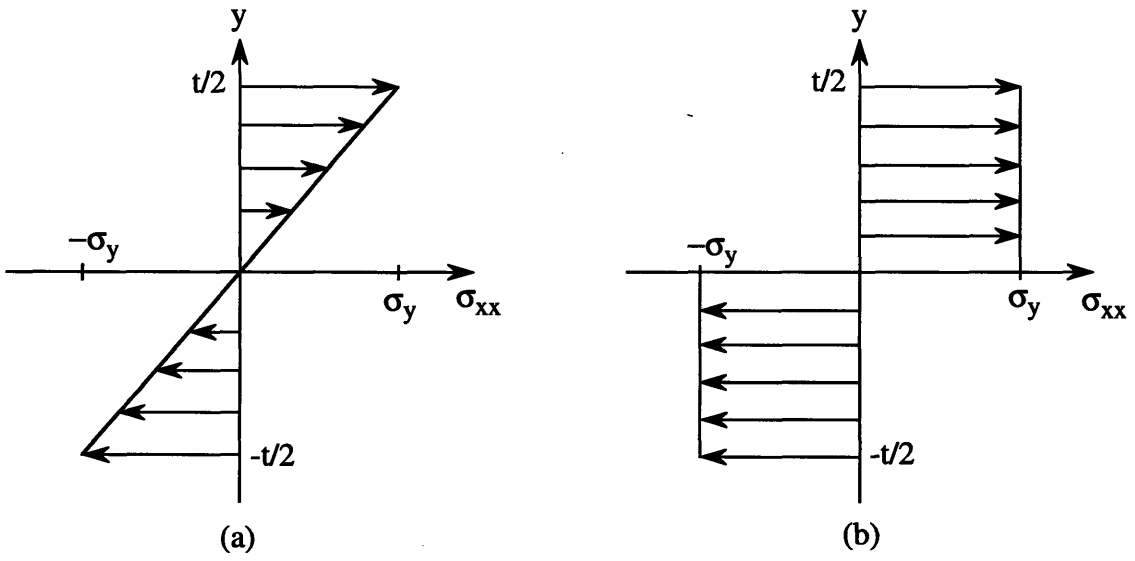

Figure 1.8: Stress distribution in the sheet during bending: (a) Elastic bending (Note that the top and bottom surface of the sheet just reach initial yield, σ_y); (b) Plastic Bending.

When the sheet is formed until fully plastic, as shown in Figure 1.8 (b), the corresponding stress distribution can simply be written in a form of

$$\sigma_{xx} = \begin{cases} \sigma_y & ,0 < y \le \frac{t}{2} \\ -\sigma_y & ,-\frac{t}{2} \le y < 0 \end{cases} \tag{1.6}$$

Since the bending moment in the sheet is obtained from the expression $M = \int \sigma_{xx} y dA$, the bending moment corresponding to the stress distribution in the loaded sheet (See Figure 1.8 (b)) having a unit width, $b = 1$, is

$$M_{bend} = \int_{-\frac{t}{2}}^{0} (-\sigma_y) y dA + \int_{0}^{\frac{t}{2}} (\sigma_y) y dA \tag{1.7}$$

$$= \int_{-\frac{t}{2}}^{0} (-\sigma_y) y(1) dy + \int_{0}^{\frac{t}{2}} (\sigma_y) y(1) dy$$

$$M_{bend} = \frac{\sigma_y t^2}{4} \tag{1.8}$$

During the elastic unloading of the sheet, the equilibrium condition has to be satisfied, which means that the total force and moment in the sheet, after unloading, have to be equal to zero ($\sum F = 0, \sum M = 0$). The stress distribution in Figure 1.8 (b) clearly shows that the force equilibrium condition is already satisfied. The moment equilibrium condition, however, requires some of the unloading moment to be removed from the loaded sheet as illustrated by the following:

$$\sum M = 0 = M_{bend} + M_{unload1}$$

$$\therefore M_{unload1} = -M_{bend} = -\frac{\sigma_y t^2}{4} \tag{1.9}$$

As a result, a corresponding stress distribution due to this unloading moment, $M_{unload1}$, can be evaluated from

$$\sigma_{unload1} = \frac{M_{unload1} y}{I} = -\frac{3\sigma_y}{t} y \tag{1.10}$$

The sketch for this unloading stress distribution is depicted in Figure 1.9. To obtain the residual stresses in the sheet after unloading, one simply superposes the stress distribution produced by unloading moment (Figure 1.9) to the bending stress distribution (Figure 1.8 (b)). Algebraically, this is equivalent to

$$\sigma_{r1} = \sigma_{xx} + \sigma_{unload1}$$

$$\sigma_{r1} = \begin{cases} \left(1 - \frac{3}{t}y\right)\sigma_y & ,0 < y \le \frac{t}{2} \\ \left(-1 - \frac{3}{t}y\right)\sigma_y & ,-\frac{t}{2} \le y < 0 \end{cases} \tag{1.11}$$

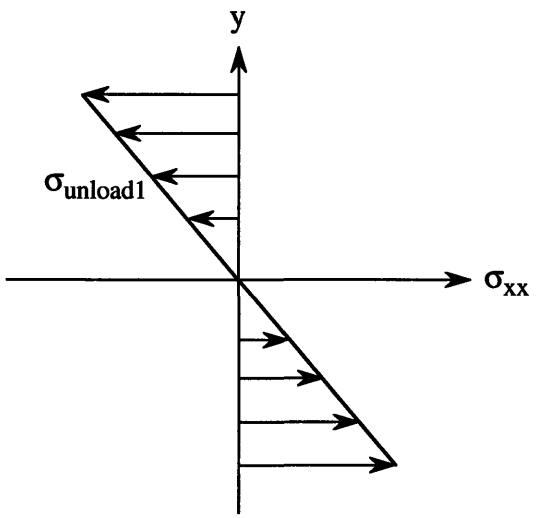

Figure 1.9: Unloading stress distribution in the sheet, $\sigma_{unload1}$.

This normal residual stress distribution in the sheet after unloading, depicted in Figure 1.10, satisfies both the force and the moment equilibrium conditions. It is interesting to note that the level of residual stresses in the sheet depends on a number of factors such as the internal stresses in the sheet due to the manufacturing methods of the sheets, e.g.- cold rolled or hot rolled, and whether the forming process involves any pre-stretching or post-stretching of the sheet. This residual stress will, in turn, affect the change in both stress distribution and part curvature during the chemical milling process.

Upon unloading, the curvature of the sheet changes and the amount of curvature that is recovered is equal to

$$\frac{1}{\rho_{unload}} = \frac{M_{bend}}{EI} = \frac{3\sigma_y}{Et} \tag{1.12}$$

This unloading curvature is often called the "springback" of the sheet. If a curvature of $\frac{1}{\rho_L}$ is imposed to the sheet, then, upon unloading of the sheet, $\frac{1}{\rho_{unload}}$ will be recovered, result-

ing in a permanent curvature $\frac{1}{\rho_P}$ of

$$\frac{1}{\rho_P} = \frac{1}{\rho_L} - \frac{1}{\rho_{unload}} \tag{1.13}$$

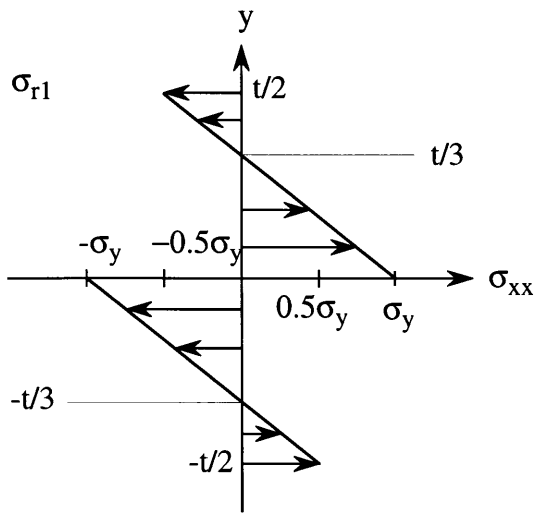

Figure 1.10: Normal residual stress distribution in the sheet after unloading from forming, σ_{r1}.

The diagram of the moment-curvature relationship can then be plotted to show the part curvature change upon unloading. (See Figure 1.11.) It should be noted here that the recovered curvature $\frac{1}{\rho_{unload}}$ essentially reduces the curvature of the sheet, hence the name "springback".

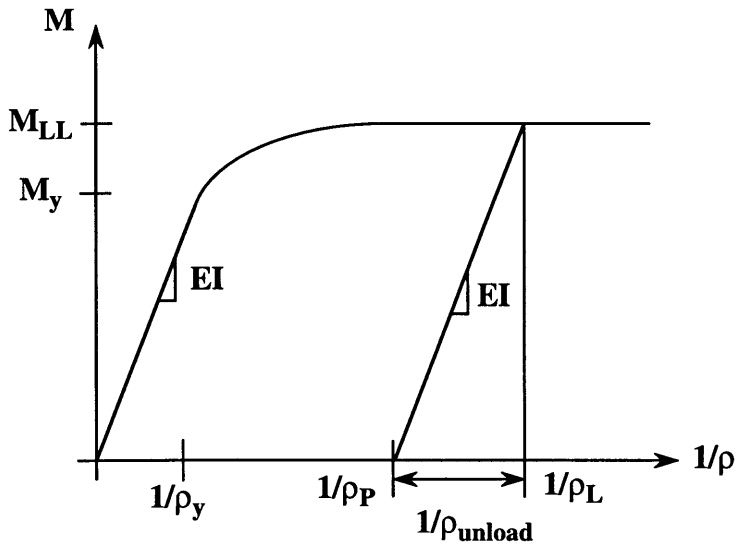

Figure 1.11: Moment-Curvature diagram illustrating the change in curvature upon unloading.

1.3.2 The Chemical Milling Process

In this section, the case of chemical milling the entire part by one-half of the sheet thickness will be considered. Readers can find an additional closed form solution for the case of chemical milling different sheet thickness in Appendix A. As described earlier, the main idea of the chemical milling process is the removal of material with zero cutting force. Therefore, the stress distribution before the sheet is re-equilibrated from chemical milling is essentially the residual stress in the sheet after unloading from the forming process and before the chemical milling process with the chemically milled section removed. Following this argument, it becomes clear to see that the stress distribution in Figure 1.12 is basically the same stress distribution as the one shown in Figure 1.10 with the bottom half of the sheet thickness removed, since, in this particular case, the sheet is chemically milled on the inside of the part or the region below the neutral axis.

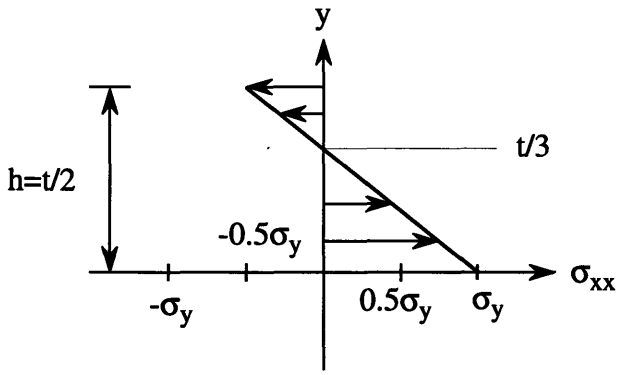

Figure 1.12: Normal stress distribution in the sheet before re-equilibrating from chemical milling.

From a careful observation of the stress distribution in Figure 1.12, one can deduce that the force and moment equilibrium conditions are not satisfied. In order to re-equilibrate the stress distribution in the sheet, the sheet is required to change its configuration to compensate for the moment and force removed as a result of chemical milling. When this occurs, the stress distribution in the sheet re-equilibrates itself until it reaches an equilibrium point. The curvature will also change upon unloading from chemical milling. A derivation for the closed form solution of the final stress distribution after chemical milling is as follows. First, one should note that the new sheet thickness h is now equal to one half of the original sheet thickness t; $h = \frac{t}{2}$. In addition, the neutral axis is now at a new location

which is at $\frac{1}{2}h$. In other cases, however, the new location of the neutral axis cannot be determined quite as easily as in this particular case. Appendix A illustrates this difference and provides calculations for the new locations of the neutral axis in different cases. The residual stress in the chemically milled sheet before re-equilibrating, in terms of the new sheet thickness h, is easily derived from the equation of a straight line.

$$y = m\sigma_x + b \qquad ,-\frac{h}{2} \le y \le \frac{h}{2} \tag{1.14}$$

Using two data points, $\sigma_x\left(y = -\frac{h}{2}\right) = \sigma_y$ and $\sigma_x\left(y = \frac{h}{2}\right) = -\frac{\sigma_y}{2}$, the values of m and b are evaluated to yield

$$b = \frac{h}{6} \text{ and } m = -\frac{2}{3}\frac{h}{\sigma_y} \tag{1.15}$$

The stress distribution in Figure 1.12 in terms of h is

$$y = -\frac{2}{3}\frac{h}{\sigma_y}\sigma_x + \frac{h}{6}$$

$$\text{or } \sigma_{r1'} = \sigma_x = -\frac{3\sigma_y}{2}\frac{1}{h}y + \frac{1}{4}y \qquad ,-\frac{h}{2} \le y \le \frac{h}{2} \tag{1.16}$$

Secondly, consider the force equilibrium condition, in order to determine the fictitious force necessary in balancing the force equilibrium equation.

$$\sum F = -\frac{1}{2}\frac{\sigma_y}{2}\left(\frac{h}{3}\right) + \frac{1}{2}\sigma_y\left(\frac{2h}{3}\right) + f = 0$$

$$\therefore f = -\frac{1}{4}\sigma_y h \tag{1.17}$$

where f is the fictitious force. From the definition of stress, $\sigma = \frac{F}{A}$, where A is the area in which the applied force F is acting, the normal stress σ_f due to the fictitious force f is, therefore,

$$\sigma_f = -\frac{1}{4}\sigma_y \tag{1.18}$$

Thirdly, it is necessary to determine the moment left in the sheet from the stress distribution in Figure 1.12. Evaluating the expression $M = \int \sigma_x y dA$ using equation (1.16) for the stress σ_x yields

$$M_{chem} = \int_{-\frac{h}{2}}^{\frac{h}{2}} \left(-\frac{3\sigma_y}{2}\frac{1}{h}y + \frac{1}{4}\sigma_y \right) y dy (1)$$

$$= -\frac{1}{2}\frac{\sigma_y}{h}y^3 + \frac{1}{8}\sigma_y y^2 \Big|_{-\frac{h}{2}}^{\frac{h}{2}} = -\frac{1}{8}\sigma_y h^2 \tag{1.19}$$

Similar to what was done for the unloading step of the forming process, the moment equilibrium condition needs to be satisfied. The unloading moment required to balance the moment equilibrium equation is essentially the negative of the moment in the sheet which was caused by material removal through chemical milling. The unloading moment for the chemical milling process is found to be

$$M_{unload2} = -M_{chem} = \frac{1}{8}\sigma_y h^2 \tag{1.20}$$

which corresponds to the unloading stress of

$$\sigma_{unload2} = \frac{M_{unload2} y}{I_{new}} = \frac{3\sigma_y}{2}\frac{1}{h}y \tag{1.21}$$

Note that I_{new} is the moment of inertia of the cross section of the sheet after chemical milling, which equals to $\frac{1}{12}h^3(1)$. Finally, the residual stress distribution in the sheet after chemical milling is determined by a superposition of the stresses due to the unloading moment $\sigma_{unload2}$, the fictitious force σ_f, and the residual stresses before chemical milling, $\sigma_{r1'}$.

$$\sigma_{r2} = \sigma_{r1'} + \sigma_{unload2} + \sigma_f = -\frac{3\sigma_y}{2}\frac{1}{h}y + \frac{1}{4}\sigma_y + \frac{3\sigma_y}{2}\frac{1}{h}y - \frac{1}{4}\sigma_y = 0 \tag{1.22}$$

It is interesting to see that, in this particular case of chemical milling the inside of the entire part by one-half of the sheet thickness, the residual stress in the sheet after chemical milling is essentially zero. In other words, the sheet is stress free after chemical milling. This is, however, purely incidental. In general, the changes in the stress distribution in the sheet during the forming and the chemical milling process will be similar to those depicted in Figure 1.13. (See also Appendix A.)

Ultimately, we are interested in the change in curvature of the sheet upon unloading from chemical milling as well as the change in the residual stress in the sheet after chemi-

cal milling. A similar approach to determining the change in curvature upon unloading from forming can also be used here. The "initial" curvature before chemical milling is the

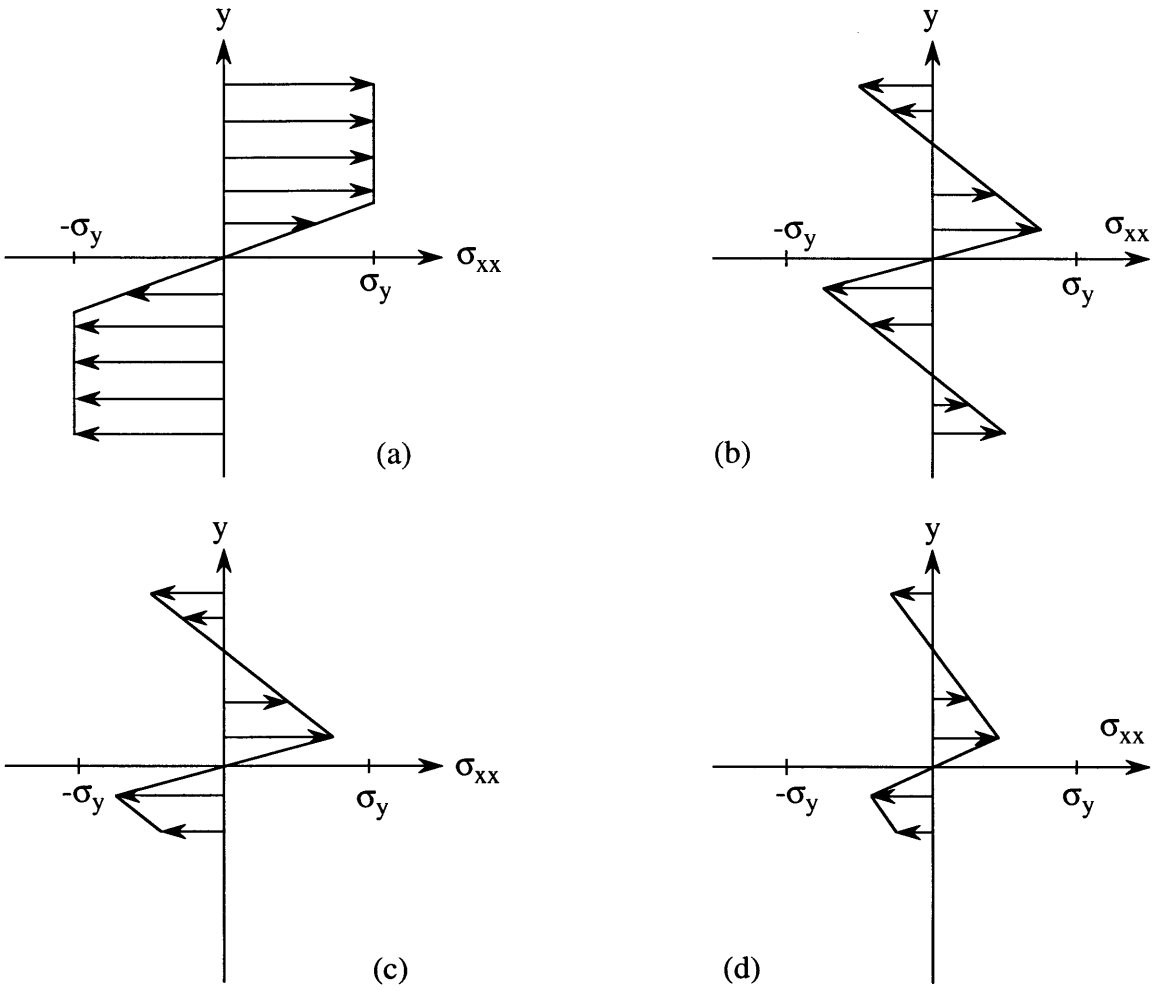

Figure 1.13: Changes of the stress distribution in the sheet during forming and chemical milling processes: (a) loaded; (b) unloaded; (c) material is removed during chemical milling; and (d) the sheet is allowed to re-equilibrate after chemical milling.

permanent curvature $\frac{1}{\rho_P}$ as a result of unloading from forming. Upon chemical milling, the amount of curvature recovered can be calculated by taking into account the effective moment left in the sheet as a result of the removal of material by the chemical milling process, M_{cm}. Then, the unloading curvature upon chemical milling is found to be

$$\frac{1}{\rho'_{unload}} = \frac{M_{cm}}{EI} = -\frac{3}{2}\frac{\sigma_y}{Eh} \tag{1.23}$$

Consequently, the final curvature after chemical milling $\frac{1}{\rho_{final}}$ is

$$\frac{1}{\rho_{final}} = \frac{1}{\rho_P} - \frac{1}{\rho'_{unload}} \tag{1.24}$$

Interestingly, the recovered curvature due to chemical milling $\frac{1}{\rho'_{unload}}$ has a negative sign, which means that the final curvature $\frac{1}{\rho_{final}}$ is increased after chemical milling. This is opposite to what was observed when the sheet is unloaded from forming; the recovered curvature upon unloading $\frac{1}{\rho_{unload}}$ in equation (1.12) reduces the loaded curvature. Clearly, the factor which determines whether the change of curvature is positive or negative is the effective moment remained in the sheet caused by the change of the residual stress in the chemical milling process. Furthermore, by examining the expression of the unloading curvature $\frac{1}{\rho_{unload}}$ in equation (1.23), it is clear to see that the change of the part curvature also depends upon the area moment of inertia I_{new} of the sheet after chemical milling. This is equivalent to stating that the change of part curvature depends on the sheet thickness removed from the sheet. It will be shown later in Chapter 4 the difference in the direction of the change of part curvature when different thicknesses of material are removed by the chemical milling process.

The residual stresses and the change in part curvature after chemical milling, as will be illustrated in simulations in the next several chapters and, also, in Appendix A, will depend on (1) the amount of material removed, (2) the location and geometry of the chemical milled regions, and (3) the residual stresses in the sheet before chemical milling. Later in Chapter 3, we will utilize finite element analysis to simulate the forming and chemical milling process similar to this analytical study. The results obtained from these numerical simulations will then be compared to the analytical results to indicate the predictive capability of the finite element simulations.

Chapter 2

The Study of Effect of Friction at The Sheet-Die Interface Using Various Finite Element Formulations

2.1 Background

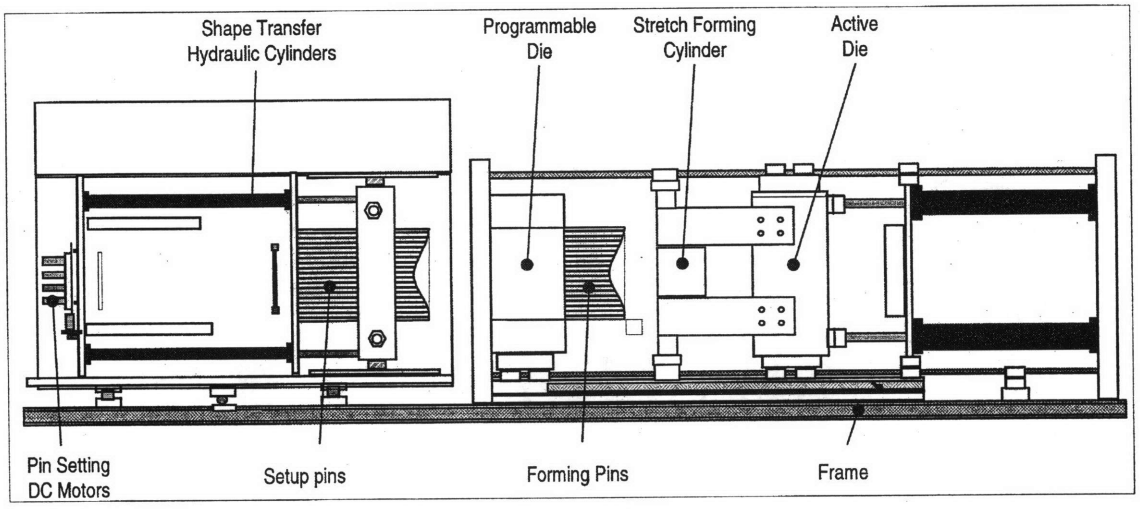

Figure 2.1: Schematic of the stretch forming machine.

Stretch forming is often used to manufacture aircraft parts and components. It is a process in which sheet metal is clamped around its edges and stretched over a die or a form block. The schematic of the stretch forming machine is depicted in Figure 2.1. The final part shape depends largely on the geometry of the die, the material properties of the sheet metal, and the loading conditions on the part. Dies for typical stretch forming operations are generally made of zinc alloys, steel, or wood. For most aerospace applications, stretch forming dies are smooth and have single or multiple radii of curvature, depending on the particular part. The terms pre-stretch and post-stretch refer to the tensile loads applied to the sheet before and after the sheet is formed over the die, respectively. During post-stretching, the sheet is stretched while in contact with the die and, therefore, there can be considerable friction between the sheet and the die. The friction force can affect the process and the final shape of the part. The friction forces have two potentially significant contributions to the process: first, the friction forces oppose the imposed post-stretch and

therefore act to reduce the effective stretch imparted to the sheet (See Figure 2.2 (a)); second, the friction forces impose a shear traction to the sheet which may or may not have a significant influence on the internal stress distribution over a boundary layer of the sheet (See Figure 2.2 (b)). This second effect of shear traction brings about an interesting question of whether there exists a shear boundary layer at the interface between the sheet and the die of any significance to the overall process. Moreover, it is of interest to determine how much and in what ways friction affects the final part shape.

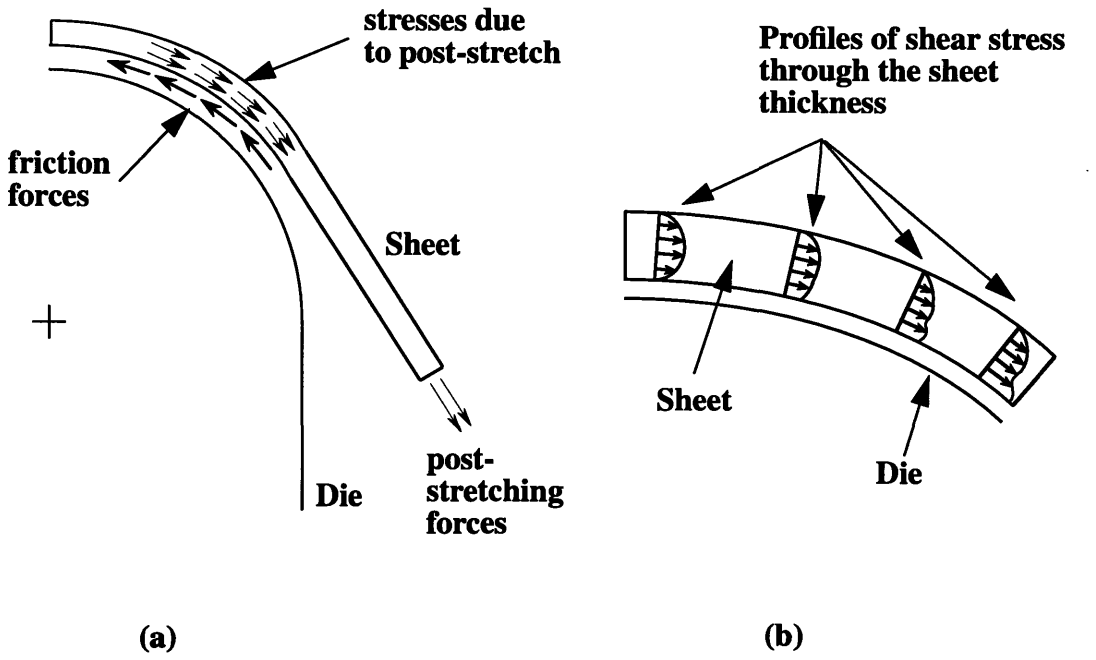

Figure 2.2: Potential effect of friction on the stretch forming process: (a) friction forces oppose the post-stretching; and (b) effect of shear traction over a boundary layer of the sheet.

ABAQUS, a commercial finite element analysis package, is chosen to be a tool to study the effect of friction and also for the investigation of the chemical milling process, which is discussed in the next chapters. With the help of finite element analysis, one is able to simulate the sheet forming process and to determine the effect of friction on the stretch forming process. Since the sheet undergoes large rotation, bending and stretching during stretch forming, shell elements (ABAQUS type S4R) appear to be ideal for these simulations because of their ability and efficiency to capture bending and stretching loading conditions. Also, the nature of their degrees of freedom (translational plus rotational)

provides an ease in applying the loading conditions imposed on the sheet by the stretch grips. However, the friction during post-stretching may transmit significant shear tractions to the sheet. While the effect of the friction forces in retarding stretching will be captured by shell elements, conventional shell elements will not capture shear boundary layer effects on the stress distribution because of the assumptions inherent in the shell element formulations. (Specifically, this assumption corresponds to the Kirchhoff beam theory which states that the line normal to the neutral axis of a beam will remain plane throughout the deformation. This assumption, in effect, neglects any contributions due to transverse shear deformations.) However, it is also not clear the level of importance of such shear boundary layer effects. In this chapter, we will first investigate the effects of friction on the stress distribution in the sheet during forming with simulations which utilize continuum elements (which do not possess any restricting assumptions in their formulations). We will then compare these results to results obtained using both non-conventional and conventional shell elements.

2.2 Continuum versus Shell Element Formulations

Before any finite element simulation is initiated, it would be wise for the finite element user to be familiar with the general finite element formulations and the specific details about the elements s/he chooses to use in her/his simulations. For the reasons mentioned earlier, the two primary types of elements used in simulations of stretch forming process and chemical milling process are continuum and shell elements. During the past decades, there has been extensive research on the development of both continuum and shell elements. The reference section provides some of the relevant literature to the topic of finite element formulations and methodology. The readers are encouraged to utilize these references for a more in-depth study of finite element analysis. This section is mainly to provide general information on the specific types of elements used in the stretch forming and chemical milling simulations, in addition to a general overview of the formulations of both continuum and shell elements.

2.2.1 General Continuum Element Formulations

The fundamental concept of the formulations of most continuum elements is generally developed from the isoparametric formulation. In the isoparametric formulation, natural coordinate systems ($\xi\eta$ or $\xi\eta\zeta$) are used to approximate the positions and the displacements. In other words, the coordinates and displacements are interpolated from the nodal values using the interpolation function, which is expressed in terms of the natural coordinates ξ,η,ζ. The Jacobian transformation matrix $[J]$ must, therefore, be invoked to relate the global coordinates x,y,z to the natural coordinates ξ,η,ζ. In most cases, the numerical integrations are required when evaluating the element stiffness matrix. In this section, the formulation of a four-node plane bilinear Isoparametric element will be considered.

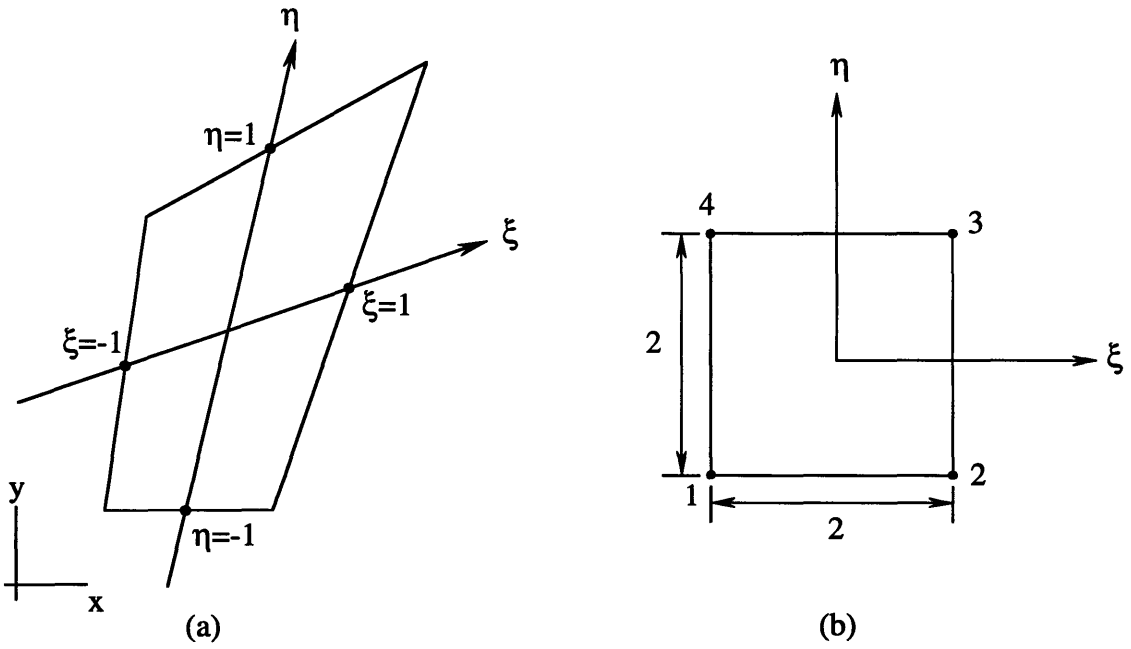

Figure 2.3: (a) 4-node planar bilinear element in xy space; (b) corresponding planar isoparametric element in $\xi\eta$ space.

A four-node plane isoparametric element with an arbitrary quadrilateral shape in xy space is shown in Figure 2.3 (a). When this planar isoparametric element is mapped into the planar natural coordinates ξ,η, the corresponding isoparametric element in $\xi\eta$ space is then represented by Figure 2.3 (b). Subsequently, the positions and displacements of each node are described in terms of natural coordinates.

$$x = \sum N_i x_i \quad \text{and} \quad u = \sum N_i u_i$$
$$y = \sum N_i y_i \quad v = \sum N_i v_i \tag{2.1}$$

where the individual interpolation functions are

$$N_1 = \frac{1}{4}(1-\xi)(1-\eta) \qquad N_3 = \frac{1}{4}(1+\xi)(1+\eta)$$
$$N_2 = \frac{1}{4}(1+\xi)(1-\eta) \qquad N_4 = \frac{1}{4}(1-\xi)(1+\eta) \tag{2.2}$$

Note that the interpolation functions in equation 2.2 dictate the orientation of $\xi\eta$ axes with respect to xy axes and the positions of each node in terms of natural coordinates system, as shown in Figure 2.3 (b), will not be changed. For example, node 1 is always at $\xi = \eta = -1$, node 2 is always at $\xi = 1$ and $\eta = -1$, and so on. In addition, the point $\xi = \eta = 0$ is regarded as the center of the element, but is not necessary the centroid of the element area [4].

Since the strain field of the element is evaluated by differentiating the interpolation matrix $[N]$, the differentiation then must be made with respect to the natural coordinates $\xi\eta$, as follows. Using Chain rule, we obtained

$$\frac{\partial u}{\partial x} = \frac{\partial u}{\partial \xi}\frac{\partial \xi}{\partial x} + \frac{\partial u}{\partial \eta}\frac{\partial \eta}{\partial x}$$
$$\frac{\partial u}{\partial y} = \frac{\partial u}{\partial \xi}\frac{\partial \xi}{\partial y} + \frac{\partial u}{\partial \eta}\frac{\partial \eta}{\partial y} \tag{2.3}$$

for the displacement u. However, the partial derivatives of ξ and η with respect to x and y are not readily available. Therefore, it is necessary to find the inverse of the equation $[B] = [\Gamma][N]$, where $[\Gamma]$ is the matrix of the partial derivatives of ξ and η with respect to x and y. First, we write

$$\frac{\partial u}{\partial \xi} = \frac{\partial u}{\partial x}\frac{\partial x}{\partial \xi} + \frac{\partial u}{\partial y}\frac{\partial y}{\partial \xi} \quad \text{or} \quad \begin{Bmatrix} \frac{\partial u}{\partial \xi} \\ \frac{\partial u}{\partial \eta} \end{Bmatrix} = \begin{bmatrix} \frac{\partial x}{\partial \xi} & \frac{\partial y}{\partial \xi} \\ \frac{\partial x}{\partial \eta} & \frac{\partial y}{\partial \eta} \end{bmatrix} \begin{Bmatrix} \frac{\partial u}{\partial x} \\ \frac{\partial u}{\partial y} \end{Bmatrix}$$
$$\frac{\partial u}{\partial \eta} = \frac{\partial u}{\partial x}\frac{\partial x}{\partial \eta} + \frac{\partial u}{\partial y}\frac{\partial y}{\partial \eta} \tag{2.4}$$

Similarly, for the displacement v,

$$\begin{Bmatrix} \frac{\partial v}{\partial \xi} \\ \frac{\partial v}{\partial \eta} \end{Bmatrix} = \begin{bmatrix} \frac{\partial x}{\partial \xi} & \frac{\partial y}{\partial \xi} \\ \frac{\partial x}{\partial \eta} & \frac{\partial y}{\partial \eta} \end{bmatrix} \begin{Bmatrix} \frac{\partial v}{\partial x} \\ \frac{\partial v}{\partial y} \end{Bmatrix} \tag{2.5}$$

The Jacobian transformation matrix $[J]$ is then defined as

$$[J] = \begin{bmatrix} \frac{\partial x}{\partial \xi} & \frac{\partial y}{\partial \xi} \\ \frac{\partial x}{\partial \eta} & \frac{\partial y}{\partial \eta} \end{bmatrix} \tag{2.6}$$

As illustrated here, the Jacobian matrix essentially maps the differentiation and acts to relate the global coordinates x,y,z to the natural coordinates ξ,η,ζ. The inverse of Jacobian matrix $[J]$ is equal to the matrix $[\Gamma]$ and equation 2.3 can be rewritten as

$$\begin{Bmatrix} \frac{\partial u}{\partial x} \\ \frac{\partial u}{\partial y} \end{Bmatrix} = [J]^{-1} \begin{Bmatrix} \frac{\partial u}{\partial \xi} \\ \frac{\partial u}{\partial \eta} \end{Bmatrix} \text{ and, similarly, } \begin{Bmatrix} \frac{\partial v}{\partial x} \\ \frac{\partial v}{\partial y} \end{Bmatrix} = [J]^{-1} \begin{Bmatrix} \frac{\partial v}{\partial \xi} \\ \frac{\partial v}{\partial \eta} \end{Bmatrix} \tag{2.7}$$

where $\frac{\partial u}{\partial \xi} = \sum_i \frac{\partial N_i}{\partial \xi} u_i$ and so on. Generally, the Jacobian matrix is expressed as a function of the natural coordinates ξ and η. If the elements are in geometrically nice shapes, such as rectangular or parallelograms, the Jacobian matrix will contain terms of nodal positions in Cartesian coordinates and is therefore a constant.

Now the formulation of the planar bilinear isoparametric element can be completed. From the basic mechanics of solids, the strain-displacement relationship can be written as

$$\{\varepsilon\} = \begin{Bmatrix} \varepsilon_{xx} \\ \varepsilon_{yy} \\ \gamma_{xy} \end{Bmatrix} = \begin{bmatrix} 1 & 0 & 0 & 0 \\ 0 & 0 & 0 & 1 \\ 0 & 1 & 1 & 0 \end{bmatrix} \begin{Bmatrix} \frac{\partial u}{\partial x} \\ \frac{\partial u}{\partial y} \\ \frac{\partial v}{\partial x} \\ \frac{\partial v}{\partial y} \end{Bmatrix} \tag{2.8}$$

Then, use equation 2.7 to obtain

$$\begin{Bmatrix} \frac{\partial u}{\partial x} \\ \frac{\partial u}{\partial y} \\ \frac{\partial v}{\partial x} \\ \frac{\partial v}{\partial y} \end{Bmatrix} = \frac{1}{detJ} \begin{bmatrix} J_{22} & -J_{12} & 0 & 0 \\ -J_{21} & J_{11} & 0 & 0 \\ 0 & 0 & J_{22} & -J_{12} \\ 0 & 0 & -J_{21} & J_{11} \end{bmatrix} \begin{Bmatrix} \frac{\partial u}{\partial \xi} \\ \frac{\partial u}{\partial \eta} \\ \frac{\partial v}{\partial \xi} \\ \frac{\partial v}{\partial \eta} \end{Bmatrix} \tag{2.9}$$

$$\begin{Bmatrix} \frac{\partial u}{\partial \xi} \\ \frac{\partial u}{\partial \eta} \\ \frac{\partial v}{\partial \xi} \\ \frac{\partial v}{\partial \eta} \end{Bmatrix} = \begin{bmatrix} \frac{\partial}{\partial \xi} & 0 \\ 0 & \frac{\partial}{\partial \eta} \\ \frac{\partial}{\partial \xi} & 0 \\ 0 & \frac{\partial}{\partial \eta} \end{bmatrix} \begin{Bmatrix} u \\ v \end{Bmatrix} = [\partial]_{\xi,\eta}[N]\{d\} = [D]\{d\} \tag{2.10}$$

Finally, by putting equation 2.8 to 2.10 together, the interpolation matrix $[B]$ for the strain field is found to be

$$[B] = \begin{bmatrix} 1 & 0 & 0 & 0 \\ 0 & 0 & 0 & 1 \\ 0 & 1 & 1 & 0 \end{bmatrix} \frac{1}{detJ} \begin{bmatrix} J_{22} & -J_{12} & 0 & 0 \\ -J_{21} & J_{11} & 0 & 0 \\ 0 & 0 & J_{22} & -J_{12} \\ 0 & 0 & -J_{21} & J_{11} \end{bmatrix} [D] \tag{2.11}$$

For a linear elastic material, the element stiffness matrix is, therefore,

$$[k] = \iint [B]^T[E][B]t dx dy = \int_{-1}^{1}\int_{-1}^{1} [B]^T[E][B]t detJ d\xi d\eta \tag{2.12}$$

It is important for the readers to realize that all the derivations for the finite element formulations shown here in this section are for small strain, linear elastic material. All of the finite element simulations presented in this thesis, however, include nonlinear material effect as well as nonlinear geometry effect. The nonlinearity usually arises from the nonlinear material properties and changes in geometry. It presents various problems and difficulties in terms of finite element formulations as well as the convergence of the solutions. Also, note that $[B]^T[E][B]detJ$ determines the order of the polynomial and are usually integrated numerically. The accuracy of the solution depends on the integration method and the degree of precision used to evaluate the terms in equation 2.12. Usually, the integration

is done by the Gauss Quadrature Method, in which the integral is approximated by a number of sampling points and some weighing functions. The formula for the Gauss Quadrature approach is shown in equation 2.13.

$$I = \int_{-1}^{1} f(\xi)d\xi \cong W_1 f(\xi_1) + W_2 f(\xi_2) + \ldots + W_n f(\xi_n) \tag{2.13}$$

Clearly, when the n-point Gauss Quadrature is used to integrate a polynomial of order $2n-1$, an exact solution can be obtained. If the function $f(\xi)$ is not a polynomial, Gauss Quadrature is inexact. By increasing the number of points, however, the accuracy of the integration result increases. The term 'full integration' usually refers to the order of Gauss Quadrature required to integrate the element stiffness matrix $[k]$ exactly. The term 'reduced integration', on the other hand, represents the integration of one order lower than full integration. For some elements, reduced integration will produce more accurate and efficient results than full integration. The issues of which methods to use to integrate the element stiffness matrix are discussed in details in ***Concepts and Applications of Finite Element Analysis, 3rd Edition*** by Cook. The next two sections and a later section on shell elements give an overview of the specific continuum elements and shell elements provided by ABAQUS. This is in reference to the ***ABAQUS Theory Manual Version 5.5***. The readers are advised to refer to the ABAQUS manual for more specific details of each element.

2.2.2 CPE4 Solid Element

The type of continuum elements of interest in the forming and chemical milling simulations is the two-dimensional planar solid (continuum) element, particularly the ABAQUS type CPE4. CPE4 element is a 4-node bilinear plane strain element. It is considered to be a first-order (linear) interpolation element and has only two translational degrees of freedom, u_x and u_y. Subsequently, the element output provides four components of stresses, namely σ_{xx}, σ_{yy}, σ_{zz}, and τ_{xy}, and their corresponding strain components. Full integration scheme is used with this type of element and the element stiffness matrix is integrated at the four Gauss points in each element.

CPE4 is essentially an isoparametric element with first order interpolation. Therefore, the formulation for CPE4 is similar to what was shown in the previous section. However, ABAQUS uses a technique known as the selectively reduced integration technique to inte-

grate the terms in the element stiffness matrix. This technique replaces the actual volume changes at the Gauss points with the average volume change of an element, which helps to prevent mesh locking and, thus, provides accurate solutions in the incompressible or nearly incompressible cases. In addition, ABAQUS uses the average strain in the third or out-of-plane direction for the plane strain problems. Therefore, in the two-dimensional elements such as CPE4, only in-plane strains are modified. It should then be noted that this might cause a slightly different behavior between using plane strain elements and three-dimensional solid elements with plane strain boundary conditions.

2.2.3 CPE8R Solid Element

Continuum elements of ABAQUS type CPE8R is a higher order element than the CPE4 continuum elements. CPE8R is an 8-node biquadratic element that utilizes a reduced integration scheme. Since CPE8R is a second-order element, Gauss integration is often used because of its efficiency and a high level of accuracy of strain predictions at the Gauss points. As mentioned earlier, reduced integration uses one order less than full integration to integrate the element's internal forces and stiffness, thereby reducing the number of constraints in an element. The method, therefore, helps to avoid the problem of mesh locking. However, the reduction in integration order introduces the probability of activating zero-energy (often called hour glass) modes.

2.2.4 General Shell Element Formulations

A definition of a shell is a structure which can be derived from a thin plate by initially forming the middle plane to a singly or doubly curved surface [5]. In other words, the curved shape of a shell is produced when forces and moments are applied to a thin plate. A shell is usually thin in comparison to its span. The stresses in shells are, in general, composed of bending stress and membrane stress. Bending stress in a shell corresponds to the bending stress in a plate, and produces bending and twisting moments. Membrane stress corresponds to stress in a plane stress problem and produces a tangential force to the mid-surface. Shell theories are limited to small deflections unless higher-order terms are added to account for membrane strains associated with the rotation of shell midsurface. In classical shell theory, two kinds of shells are distinguished: (1) thin shells, of which transverse

shear deformation is negligible and is not accounted for; and (2) thick shells, of which transverse shear deformation and the effects of thickness-direction normal stresses are accounted for.

Shell elements are considered to be structural elements, in which the displacements u,v,w are interpolated in terms of midsurface displacements and rotations. According to Bathe, structural elements such as shells are, in essence, "a continuum isoparametric element formulation with displacement constraints."[6] There are generally three approaches in formulating shell elements: use of flat elements, curved elements, and Mindlin-type elements (also known as degenerated solid elements). The main concept of each approach will be briefly explained in this section. The focus is, however, on the formulation of isoparametric shell elements of general shape.

The use of flat elements in modeling a curved shell basically combines a plane membrane element with a plate bending element. In other words, the element stiffness equation for the flat element is consisted of two independent sources of contribution to the total strain energy: a membrane contribution and a bending contribution. Even though this formulation is easier and simpler than other approaches, it is not particularly accurate because the element does not provide a coupling of bending and membrane actions in an individual element. Similar to using a straight element to model an arc, numerical difficulties due to spurious bending moments can occur when flat elements are used to model a shell.

When curved elements are used to model a shell, it is often found that they are less accurate than flat elements. A curved element is typically more complicated than a flat element because its geometry is more complicated. In addition, a curved element is too stiff, especially when a shell is thin and has a large rise-to-span ratio. These difficulties are due to what is called membrane locking. It is the condition in which the element is severely constrained, causing the element to be too stiff, i.e. it cannot bend. In general, the user of curved elements need to supply additional information to the nodal coordinates in order to describe element geometry [4].

The Mindlin-type shell elements occupy the middle ground between flat elements and curved elements both in terms of accuracy and ease of use. They are similar to the Mindlin

beam elements in that the formulation is based on the Timoshenko beam theory, which recognizes the effects of transverse shear strain and averages these effects over the cross section of the beam. As a result, the Mindlin-type shell elements can account for transverse shear deformation. The element stiffness matrix for the Mindlin-type shell elements is derived from taking into account the strain energy U_m from membrane strain ε_m, U_b from curvature change κ, and U_s from transverse shear strain γ_{zs}.[7] Numerical difficulties due to element locking can occur as the thickness of shell approaches zero. This problem can be avoided by way of reduced integration. For instance, if U_m and U_s are integrated with one-point rule, only two constraints are imposed on the element and the resulting mesh does not lock.

In the case of isoparametric general shell elements, a shell of general shape can be modeled by a three-dimensional solid element which has small thickness compared to other dimensions. The main idea in formulating the isoparametric shell element is based on the concept of degenerated solids, which is illustrated in Figure 2.4. The solid element in Figure 2.4 (a) is used as a starting geometry and has 20 nodes and 60 degrees of freedom. With three nodes along the thickness-direction lines, this element has too many degrees of freedom. By eliminating the middle nodes, the thickness-direction strain ε_3 is essentially modeled as a constant through the shell thickness. Note that the subscript 3 is used to indicate the direction normal to the midsurface of a shell. This reduction in the number of nodes and degrees of freedom results in an element in Figure 2.4 (b).

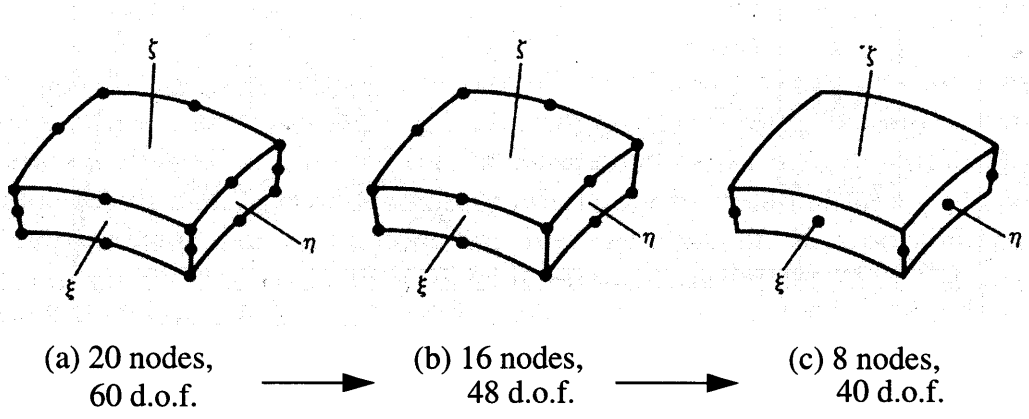

Figure 2.4: Illustration of the concept of a degenerated solid.

As the element becomes thinner, stiffness coefficients associated with the thickness-direction strain ε_3 become much larger than other stiffness coefficients, which can cause numerical difficulties. In order to avoid this problem, each pair of the thickness-direction nodes can be constrained to have the same thickness-direction displacement, resulting in only five degrees of freedom for each pair of nodes. Further reduction can be accomplished by attaching these five degrees of freedom, three translations and two rotations, to one single node at the midsurface of a shell element, as shown in Figure 2.4 (c). The final form of shell elements then has only midsurface nodes and can be formulated for a four-node or nine-node element. Since all of the isoparametric shell elements are considered to be of Mindlin type, then the effects of transverse shear deformations are accounted for in the element formulation. As with other aforementioned elements, isoparametric shell elements may encounter problems associated with element locking. These problems can be avoided by choice of geometry, shape functions, type and number of degrees of freedom, and the chosen numerical integration schemes.

As for the formulations of the shell elements of general shape, one follows the standard procedure for the isoparametric formulation. First, the generalization of the position of an arbitrary node in an element, as depicted in Figure 2.5 (a), is considered. Then, the Cartesian coordinates of an arbitrary node in an element can be expressed as

$$\begin{Bmatrix} x \\ y \\ z \end{Bmatrix} = \sum N_i \begin{Bmatrix} x_i \\ y_i \\ z_i \end{Bmatrix} + \sum N_i \zeta \frac{t_i}{2} \begin{Bmatrix} l_{3i} \\ m_{3i} \\ n_{3i} \end{Bmatrix} \tag{2.14}$$

where l_i,m_i,n_i are direction cosines of the line jik perpendicular to the midsurface plane, $x_i = (x_j + x_k)/2$ and similarly for y_i and z_i, and shape functions N_i are functions of ξ and η, but are independent of ζ [4]. The form of shape functions N_i depend on the number of nodes in an element and can be obtained from the standard isoparametric formulations. Figure 2.5 (b) shows orthogonal vectors at node i, in which vectors $\mathbf{V}_{1i}$ and $\mathbf{V}_{2i}$ are tangent to the midsurface. Both $\mathbf{V}_{1i}$ and $\mathbf{V}_{2i}$ are used to define the directions of nodal rotation degree of freedom α_i and β_i. The vector $\mathbf{V}_{3i}$ is defined as a thickness-direction vector and has l_i,m_i,n_i components. A similar approach in finding the Jacobian matrix as the one in Section 2.2.1 was taken and found the terms in the Jacobian matrix to be

$$
\begin{aligned}
x_{,\xi} &= \sum N_{i,\xi}(x_i + \zeta t_i l_{3i}/2) \\
x_{,\eta} &= \sum N_{i,\eta}(x_i + \zeta t_i l_{3i}/2) \\
x_{,\zeta} &= \sum N_i(t_i l_{3i}/2)
\end{aligned}
\tag{2.15}
$$

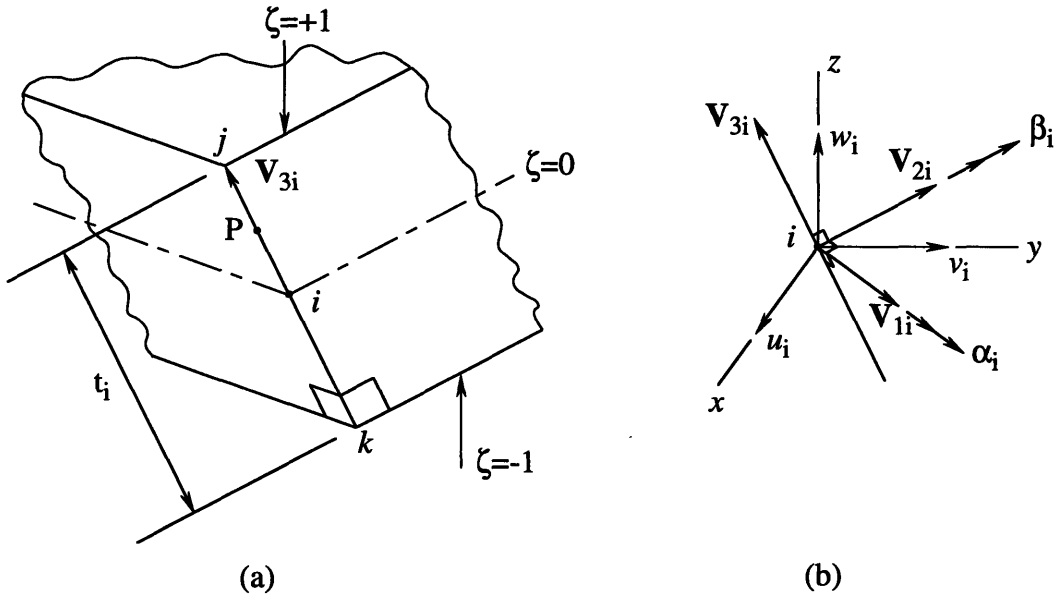

Figure 2.5: (a) An arbitrary node i in a shell element; (b) Orthogonal vectors at node i.

With five degrees of freedom at node i, the displacement of an arbitrary point P on the line perpendicular to the midsurface plane will consist of the displacement of node i and the displacement relative to node i due to rotation of vector $\mathbf{V}_{3i}$. In general, the displacement field of an arbitrary point can be expressed as

$$
\begin{Bmatrix} u \\ v \\ w \end{Bmatrix} = \sum N_i \begin{Bmatrix} u_i \\ v_i \\ w_i \end{Bmatrix} + \sum N_i \zeta \frac{t_i}{2} [\mu_i] \begin{Bmatrix} \alpha_i \\ \beta_i \end{Bmatrix}
\tag{2.16}
$$

where $[\mu_i]$ is the matrix of direction cosines. The first term on the r.h.s. refers to the displacement of node i while the second term is from the relative displacement due to the rotational degrees of freedom. The strain-displacement relationships are

$$\begin{Bmatrix} \varepsilon_x \\ \varepsilon_y \\ \varepsilon_z \\ \gamma_{xy} \\ \gamma_{yz} \\ \gamma_{zx} \end{Bmatrix} = [H] \begin{Bmatrix} u_{,x} \\ u_{,y} \\ u_{,z} \\ v_{,x} \\ v_{,y} \\ \cdots \\ w_{,z} \end{Bmatrix} \text{ and } \begin{Bmatrix} u_{,x} \\ u_{,y} \\ u_{,z} \\ v_{,x} \\ v_{,y} \\ \cdots \\ w_{,z} \end{Bmatrix} = \begin{bmatrix} J^{-1} & 0 & 0 \\ 0 & J^{-1} & 0 \\ 0 & 0 & J^{-1} \end{bmatrix} \begin{Bmatrix} u_{,\xi} \\ u_{,\eta} \\ u_{,\zeta} \\ v_{,\xi} \\ v_{,\eta} \\ \cdots \\ w_{,\zeta} \end{Bmatrix} \tag{2.17}$$

Using equation 2.16 to find the partial derivatives of the displacement u,v,w with respect to ξ,η,ζ in equation 2.17, one obtains

$$\left[\varepsilon_x \ \varepsilon_y \ \varepsilon_z \ \gamma_{xy} \ \gamma_{yz} \ \gamma_{zx}\right]^T = \sum [B_i] \left[u_i \ v_i \ w_i \ \alpha_i \ \beta_i\right] \tag{2.18}$$

in which $[B_i]$ is the complete strain-displacement matrix. Finally, the element stiffness matrix for an isoparametric general shell element can be written as

$$[k] = \int_{-1}^{1}\int_{-1}^{1}\int_{-1}^{1} [B]^T [E][B] det[J] d\xi d\eta d\zeta \tag{2.19}$$

2.2.5 S4R Shell Element

A specific type of shell elements used in our simulations is the shells of ABAQUS type S4R. It is a 4-node, first-order, doubly curved element that is valid for both thick and thin shell applications and can account for finite membrane strains. In using S4R as "thick" shell elements, the modeling issue pertains to the case in which the transverse shear flexibility is important. In other words, the effect of transverse shear deformation is significant and should be included in the modeling of the shell elements. The "thin" shell applications refer to the situation where the thickness of shells is much smaller than other dimensions and the effect of transverse shear deformation is negligible. Hence, the Kirchhoff constraints (the plane normal to the midsurface remains plane during deformation) are imposed algebraically. Furthermore, S4R allows transverse shear stress as an output. It also utilizes a reduced integration scheme in the element formulation. The finite strain shell element formulation for ABAQUS type S4R element is discussed in details in the ***ABAQUS Theory Manual Version 5.5***. [8]

2.3 Simulations and Analysis of Stretch Forming

2.3.1 Testing Parameters and Setups

As mentioned previously, the two main objectives in this preliminary study were to analyze the effect of a shear boundary layer, if it exists at all, at the sheet-die interface, and to examine the capability of various finite element formulations to capture these effects. A matrix of test cases was setup and simulated using ABAQUS. The problem was the one in which an aluminum (Al-2024O: E = 68.9 GPa and σ_y = 76.1 MPa) sheet with a dimension of 60cm x 15cm x 1.6mm (24.0"x6.0"x0.063") is pre-stretched to just below the yield point, wrapped over a 12.5 cm (5.0")-radius smooth, cylindrical die to an angle of 30 degrees, and post-stretched to approximately 5.0% nominal strain. The stress-strain curve showing the material behavior of the Al-2024O is shown in Figure 5.1. Testing parameters in the simulations varied from no friction to a friction coefficient of 0.2 between the sheet and the die, and from using both 1st- and 2nd-order plane strain continuum elements (ABAQUS type CPE4 and CPE8R) to using various kinds of shell elements (ABAQUS type S4R). The aspect ratio of the elements used in each case of simulations is tabulated in the table 2.1. The plane strain condition used in the simulations eliminates the effect of an anticlastic curvature at the edges and causes the stress to be constant across the width of the sheet. This is essentially equivalent to modeling the middle section of the sheet and neglecting any effects at the edges

Types of Elements Used In Simulation	Aspect Ratio of Elements (for the elements in contact with the die)
1st-order Plane Strain Continuum Elements	1:1
2nd-order Plane Strain Continuum Elements	1:1
Shell Elements of 5 Section Points	1:3
Shell Elements of 11 Section Points	1:3
Shell Elements of Composite Type	1:3

Table 2.1: Aspect ratio of the elements used in the simulations.

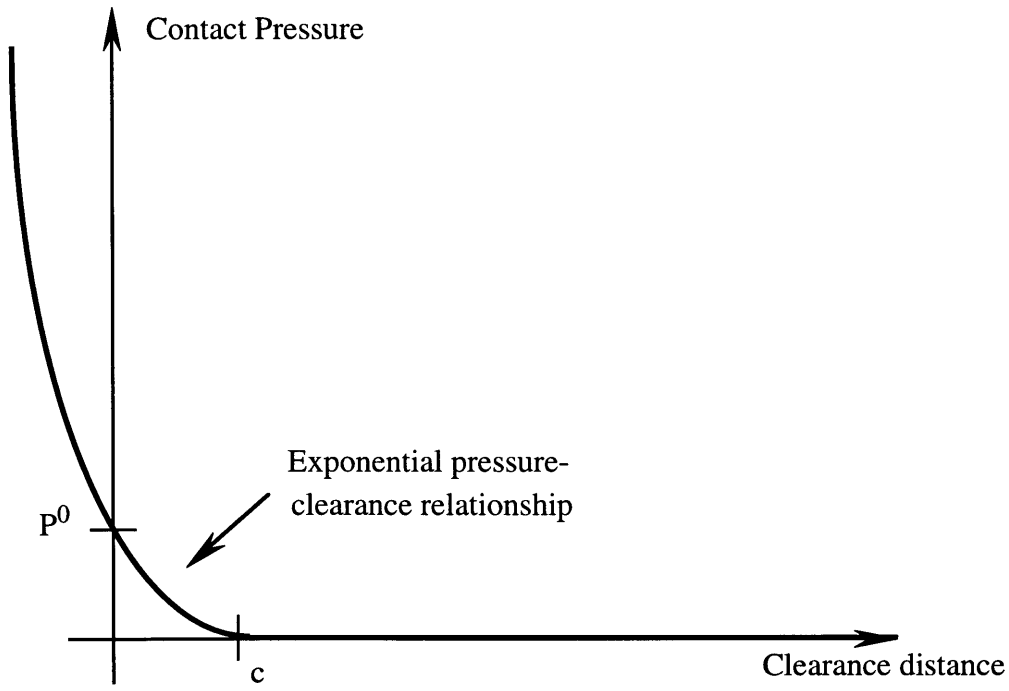

Figure 2.6: "Softened" pressure-clearance relationship for contact.

The die was modeled as a rigid surface, whereas the sheet was modeled as a deformable surface. The contact interactions between the two surfaces were defined as having friction coefficient of user-specified value with a "softened contact" characteristic. The "softened contact" option was essentially a pressure-clearance relationship for interface elements. It allowed an exponential increase in the pressure transmitted between surfaces as the distance between two surfaces decreases below the zero-pressure clearance. This pressure-clearance relationship used in the "softened contact" scheme is also illustrated in Figure 2.6. This modeling of contact was mainly used for numerical reasons; the "softened contact" option acts to ease convergence in the contact solution by gradually ramping up contact.

There is, however, a slight difference between modeling contact of shell elements and that of continuum elements. In using shell elements, effectively the sheet has "zero" thickness and is represented by a plane, as illustrated in Figure 2.7 (a), because of the characteristics of shell elements. When the continuum elements are used, however, the entire cross section of the sheet is modeled. (See Figure 2.7 (b)) Therefore, the modifications have to be made to the pressure-clearance relationship for both cases. The differences in the val-

ues for the clearance distance and the pressure at zero clearance are shown in Figure 2.7. In addition, the friction model that ABAQUS provides is similar to the classical Coulomb friction model, in which the contact surfaces do not slide over each other as long as the magnitude of shear stress is less than the coefficient of friction, μ, times the normal stress between them.[9]

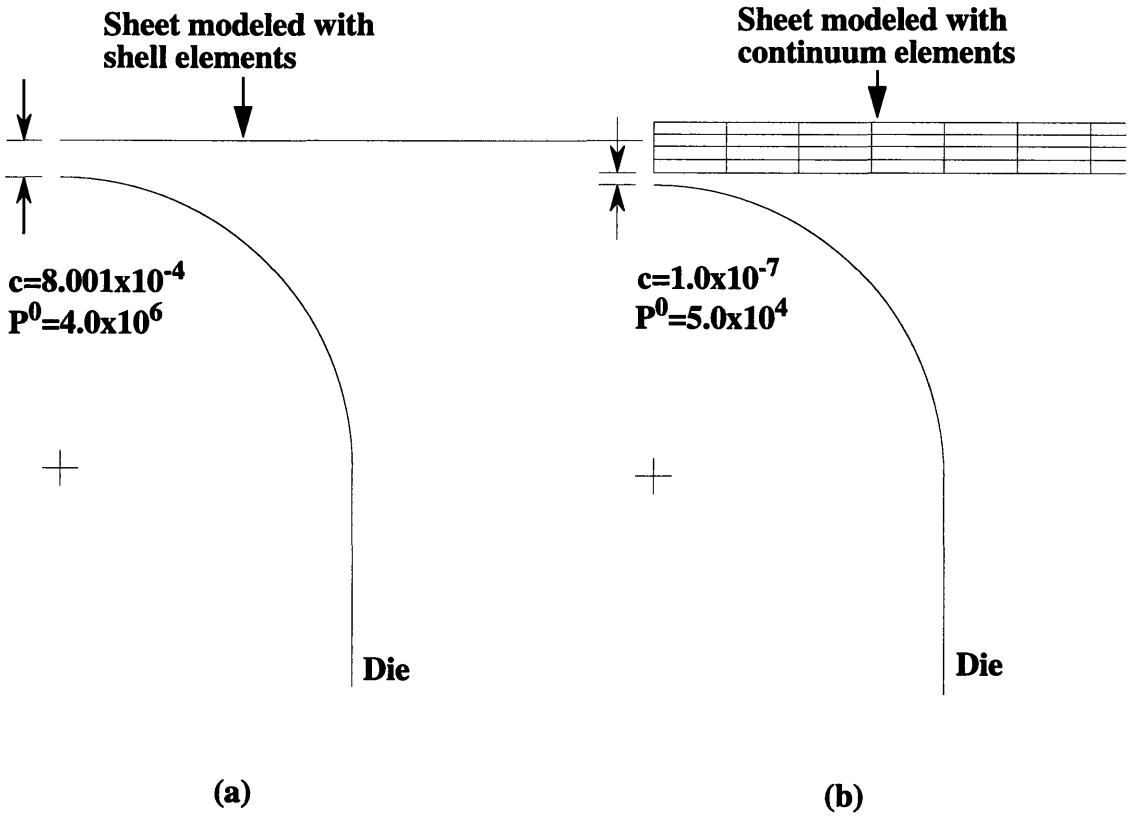

Figure 2.7: Differences in modeling contact between (a) shell elements and (b) continuum elements

Taking advantage of the symmetry of the problem, half of the sheet was modeled. The purpose was to reduce the problem size in terms of memory storage and CPU time. Figure 2.8 illustrates the model of half of the sheet using plane strain continuum elements after it was formed over a die. It should also be noted that the mesh in the region near the center of the die is much more refined than those at the gripping end of the sheet. This is to ensure that correct curvature of the part is obtained during simulations. In order to observe the effect of friction at the sheet-die interface, the sheet was modeled such that the mesh of

the bottom half of the sheet near the die was more refined, as shown in Figure 2.8. Furthermore, the modeling of the sheet has also taken into account the effects of aspect ratio of the continuum elements, the topic which will be discussed in more details in the Appendix B.

When shell elements were used, the model of the sheet was further simplified to a 1/4-inch strip by imposing plane strain constraints on its edges. The plane strain constraints impose a symmetry about the y-axis or the centerline of the sheet. Equivalently, this means that, for both edges of the sheet, the displacement u_y and the rotations about the x- and z-axes are fixed ($u_y = \phi_x = \phi_z = 0$). A three-dimensional view and a side view of the model of the sheet using shell elements are shown in Figures 2.9 (a) and (b), respectively. Similar to the plane strain continuum element model, the mesh of the shell element model was also more refined at the region near the center of the die. As for the refinement in the thickness direction of shell elements, ABAQUS allows users to specify the number of section points through the sheet thickness, which is used to calculate the shell section behavior. Increasing the number of section points would produce more accurate results for nonlinear or complex problems. This is equivalent to refining the mesh in the thickness direction for the case of using plane strain continuum elements. In this particular study, the number of section points through the thickness of shell elements varied from five, ABAQUS default value, to eleven section points. In addition, a composite layer type of shell elements was utilized. Composite shells effectively allow the user to vary the thickness, number of integration points, material, and orientation for each layer of the composite shells. In this particular model, a two-layer composite shell, of which the thickness of the layer near the die was a quarter of the thickness of the sheet, was considered. This made the localization of the section points near the die possible. Consequently, the use of composite shell elements helped to ascertain the presence of any shear boundary layer effect from friction.

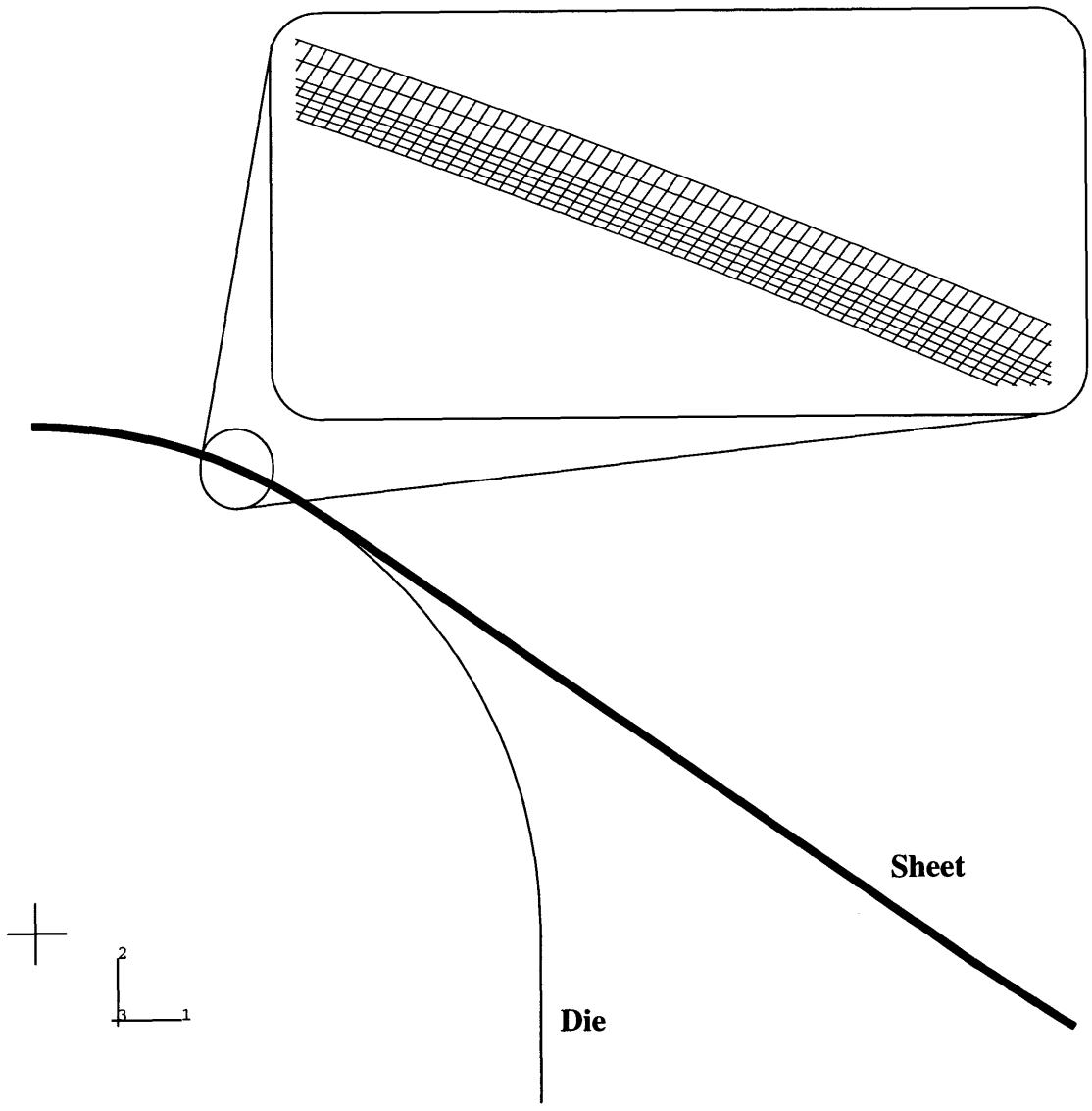

Figure 2.8: Plane Strain Continuum element model of the sheet forming over the die.

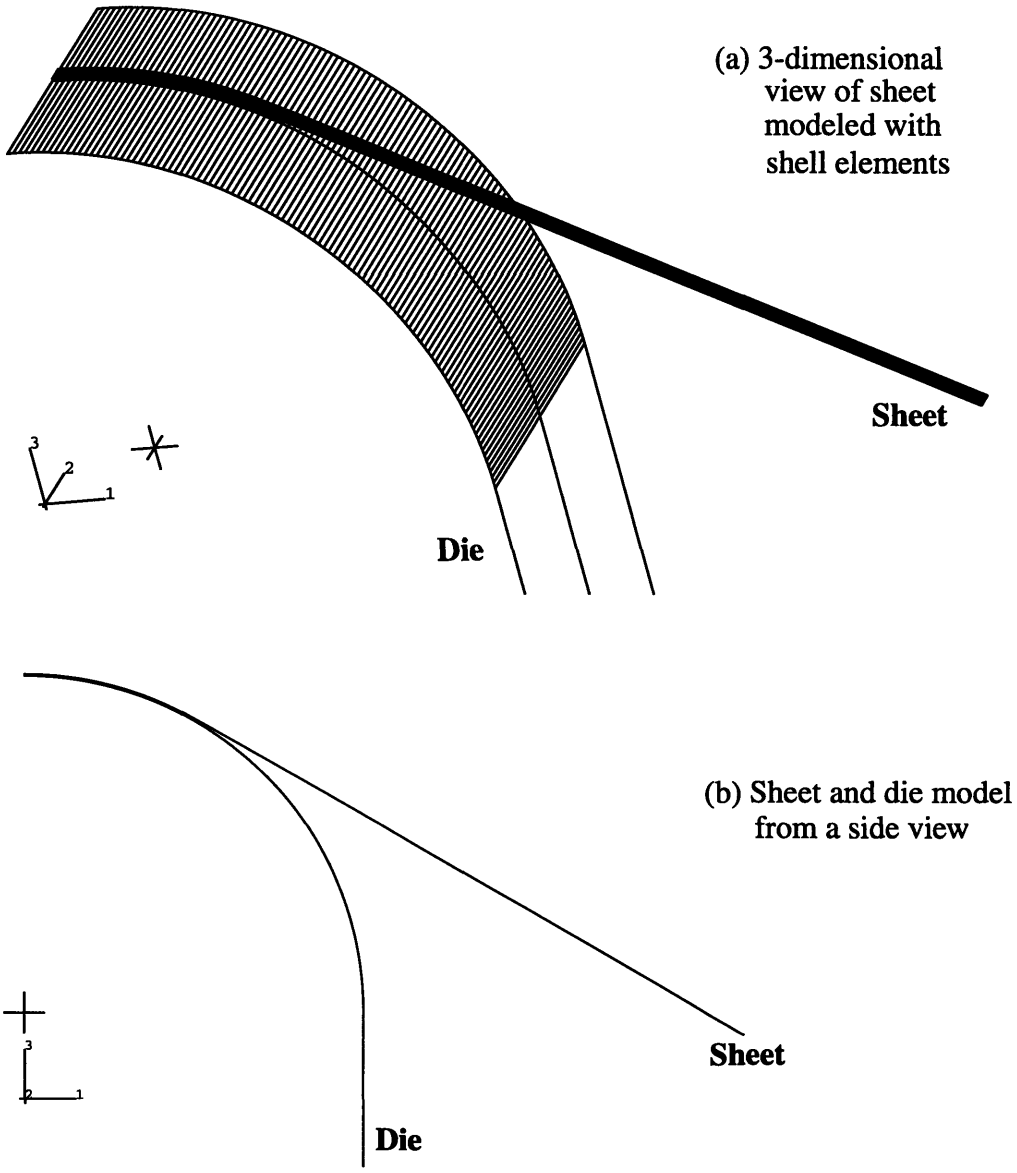

Figure 2.9: (a) 3-D view; (b) Side view of the Shell element model of the sheet.

2.3.2 Results From The Simulations of The Stretch Forming Process

In this section, some of the simulation results for the stretch forming process will be shown. The outline of the presentation of the results will be in the order of the process itself: pre-stretching, wrapping, post-stretching, and, finally, unloading. The distributions through the sheet thickness for the in-plane normal stress σ_{xx} (also referred to as σ_{11}) and the normal strain ε_{xx} (ε_{11}) in each stage of the process are considered. The results shown

in this section were taken from the simulations using shell elements of five section points only. The results from the other simulations using different types of elements and their comparisons will be shown and discussed in the next section.

The simulation results shown here are taken from a region along the sheet which contacts the die during wrap. This region is depicted in Figure 2.15. The first step of the simulation corresponds to the pre-stretching of the sheet. When the sheet is pre-stretched, the stretching force simply produces the constant tensile stresses in the sheet as shown in Figure 2.10 (a). The corresponding normal strain distribution in the sheet is also depicted in Figure 2.10 (b), which follows the material constitutive law relating stress and strain.

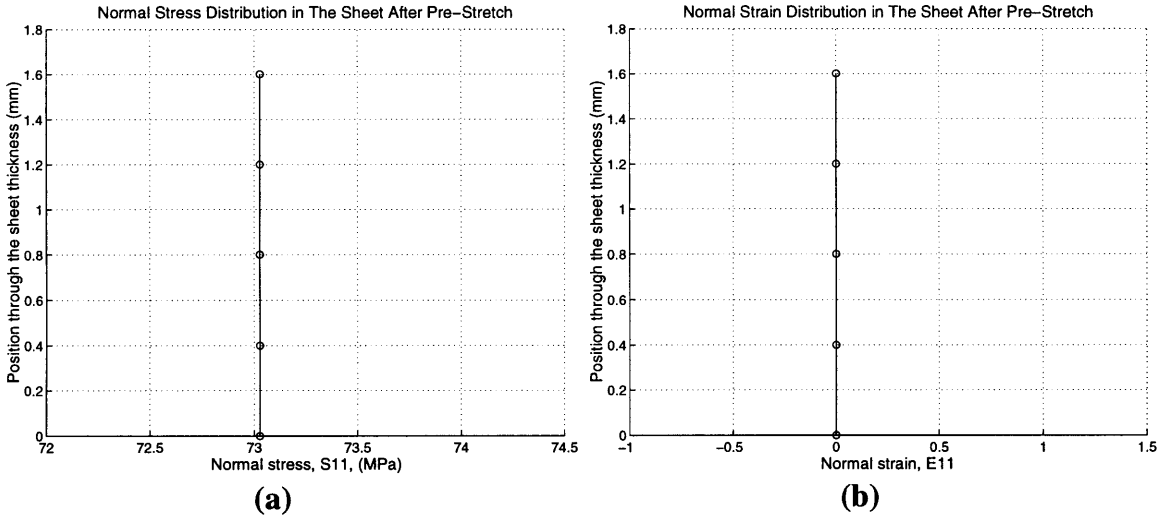

Figure 2.10: (a) Normal stress distribution σ_{11};(b) normal strain distribution ε_{11} in the sheet after pre-stretch.

After the pre-stretching is completed, the sheet is wrapped over a die. The wrapping step basically acts to bend the sheet. This bending stress depends on the cross section of the sheet, the radius of curvature of the die, the bend angle, and the material. Since the sheet is pre-stretched prior to forming, the loaded stress distribution will not look like the one in Figure 1.8. The strain from bending or forming is essentially added to the strain due to the pre-stretching step. With numerical simulations, the stress and strain distribution in the sheet after the forming step are shown in Figures 2.11 (a) and (b), respectively.

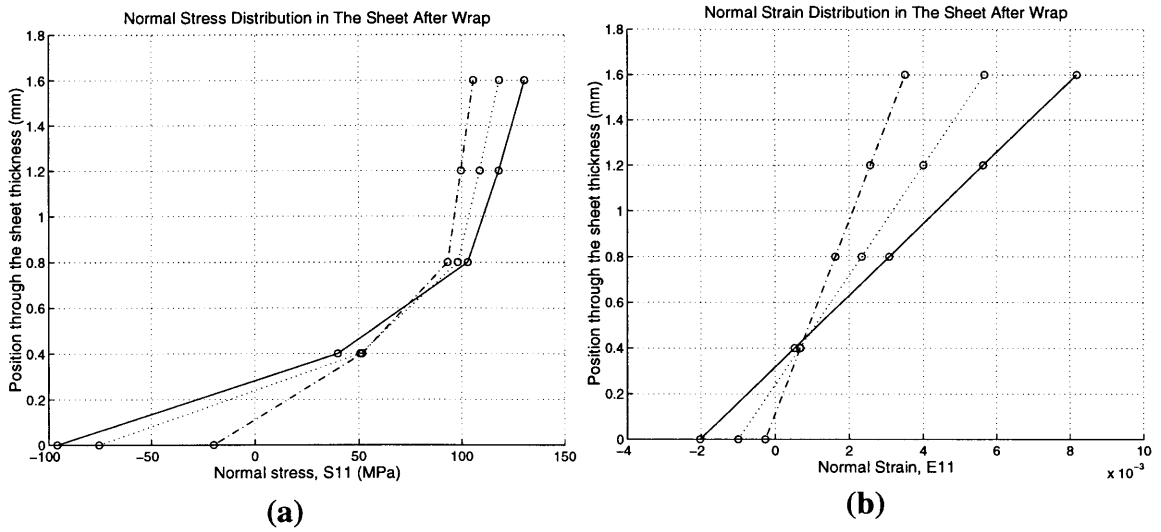

Figure 2.11: (a) Normal stress distribution σ_{11};(b) normal strain distribution ε_{11} in the sheet after wrapping or forming.

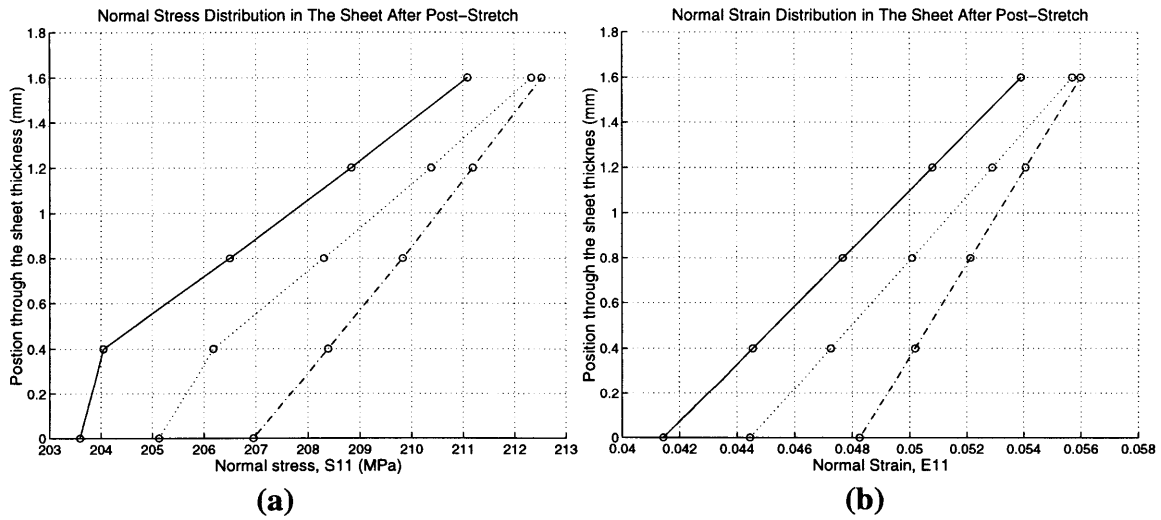

Figure 2.12: (a) Normal stress distribution σ_{11};(b) normal strain distribution ε_{11} in the sheet after post-stretch; Note that the stress varies slightly through the thickness.

The post-stretching of the sheet after wrapping is usually implemented in the manufacturing process of the aircraft sheet components. This step is included to reduce the amount of springback in the sheet. The post-stretching adds a constant tensile stress to the sheet, which, if done properly, would wipe out the stress distribution through the thickness (making the stress through the thickness constant) and thus eliminate any bending moment. This essentially means that when the sheet is unloaded, there would be no springback

associated with moment recovery which is the major aspect of the part shape change in unloading. Figures 2.12 (a) and (b) depict the simulation results on the stress and its corresponding strain distribution in the sheet after post-stretch.

The final step in the simulation is the unloading step, in which the sheet is released from the gripper and is allowed to springback. It is equivalent to, in the simulations, eliminating all contact and allowing the sheet to ramp to equilibrium. The simulation results, shown in Figures 2.13 (a) and (b) show the stress and strain distributions after the sheet was unloaded and reached equilibrium. It should be noted that the stress distribution after unloading has a typical characteristic of the residual stress and that the residual stress in the sheet, in this particular case, is practically zero.

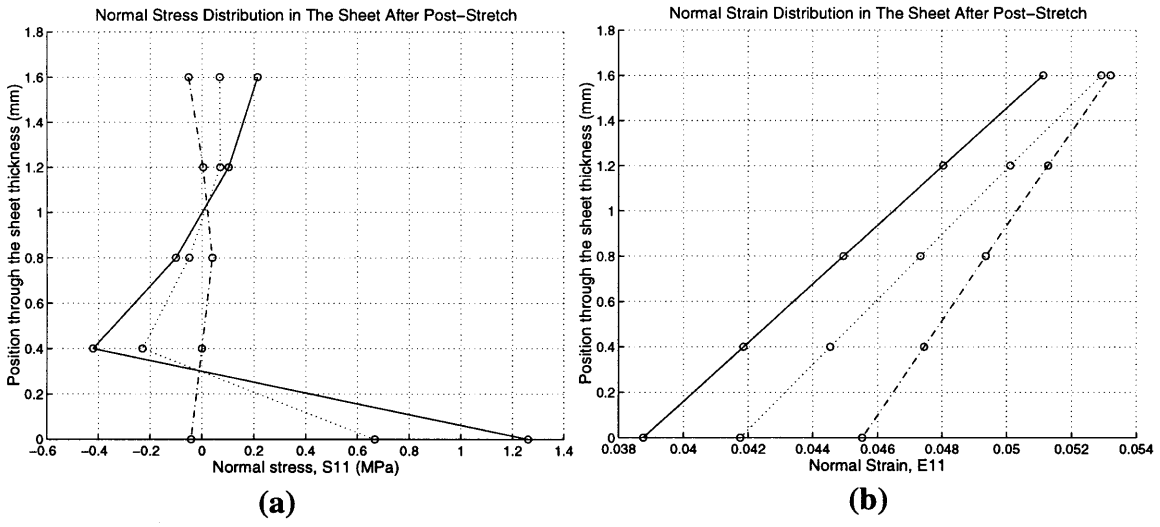

Figure 2.13: (a) Normal stress distribution σ_{11};(b) normal strain distribution ε_{11} in the sheet after final unloading from wrap and post-stretch.

After examining the stress and strain distribution in the sheet during each step of the process, it is imperative that the part configurations during loaded and unloaded stage are considered. Figure 2.14 depicts the loaded shape after wrap as compared to the unloaded shape. It is apparent, from the illustration in Figure 2.14, that the change of the part shape or the springback of the sheet is quite small. This is mainly due to the presence of a post-stretch in the overall stretch forming process. As discussed earlier, post-stretching tends to wipe out any residual stresses and make the stress distribution constant, hence resulting in zero moment, which significantly reduces any springback in the part.

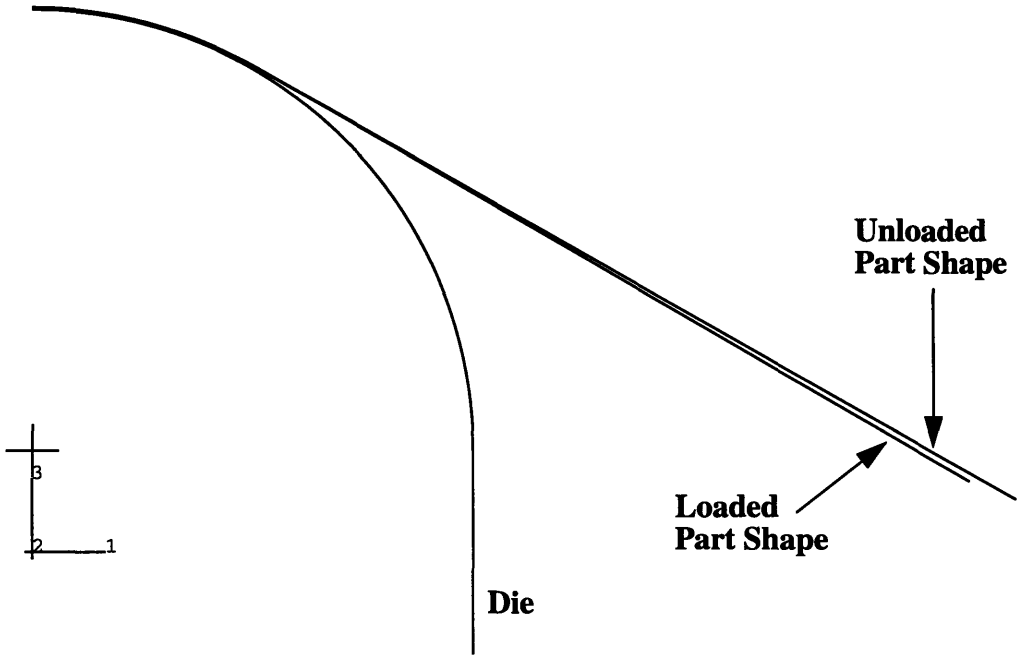

Figure 2.14: Comparison between a loaded shape after wrapping and an unloaded shape.

2.3.3 Comparison and Analysis of Simulation Results

In order to understand the effect of friction at the sheet-die interface, a number of cases were simulated. Different types of elements and two values of friction coefficients were used such that the stress distribution through the thickness of the sheet from each simulation could be compared with others. Because friction mostly exhibited significant effect during post-stretching, much of the analysis and comparison of results focused on what happened to the sheet during and after post-stretching. Moreover, the area of the sheet, in which the effect of friction was most apparent, was at the end of the contact area between the sheet and the die. In this region, there were considerable shear tractions and interactions between the sheet and the die due to friction. This area is indicated in a circle in Figure 2.15. Most of the results used in the comparison and analysis of different cases of simulations would be from the end of post-stretch and from different locations along the sheet within the area of interest circled in Figure 2.15.

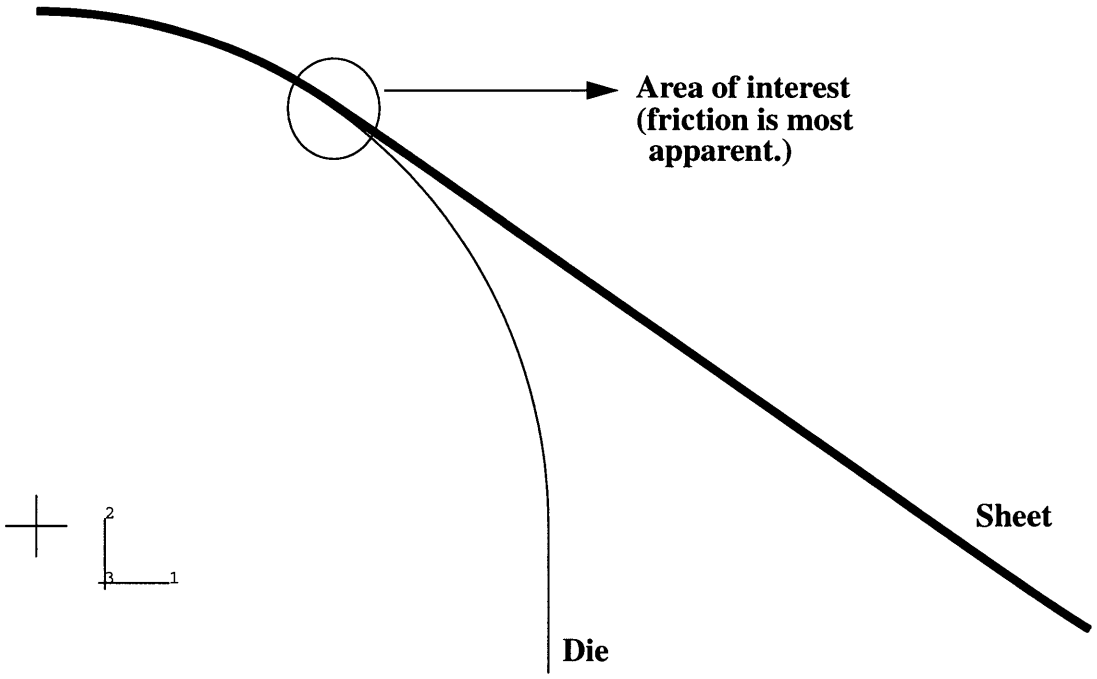

Figure 2.15: Area of the sheet where the effect of friction is most apparent.

In order to determine whether friction produces any shear boundary layer effect on the stress distribution through the sheet thickness, simulation results from the two cases of no friction and friction coefficient of 0.2 for both 1st- and 2nd-order plane strain continuum elements are compared and shown in Figure 2.16. From the comparison of the stress distributions between the case modeled with and without friction, the spread of stress distribution profile at different locations along the length of the sheet appears to be increased for the case of modeling with a friction coefficient of 0.2. It seems as though the effect of friction is only manifested in reducing the amount of axial force transmitted along the length of the sheet and does not impose any shear boundary layer. This hypothesis became even more conclusive when one considered the contour plot of normal stress, σ_{11}, in the sheet, after post-stretch, modeled by plane strain continuum elements, as shown in Figure 2.17.

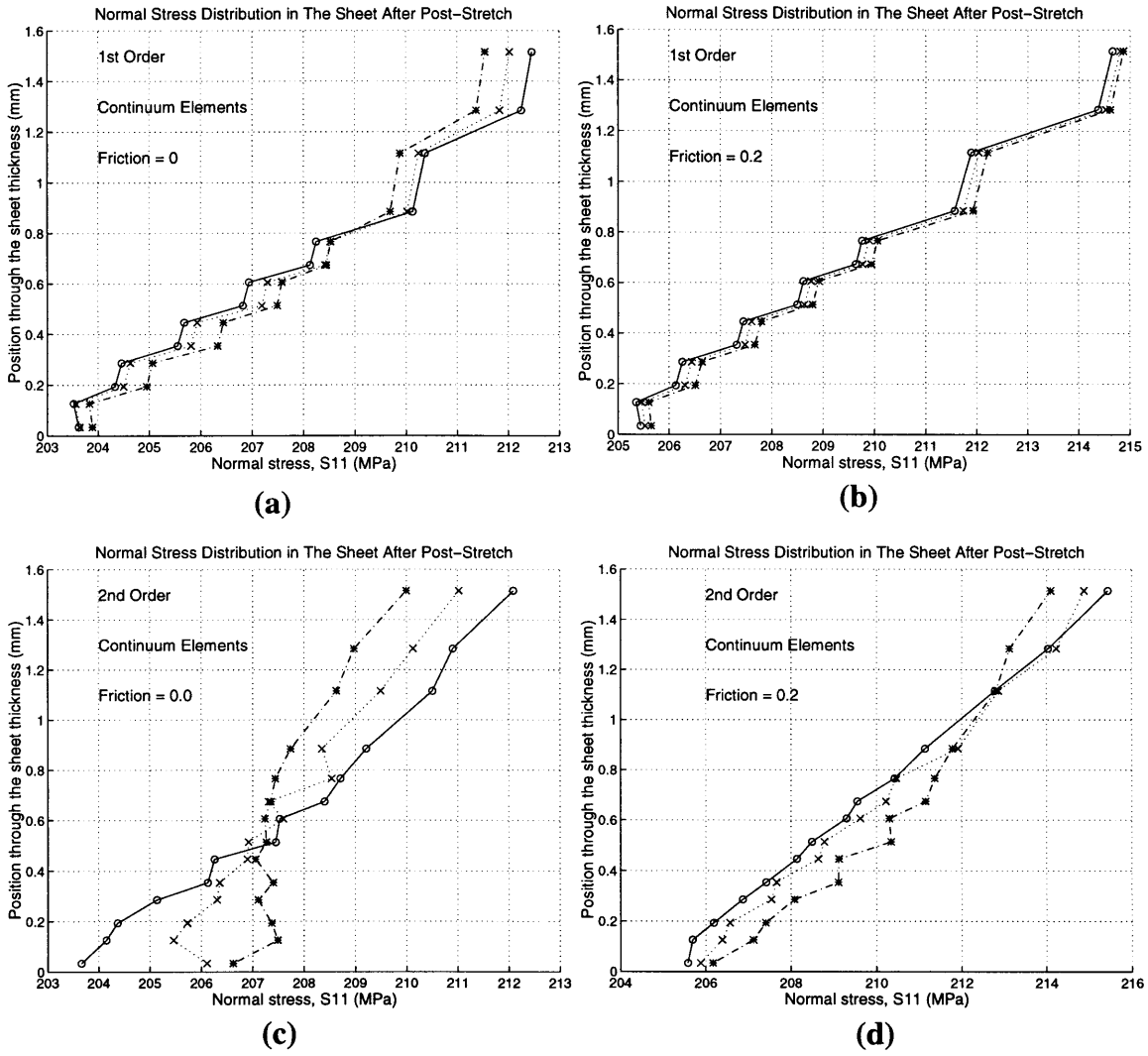

Figure 2.16: Stress distribution in the sheet after post-stretch for different cases of simulations using: (a) 1st-order plane strain continuum elements, $\mu = 0.0$; (b) 1st-order plane strain continuum elements, $\mu = 0.2$; (c) 2nd-order plane strain continuum elements, $\mu = 0.0$; (d) 2nd-order plane strain continuum elements, $\mu = 0.2$.

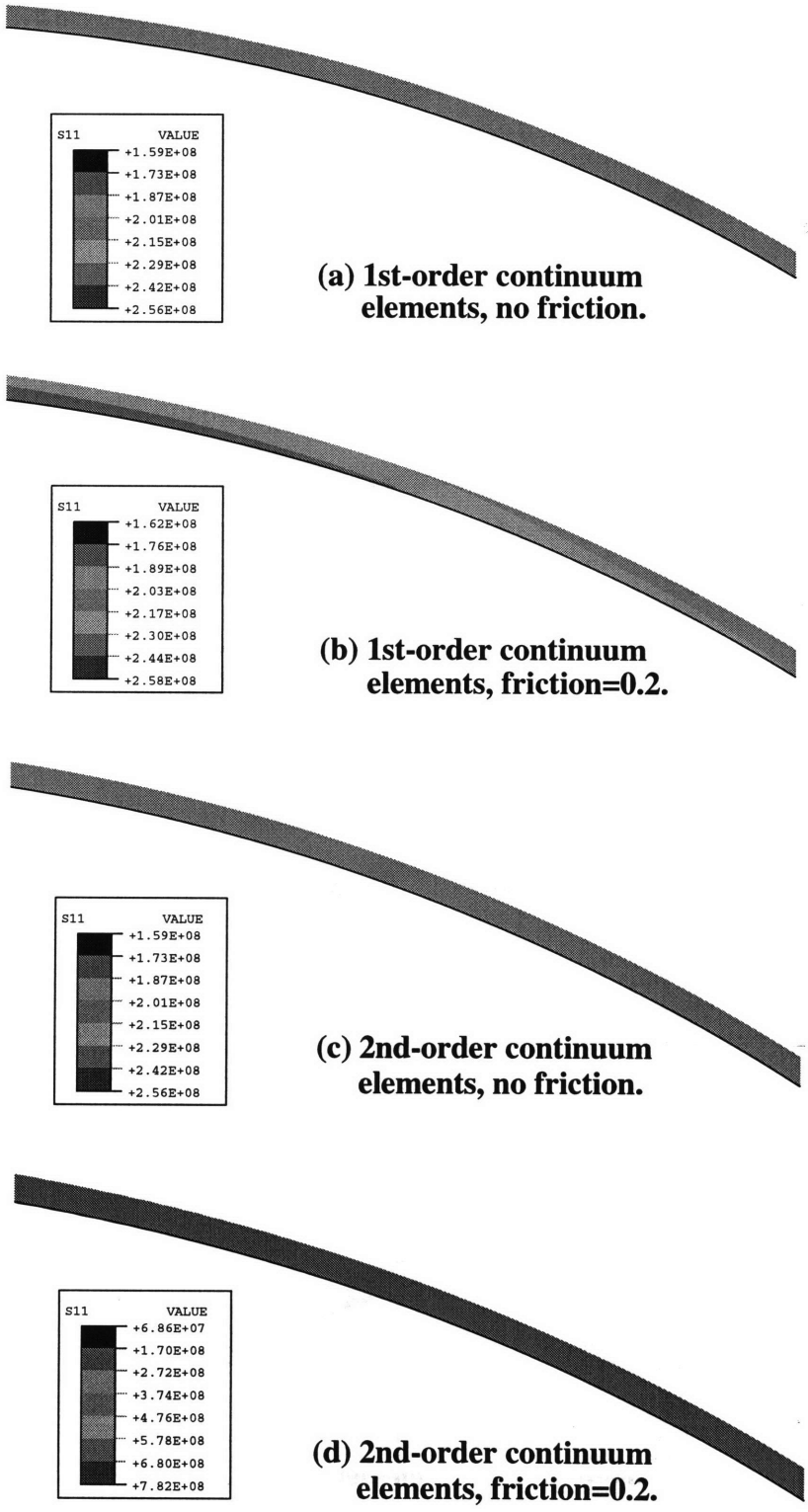

Figure 2.17: Contour plots of σ_{11} after post-stretch in the sheet modeling with 1st- and 2nd-order plane strain continuum elements. (a) and (c) simulated with no friction; (b) and (d) simulated with friction (μ=0.2).

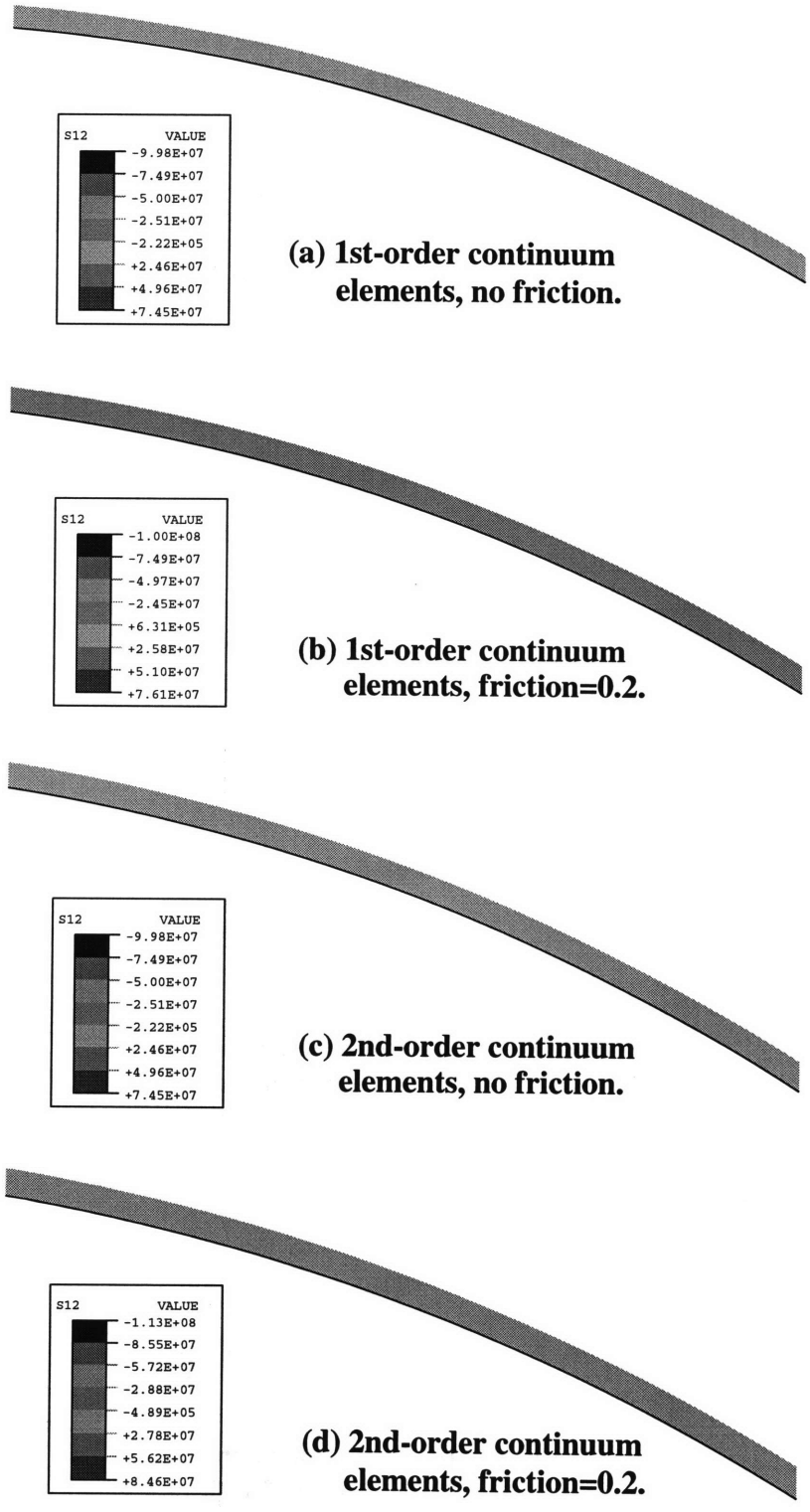

Figure 2.18: Contour plots of the shear stress (σ_{12}) after post-stretch in the sheet modeling with 1st- and 2nd-order plane strain continuum elements. (a) and (c) simulated with no friction; (b) and (d) simulated with friction (μ=0.2).

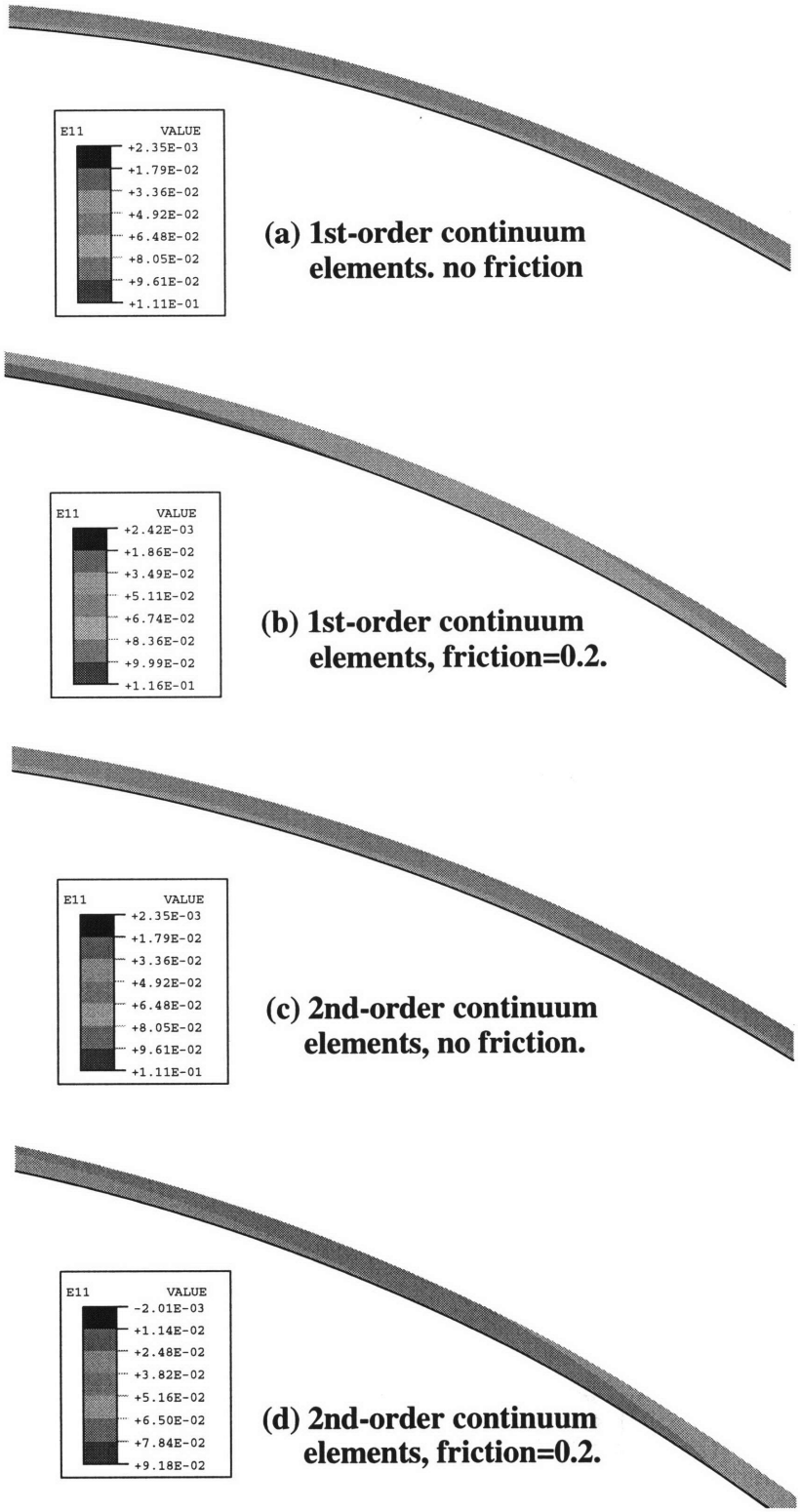

Figure 2.19: Contour plots of post-stretch membrane strain, ε_{11}, in the sheet modeling with 1st- and 2nd-order plane strain continuum elements. (a) and (c) simulated with no friction; (b) and (d) simulated with friction (μ=0.2).

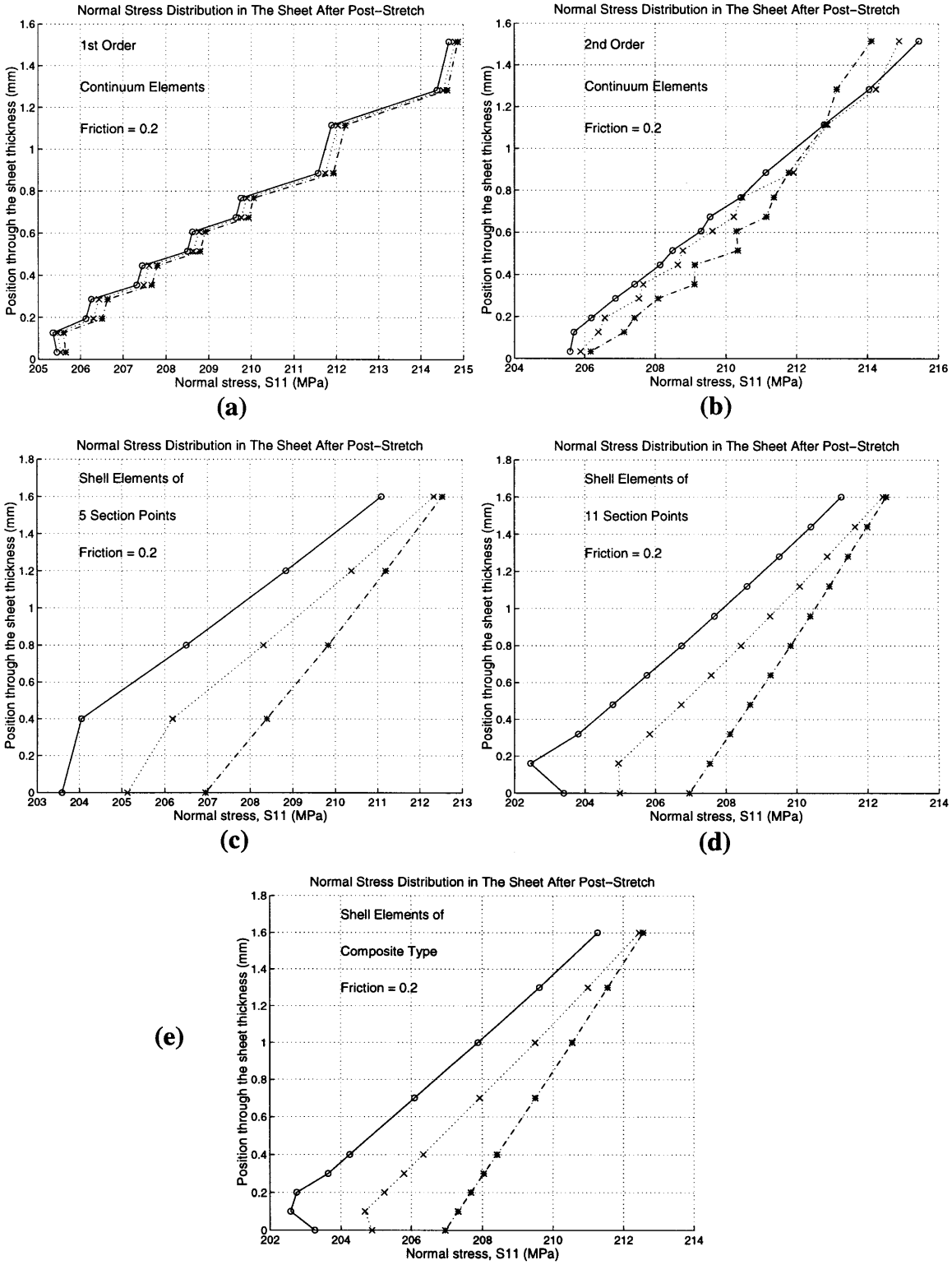

Figure 2.20: Comparison between continuum and shell elements: (a) 1st-order plane strain continuum elements, $\mu = 0.2$; (b) 2nd-order plane strain continuum elements, $\mu = 0.2$; (c) shell elements of 5 section points, $\mu = 0.2$; (d) shell elements of 11 section points, $\mu = 0.2$; (e) shell elements of composite type, $\mu = 0.2$.

The plots of the shear stress (σ_{12}) distributions in the sheet also confirm a negligible presence of shear stress (σ_{12}) found in each of the plane strain continuum element case. Furthermore, the effect of friction is visible in the variation of the post-stretch membrane strain, ε_{11}, from approximately 0.5% to 0.4% as the position is moved toward the center of the die. (see Figure 2.19) Evidently, these results indicate that friction does not produce any significant shear boundary layer effect on the stress distribution through the sheet thickness. Rather, the effect of friction is perceived as hindering post-stretching along the length, thus resulting in a post-stretch gradient.

When the result obtained from a simulation using plane strain continuum elements, shown in Figures 2.20 (a) and (b), is compared to those using shell elements, shown in Figures 2.20 (c) through (e), it can be seen that plane strain continuum elements produced stress distribution profiles through the sheet thickness similar to those obtained using shell elements. Plane strain continuum elements also predict a linear strain distribution supporting the shell element assumptions, i.e. no significant effects from shear are apparent in the strain. The level of shear stress due to friction computed using the plane strain continuum elements is found to be quite negligible and very small compared to the other stress levels, as already illustrated in Figure 2.18. Figure 2.21 compares the level of shear stress (σ_{12}) in the sheet after post-stretch as obtained from using shell elements and that obtained from using continuum elements, in the case where friction is present at the sheet-die interface.

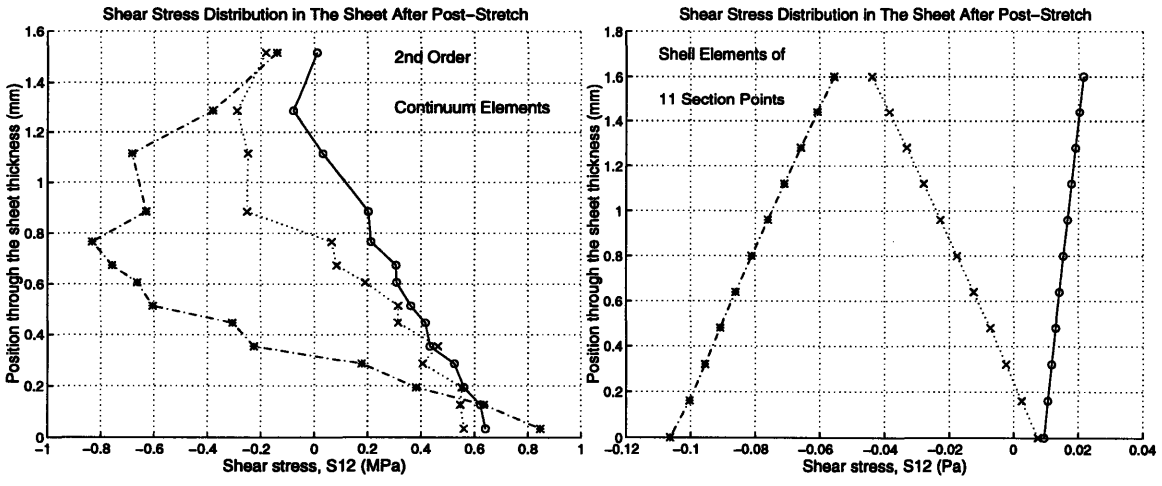

Figure 2.21: Comparison of shear stress (σ_{12}) distribution between continuum and shell elements.

The only subtle difference between using continuum versus shell elements is that the plane strain continuum elements does not display the reversal in stress distribution near the die, as observed in shell elements. The reason for this subtlety is to be found in minor geometric modeling differences between the two cases. It was mentioned earlier in this chapter about the differences between the model of the sheet using shell elements versus using continuum elements; shell elements model the entire sheet as a curved shell having "zero" thickness while continuum elements model the entire cross section of the sheet. (See Figures 2.8 and 2.9) This modeling scheme, in essence, affects the bending radius of the sheet. In other words, when the continuum elements are used, the bending radius is basically the radius of the die, R_{die}. However, when shell elements are used, the bending radius is shifted by an amount equal to one-half the sheet thickness because of how the sheet is modeled. Therefore, the actual bending radius for the sheet modeled with shell elements is $R_{die} + \frac{t}{2}$. This subtle difference in the modeling of the sheet is depicted in Figure 2.22.

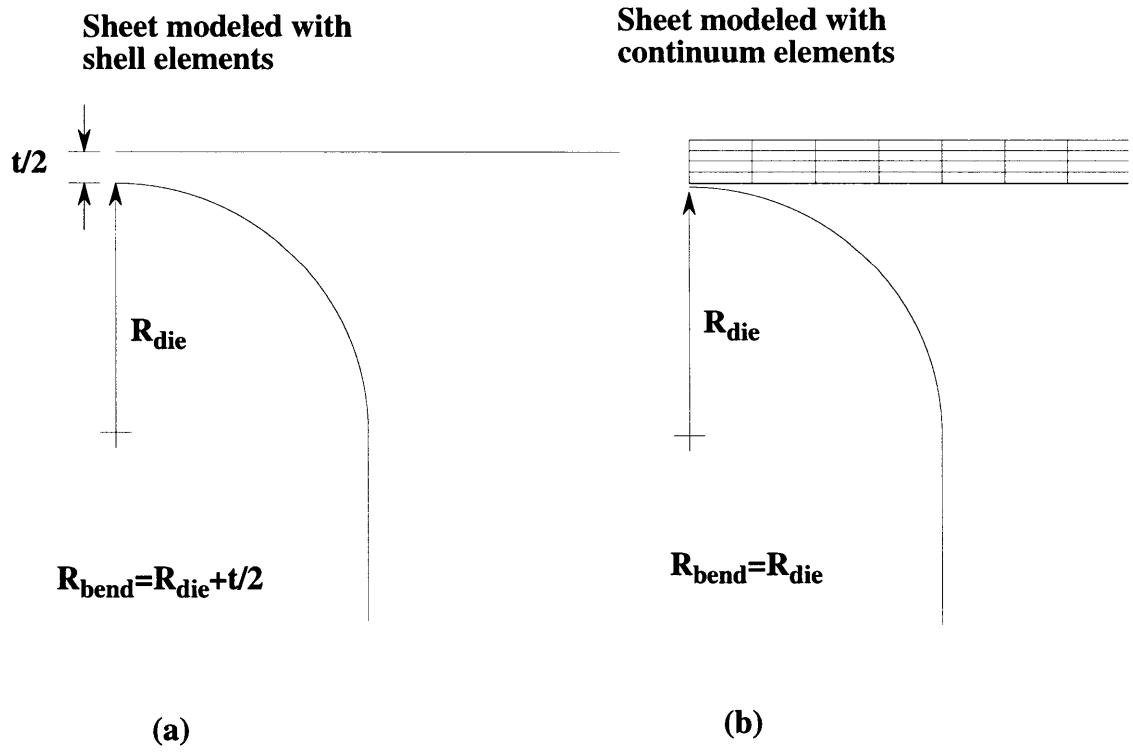

Figure 2.22: A slight distinction in bending radii when different types of elements are used.

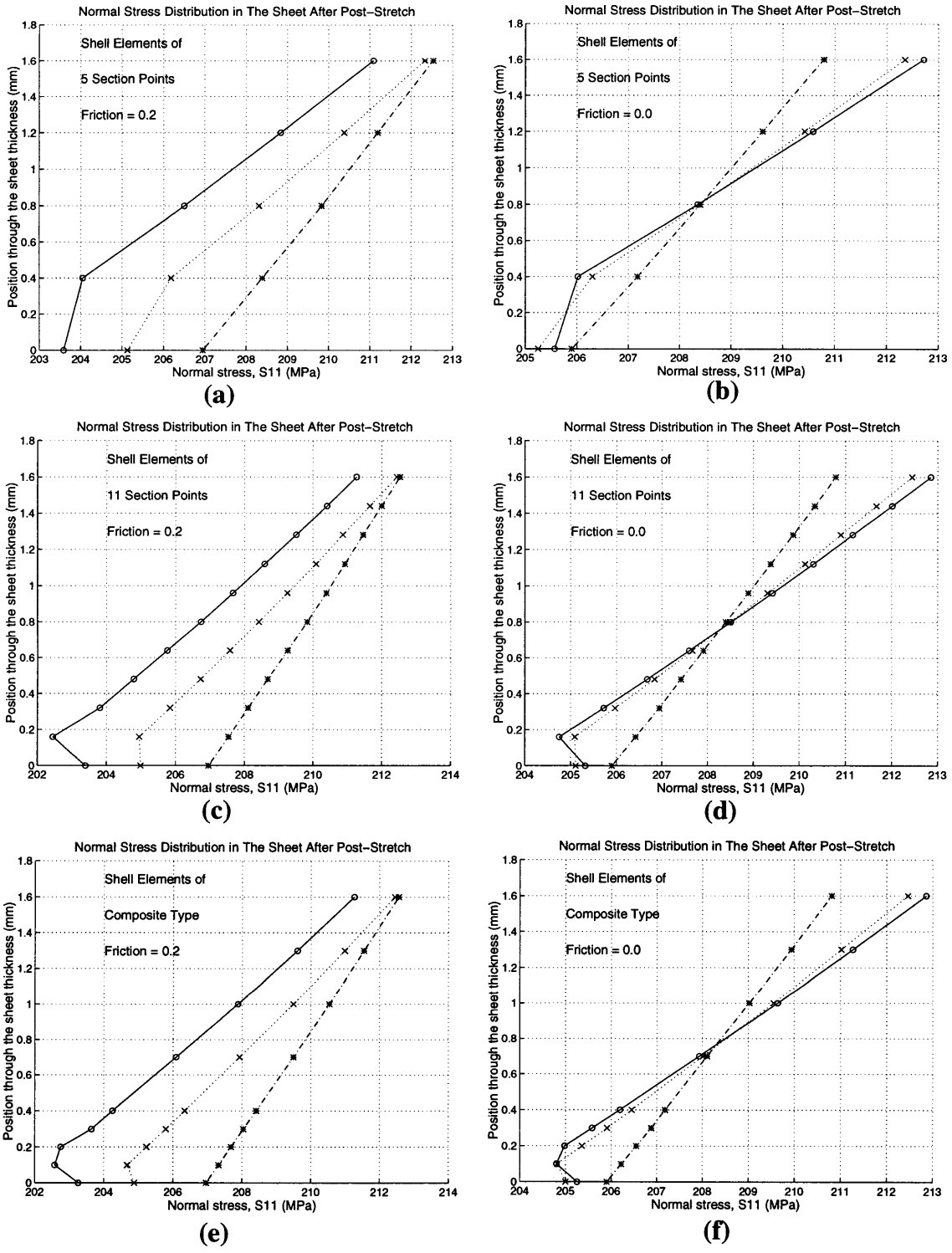

Figure 2.23: Comparison of stress distribution in the sheet after post-stretch between different cases of shell elements: (a) shell elements of 5 section points, μ=0.2; (b) shell elements of 5 section points, μ=0.0; (c) shell elements of 11 section points, μ=0.2; (d) shell elements of 11 section points, μ=0.0; (e) shell elements of composite type, μ=0.2; (f) shell elements of composite type, μ=0.0.

Results from simulations of various cases of shell elements are illustrated in Figures 2.23 (a) through (c), which correspond to the case of using shell elements of five section points, eleven section points, and composite type, respectively. A comparison of stress distributions for these three cases shows that when the number of section points through the thickness is increased (i.e. from five to eleven section points) or is localized in a small region through the use of composite-type shells, shell elements are able to acquire more details and smoother distributions in that region. Furthermore, it is obvious from this comparison that shell elements with higher number of section points through the thickness will predict a more accurate stress distribution in the sheet, and, therefore, will produce more accurate results. Even when shell elements of a high number of section points or with a localization of section points near the die are used, no dramatic difference in the characteristics of the stress distribution is observed, which implies that no boundary layer effect from friction is apparent.

Table 2.2 lists the total computational (CPU) time required to complete the simulation in different cases. The CPU time showed in this table is based on the computer time used to perform these simulations on a Hewlett-Packard computer HP-735 model, which has the clock speed of about 135 MHz. From these data, it is apparent that the simulation with the plane strain continuum models required an exceedingly large amount of CPU time to complete. The simulations with shell elements modeling, on the other hand, are much less expensive in terms of the computing time and memory required. Not only is it less computationally expensive than continuum element, but shell element also produces more accurate results, according to the simulations. In general, the case with a higher friction coefficient needed a little more CPU time than the case with zero friction. However, this distinction is quite negligible. As the number of section points of shell elements is increased, a higher CPU time is required, though, by a small amount. This suggests that a higher level of accuracy of the results can be obtained from shell elements by simply increasing the number of section through the thickness, without sacrificing a large amount of CPU time. It is interesting, however, to observe that shell elements of composite type, which produce a smoother result in stress distributions, seem to use less CPU time than the other cases of shell elements.

Type of Elements Used In Simulation	μ	Total CPU Time
1st-order Plane Strain Continuum Elements	0.0	36,339 sec
1st-order Plane Strain Continuum Elements	0.2	38,493 sec
2nd order Plane Strain Continuum Elements	0.0	72,848 sec
2nd-Order Plane Strain Continuum Elements	0.2	72,953 sec
Shell Elements of 5 Section Points	0.0	466 sec
Shell Elements of 5 Section Points	0.2	467 sec
Shell Elements of 11 Section Points	0.0	483 sec
Shell Elements of 11 Section Points	0.2	509 sec
Shell Elements of Composite Type	0.0	433 sec
Shell Elements of Composite Type	0.2	432 sec

Table 2.2: Comparison of CPU time in different cases of simulations

Chapter 3

Simulations of The Chemical Milling Process

The fundamental concept of the chemical milling process is the aspect of the removal of material from a structure or a part by way of chemical reactions. The chemical milling process differs from other traditional material removal processes such as machining or grinding in that there is zero cutting force in the chemical milling process. Therefore, in order to effectively model the chemical milling process, it is necessary that the finite element method has a capability to simulate the removal of material, hence the residual stress, from the sheet without applying any external forces to the part.

3.1 Simulation Methodology

As illustrated in the last chapter and in the Appendix B, the use of continuum elements in the chemical milling simulations is eliminated due to the inefficiency and impracticality of the number of elements required to model the sheet, as well as the inaccuracy of the results produced when elements with large aspect ratio are used. The focus is, therefore, shifted to using shell elements (ABAQUS type S4R) to model this material removal process. When shell elements are used in the chemical milling simulation, a portion of the thickness of each shell element must be removed; therefore entire elements cannot be removed as is possible when using continuum elements. Instead, an alternative material removal algorithm must be developed.

To simulate the chemical milling process, one is required to understand two fundamental concepts: first, the chemical milling process is a material removal process and any changes occurring to the part are due to the change in the internal residual stresses in the part; and, second, the formulation of shell elements of ABAQUS type S4R is such that the stress distribution is described by providing the stress at a number of discreet integration points through the thickness of the shell. Recognizing these two concepts, the simulation must ensure that an accurate residual stress distribution in the part is attainable after forming but before chemical milling. Moreover, the specific location of through thickness integration points of a shell element will be modified when the thickness is changed as a result

of material removal from chemical milling. Therefore, the simulation of chemical milling will first require the stress state through the thickness to be transformed from a discreet representation at specific integration points through the thickness to a continuous function representation through the thickness; that portion of the thickness to be chemical milled is then removed; the stress distribution through the remaining thickness is then transformed to the integration points of a shell element of the new chemical milled thickness. This procedure can be numerically facilitated in the commercial code ABAQUS via the use of "user subroutines" as described later.

The simulation of the entire process consists of the forming simulation and the chemical milling simulation. Initially, the stretch forming process is simulated so that the residual stresses in the unloaded part before chemical milling can be evaluated. After the forming simulation is completed, the data of stresses and nodal coordinates of the unloaded sheet is obtained from a simple FORTRAN program or an ABAQUS Post Output option. This procedure is represented in a schematic shown in Figure 3.1.

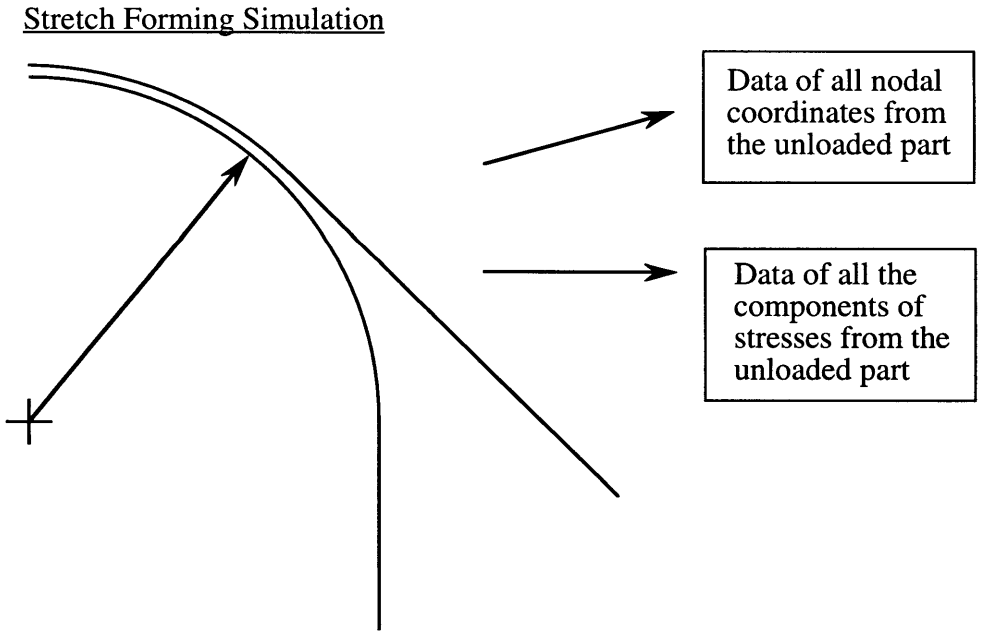

Figure 3.1: Schematic of data obtained from a forming simulation.

The chemical milling simulation then begins by generating the unloaded shape of the sheet as a starting geometry and imposing the residual stresses in the sheet. At this point, the reduced shell thickness is incorporated to selected regions of the sheet according to the

chemical milling specifications. The imposition of residual stresses is achieved by the SIGINI user subroutine. The user subroutine SIGINI allows the user to impose a residual stress distribution. The user subroutine SIGINI acts to assign the residual stress data from the unloaded state of the forming simulation to all elements and element section points.

Since, in the chemical milled sections, the thickness of the sheet changed, finite element section points in the non-chemical milled sections will be at different locations from the chemical milled sections. Therefore, for each chemical milled element, the residual stress distribution is modified to account for the removal of material thickness. This modification or mapping of the residual stress distribution in the chemical milled sections is accomplished through a curve fit of data. This curve fitting algorithm, which must be done with care, is illustrated in Figure 3.2. A curve fit with piece-wise linear interpolation is chosen for all the chemical milling simulations.

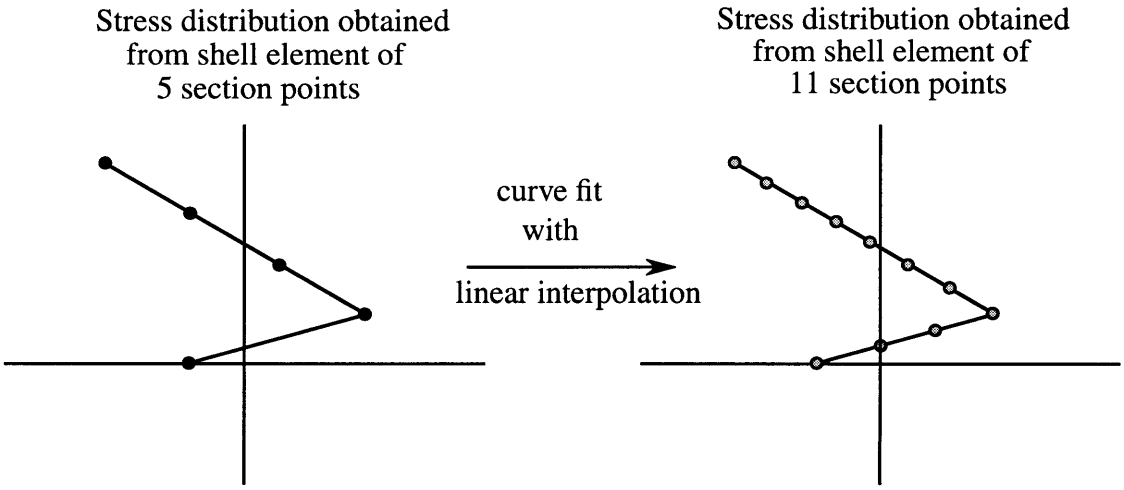

Figure 3.2: Illustration of linear interpolation curve fitting of residual stress distribution in the chemical milled section of the sheet.

Furthermore, only certain regions or pockets are removed from most of the parts. It is, therefore, necessary to distinguish chemical milled elements from non-chemical milled elements; a curve fit of "initial" residual stress distribution (i.e. prior to re-equilibration) is required for the chemical milled elements while no changes in the mapping of residual stress distribution are needed for the non-chemical milled elements. The procedure for determining the elements to be chemical milled simply involves a loop to check each element against a set of chemical milled elements. When the residual stresses are imposed to

all of the elements and element section points, the sheet is then allowed to "unload" to an equilibrium configuration.

The overall schematic of the chemical milling simulation procedure is shown in Figure 3.3. It basically summarizes how the user subroutine SIGINI is used in the simulation and what exactly is done in the step of imposing residual stress distribution. For a standard industry practice, the entire chemical milling process is usually completed in a number of steps, often known as the multi-step chemical milling. The advantage of a multi-step chemical milling is the ability to provide a gradual transition in part thickness from thin to thick regions. The methodology for the chemical milling simulation presented here, when used repeatedly with slight changes in the sets of chemical milling elements and thicknesses, will produce final results for multi-step chemical milling.

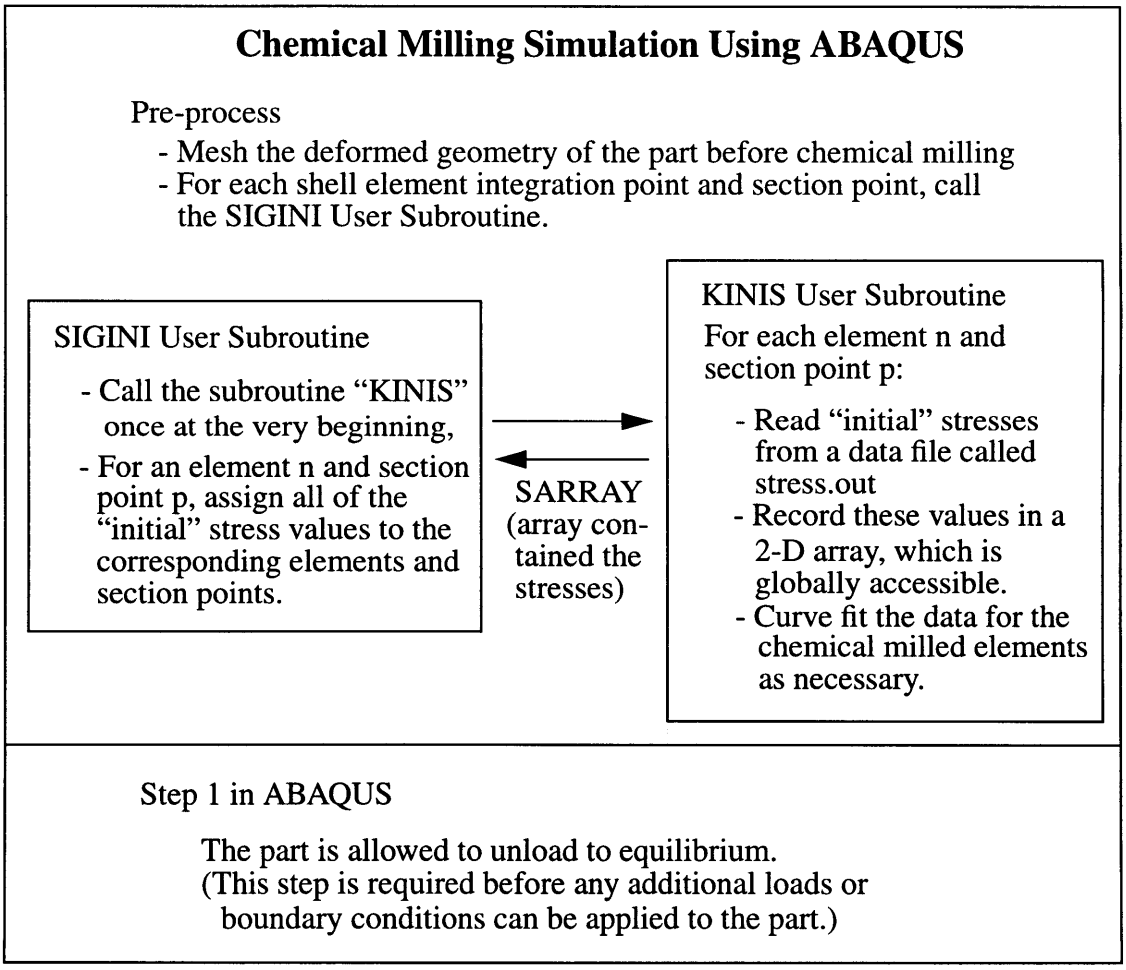

Figure 3.3: Schematic of simulation procedure using subroutine SIGINI.

3.2 Use of Shell Elements versus Continuum Elements

To ensure a viable application of the procedure to simulate the chemical milling process with shell elements, a similar preliminary study as that used in simulations with continuum elements was taken. The setup and parameters used in this simulation are the same as those presented in Appendix B. In essence, the simulation of interest was that of a strip, modeled as having an elastic-perfectly plastic material property, being formed until fully yielded and released to its unloaded configuration, after which the entire strip was chemically milled by one-half of its original thickness. In Appendix B, continuum elements were used to model the strip. This particular simulation, however, utilizes shell elements to model the strip. The last part of this section discusses the results from simulations using shell elements when compared to those obtained from simulations using continuum elements.

After the forming simulation is completed, values for the stress states are obtained from each shell element section point. Because much of the change in the residual stress state in the sheet occurs in the yielded region of the sheet, the analysis and the results from this simulation will, therefore, be pertained to this region. The stress distribution through the sheet thickness during loading and unloading stages before chemical milling is shown in Figure 3.4. When these simulation results are compared with those from the analytical solution as presented in Section 1.3.1, the agreement of the two results is evident. In short, shell elements already show a better predictive capability than continuum elements in the forming simulation.

As explained in the previous section, the chemical milling simulation requires some mapping of the stresses in the chemical milled section in the sheet. The simulation result of the stress distribution before and after chemical milling is shown in Figure 3.5. The 'x's designate the distribution of residual stress in the unloaded part before chemical milling. The 'o's designate the initial stresses to be mapped onto the chemically milled part, which are essentially linearly interpolated from the residual stresses in the unloaded part before chemical milling. Since, in this particular simulation, the bottom half of the sheet was removed by chemical milling, therefore, only the mapping of stresses in the top half of the sheet was necessary. When the sheet reached its equilibrium configuration after chemical

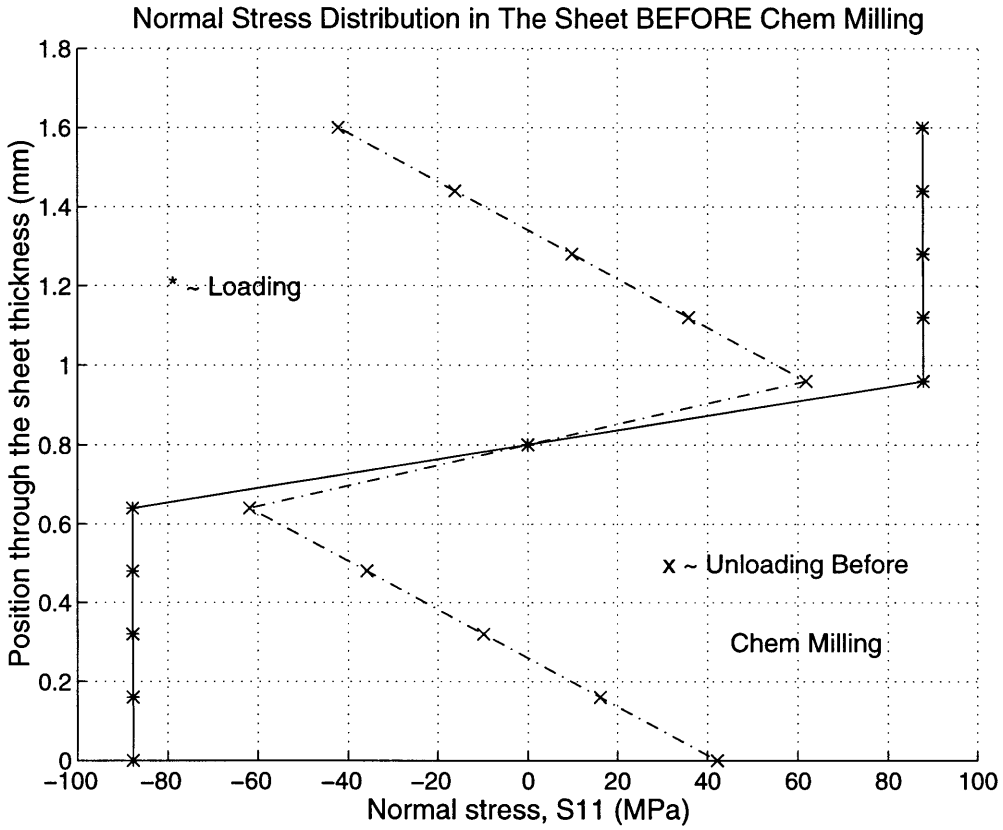

Figure 3.4: Loaded and unloaded stress distribution through the sheet thickness. (Results are taken from forming simulation using shell elements.)

milling, the residual stress distribution in the sheet is plotted and is designated by '*'s in Figure 3.5. However, this residual stress distribution after chemical milling still does not match the analytical result, which showed practically zero stress distribution in the sheet after the bottom half of the sheet was removed.

This discrepancy between the analytical solution and the result from the first attempt in simulation was found to be a result of an effect from the approximations introduced in the mapping of stresses in the region adjacent to the neutral axis. As explained in the previous section, the mapping of stresses is accomplished by a linear interpolation between stresses of two adjacent element section points. The selection of these two element section points depends solely on the position of the new element section point in the chemically milled sheet. With this rule in mind, it is clear to see that, in Figure 3.5, the mapping of stresses for the two points above the neutral axis were obtained from linearly interpolating between the values at the two innermost element section points, namely the one on the

neutral axis and another one immediately above the neutral axis. This stress distribution would be accurate only if the elastic core extends throughout this region. In other words, the mapped stress distribution implies that the elastic core of this formed sheet is in the order of 0.3 mm or about 20% of the sheet thickness. However, with the chosen material properties (E = 68.9 GPa, σ_y = 76.1 MPa) and the die radius of 5.1cm (2.0"), the elastic core can be estimated to extend for only about 0.08 mm or 5% of the sheet thickness. As a result, a more accurate estimate of stress distribution in the chemically milled part, in this particular simulation, is obtained by linearly extrapolating the stress distribution in the top portion of the sheet to the neutral axis, and neglecting the thin elastic core as indicated by 'o's in Figure 3.6.

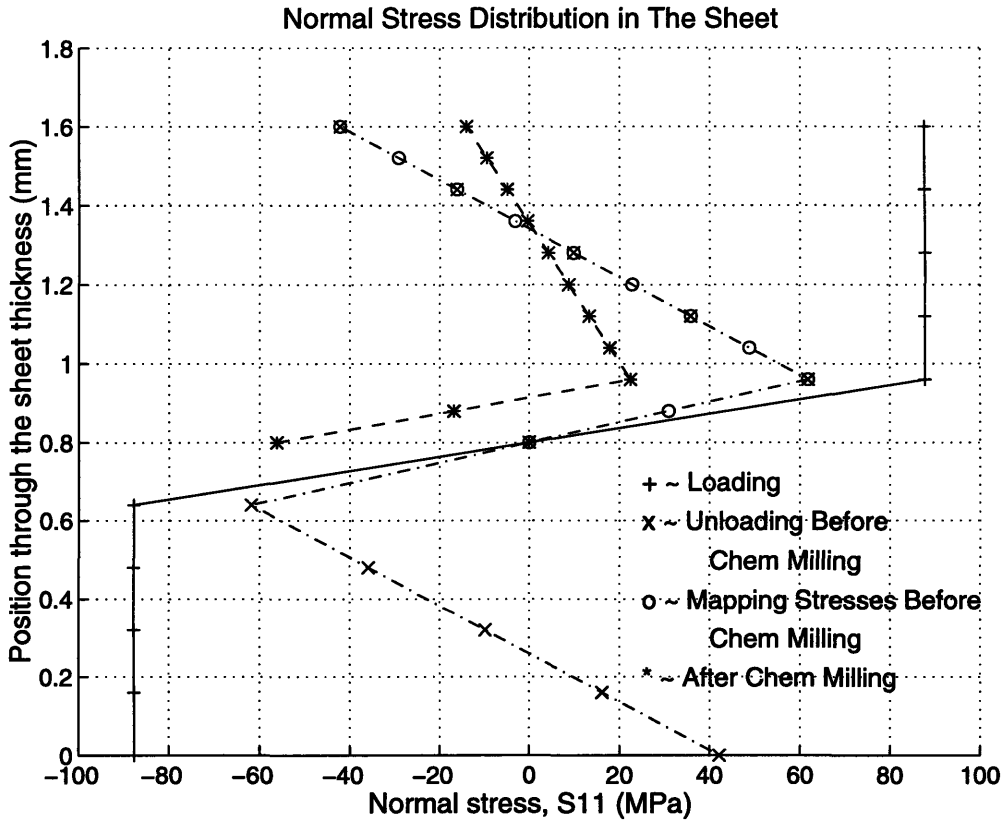

Figure 3.5: Stress distribution in the sheet BEFORE and AFTER chemical milling (1st attempt in stress mapping).

When this stress distribution with a more accurate mapping is prescribed onto the chemically milled elements and the sheet is allowed to reach its equilibrium configuration, the final residual stress distribution through the sheet thickness after chemical milling is

essentially zero. This stress distribution, as indicated by '*'s in Figure 3.6, closely matches the analytical solution presented in Section 1.3.2. The imposing of stresses in the part during chemical milling simulation not only affects the level of unloading stresses in the sheet after chemical milling, but also influences the amount of springback in the sheet as a result of chemical milling. Since the change in part curvature and configuration after chemical milling is the most critical part of the simulation, it is therefore necessary to ensure that (1) the stretch forming process produces accurate residual stress distributions in the part before chemical milling; and (2) these stresses are properly mapped onto the chemically milled elements.

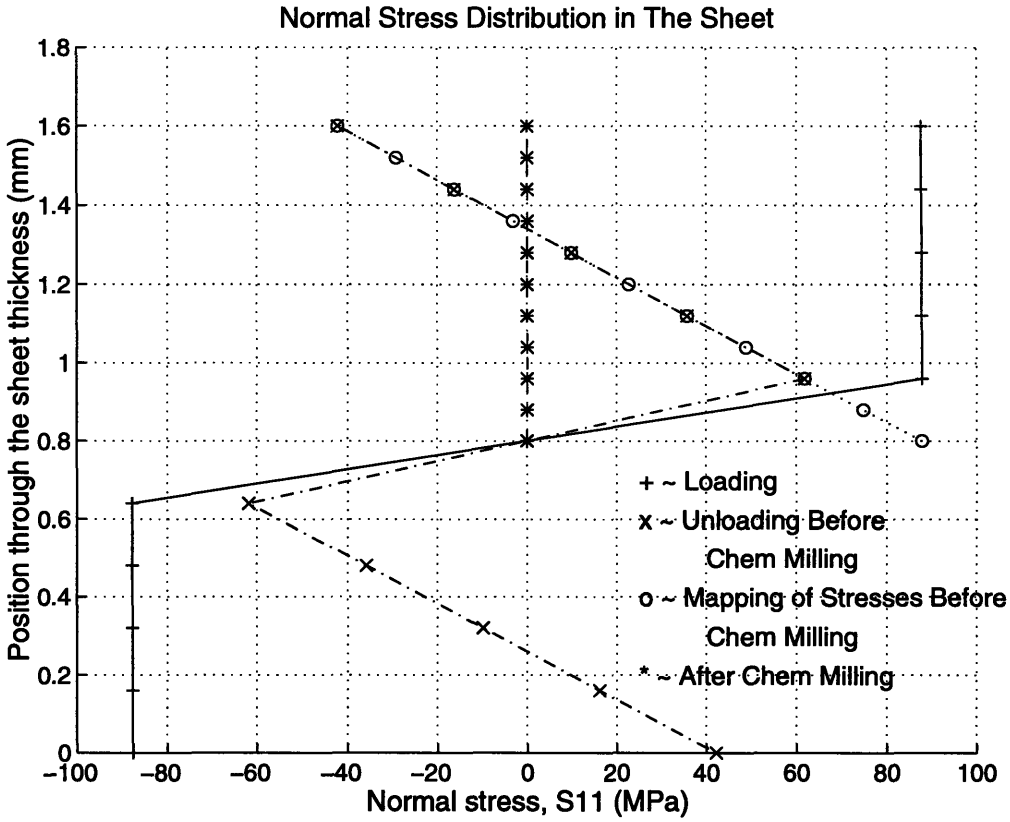

Figure 3.6: Stress distribution in the sheet BEFORE and AFTER chemical milling (accurate imposing of stresses by neglecting the thin elastic core).

The effect of stress mapping on the amount of springback in the part after chemical milling is clearly shown in Figure 3.7, which illustrates a reasonably significant difference in the change of part curvature between the two cases of mapping stresses in shell elements. Part (A) in Figure 3.7 shows the part shape before it was chemically milled. Part

(B) was the final part configuration resulting from imposing inaccurate stress distribution during chemical milling simulation, which corresponds to the stress distributions shown in Figure 3.5. Part (C), on the other hand, was the final part shape obtained from chemical milling simulation with stress distributions in Figure 3.6, which imposed a more accurate stress distribution by neglecting the thin elastic core.

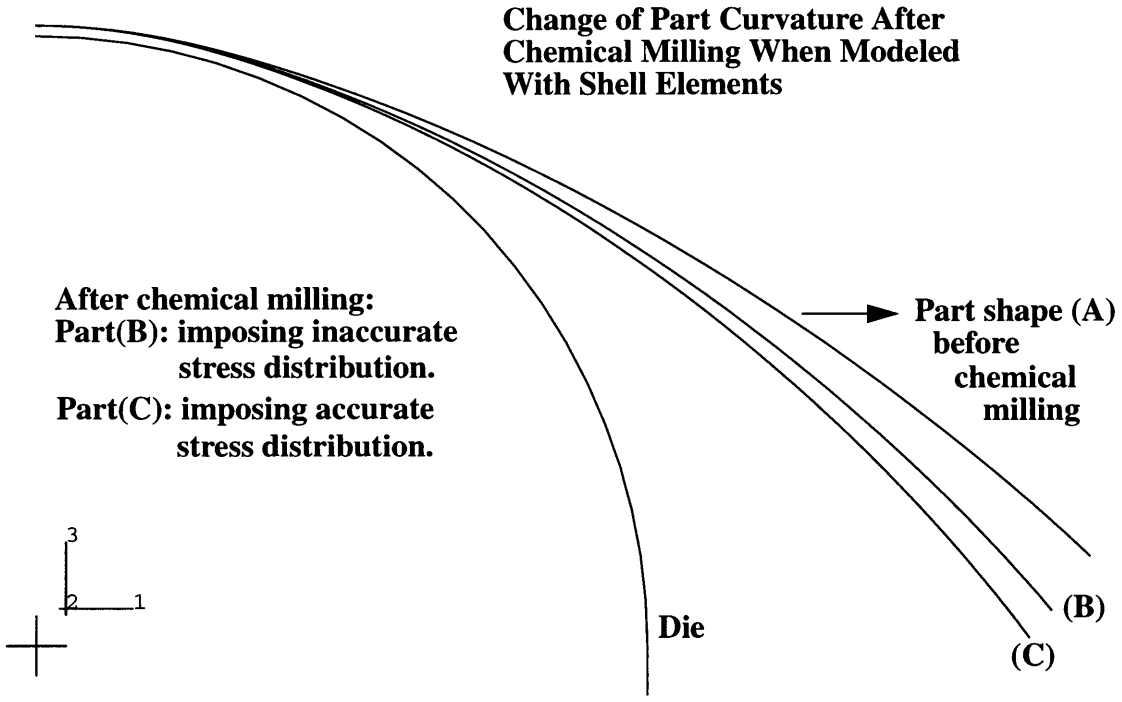

Figure 3.7: Effect of the mapping of residual stresses in the part in terms of the springback.

It is interesting to note that, in Figure 3.7, the case of imposing accurate stress distributions, Part (C), produced results which yields a greater amount of springback in the sheet than the case of imposing inaccurate stress distribution, Part (B). This result makes perfect sense from a mechanics point of view. When the material is removed from the sheet in the chemical milling process, the sheet is no longer in force or moment equilibrium. This is verified by the unloading stress distribution before chemical milling, indicated by 'o's in Figures 3.5 and 3.6, which is also the stress distribution in Part (A) in Figure 3.7.

Subsequently, the sheet has to change its configuration, or springback, as to compensate for the force and moment removed by chemical milling. The stress distribution in the sheet is consequently modified until the force and moment equilibrium are satisfied. Fig-

ure 3.8 also shows the final unloading stress distributions in the sheet after chemical milling, for both cases of stress mapping algorithms. The stress distribution designated with 'o's represents the stresses that correspond to Part (B) in Figure 3.7, which is obtained from the simulation with inaccurate imposing stresses. Similarly, the stress distribution labeled by '*'s represents those stresses in Part (C) of Figure 3.7, which utilized linear extrapolation in stress mapping during the chemical milling simulation. It is evident that, in the case of stress distribution designated with '*'s, all the stresses are completely removed from the sheet, wherein some residual stresses remain in the other stress distribution designated with 'o's. The difference in the amount of final residual stresses in the part after chemical milling gives rise to the difference in the amount of springback of the part in each case. Logically, then, the part with more stresses removed would springback more than the other one, which was observed in this particular study.

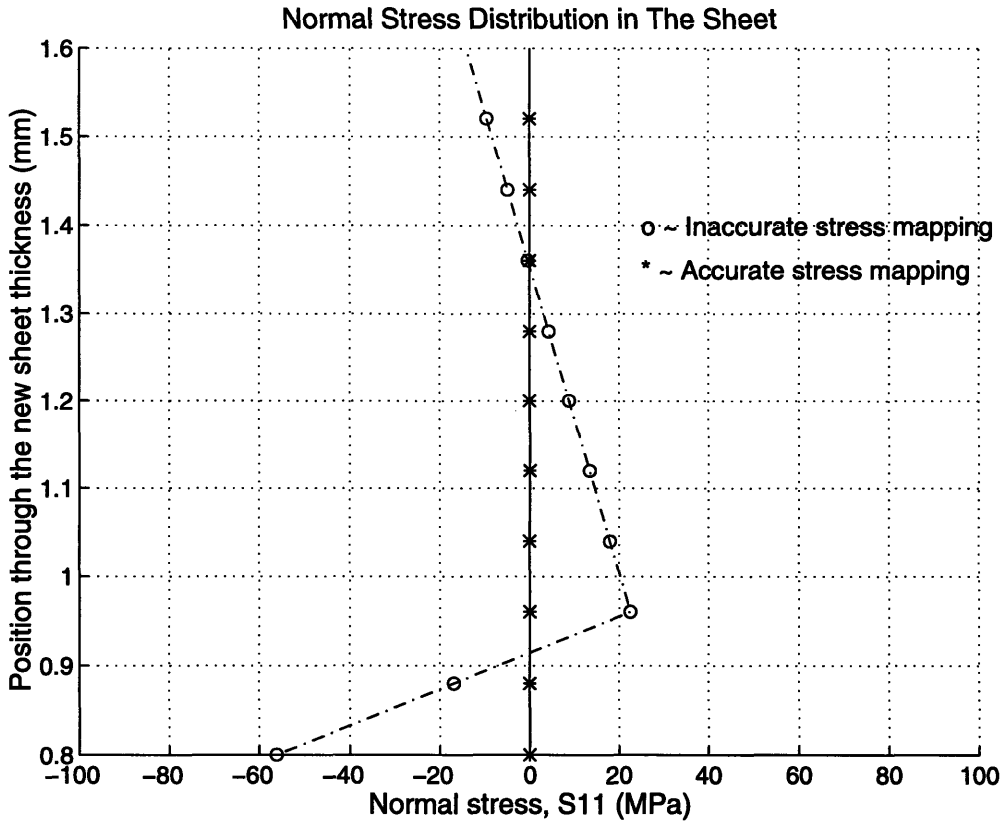

Figure 3.8: Comparison of final stress distribution after chemical milling between a case of accurate and inaccurate imposing stress distributions in the chemical milling simulations.

From the results discussed thus far, it is crucial for an effective chemical milling simulation that an accurate estimate of the residual stresses in the part before chemical milling is obtained. As illustrated in Section 2.3.3, this could be achieved by increasing the number of section points through the thickness in shell elements. Moreover, the linear extrapolation of stresses, when used carefully, could reproduce a very accurate stress distribution as shown previously, granted that the pre-conceived knowledge of the stress distribution is known prior to the simulations, which is rarely the case. Generally, a better estimate of the stress distribution in the region surrounding the neutral axis can be obtained by using a higher number of element section points. In actual stretch forming simulations, however, typical part curvatures are much less severe than the one considered in this preliminary study. Therefore, the current number of element section points through the thickness (11 points) should be adequate to capture the actual stress distribution in the sheet. Consequently, any linear extrapolation of stresses in the actual chemical milling simulation is not required and will not be implemented in the future simulations. The main reason to eliminate the extrapolation method is simply the ineffectiveness it poses on the simulations; no information on the final stress distribution after chemical milling is available prior to actual process simulations. It will be illustrated in the next chapter that the linear interpolation in the mapping of stresses is sufficient and produces accurate results when compared to the parts produced by the actual process.

At this stage, the results from chemical milling simulation using shell elements can be compared to those simulations using continuum elements in order to explicitly show a more effective modeling of the chemical milling process using shell elements. The distributions in Figure 3.9 (a) and (b) illustrate the differences in the simulation results from both types of elements before and after chemical milling, respectively. It is obvious, from looking at the comparison of stress distributions in Figure 3.9, that shell elements yield results which are more closely matched the analytical solutions than the results produced by continuum elements. Even though continuum elements of 1:1 aspect ratio seem to be in the order of the same level of accuracy as the shell elements, shell elements still has a advantage over the continuum elements in terms of the CPU time. Table 3.1, which shows the CPU time required to complete a number of different simulations, provides a rather convincing evidence supporting the use of shell elements over the continuum elements.

(Similar to the simulations in Chapter 2, all of the forming and chemical milling simulations were performed by a Hewlett-Packard computer HP-735 model, which has the clock speed of about 135 MHz.) In conclusion, shell elements prove to be more effective than continuum elements, not only in terms of the level of accuracy of the results, but also in terms of a computational time and memory required in the simulation. This effect would be even more pronounced when modeling complicated double-curvature shapes.

Elements used in the simulations	CPU Time for Forming Simulation	CPU Time for Chemical Milling Simulation	Total CPU Time
Shell Elements	6,771 sec	220 sec	6,992 sec
Continuum Elements of 1:1 Aspect Ratio	35,142 sec	544 sec	35,686 sec
Continuum Elements of 1:3 Aspect Ratio	7,481 sec	193 sec	7,674 sec
Continuum Elements of 1:6 Aspect Ratio	3,031 sec	87 sec	3,119 sec
Continuum Elements of 1:10 Aspect Ratio	1,297 sec	48 sec	1,346 sec

Table 3.1: Comparison of the CPU time in different cases of chemical milling simulations using shell and continuum elements.

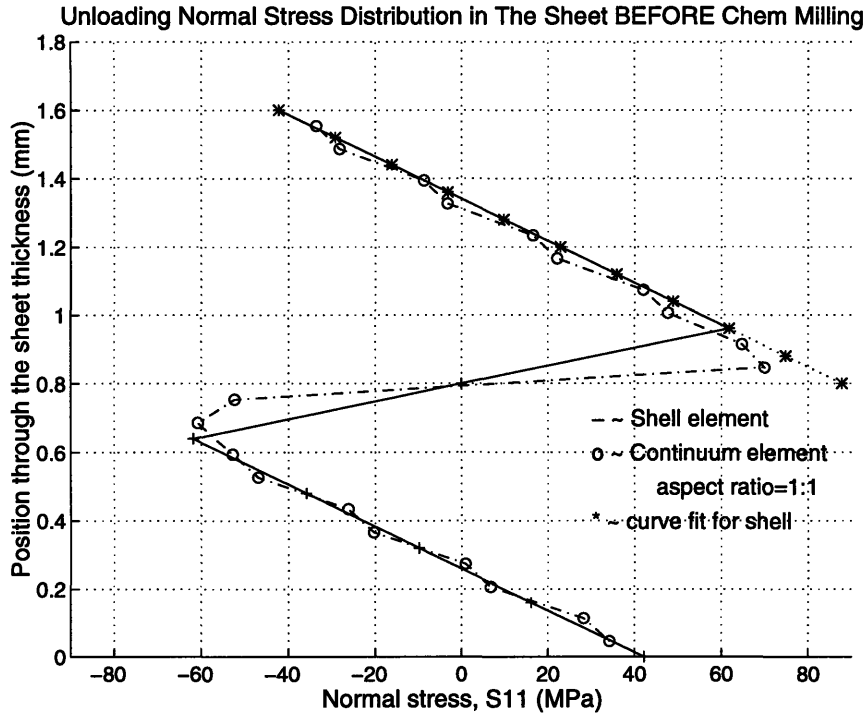

Figure 3.9: Comparison of unloading stress distribution in the sheet between shell and continuum elements. (a) BEFORE chemical milling; (b) AFTER chemical milling.

Chapter 4

Simulations of Chemical Milling Process on Parts With Simple Geometry

The development of the algorithm to simulate the chemical milling process on general shapes is completed. The next objective is to determine the accuracy of the predictive capabilities for this simulation algorithm and how well the effect of chemical milling on part shape can be modeled. In order to do this, experimental verification of the predictive ability of the model was initiated, where a set of experiments and simulations of the forming and chemical milling of several parts of simple geometry are compared. This chapter describes the forming and chemical milling conditions used in both experiments and simulations. The boundary conditions used in the numerical finite element simulations will be briefly described. The results from simulations and a discussion of the analysis on the effects of the chemical milling process, followed by a comparison between experimental and simulations results, will also be presented in this chapter.

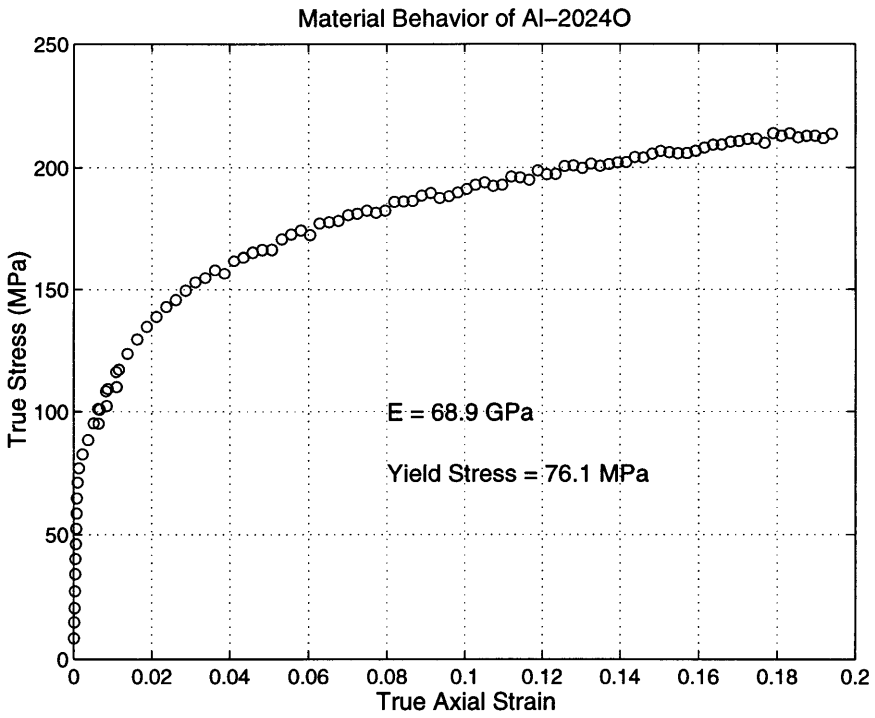

Figure 4.1: Material behavior of 2024-O.

4.1 Setup Parameters and Chemical Milling Specifications

Two sets of single radius of curvature parts were formed by using an INSTRON 1125 mechanical testing machine. The modification was made to the INSTRON 1125 such that the fixed/lower end of the INSTRON 1125 is equipped with a pair of supporting rollers and a die is attached to the moving/upper end of the INSTRON 1125, which moves downward to bend the sheet. After the sheets were formed, they were then sent to Texas Aircraft Milling for chemical milling. This simple forming setup is depicted in Figure 4.2. The two dies used in this particular forming process were cut from wooden blocks to radii of 5.8 cm (2.32") and 3.8 cm (1.52"), respectively. The sheets formed were of 1.6 mm (0.063") thick Al-2024O and have dimensions of 11.43 cm x 30.5 cm (4.5" x 12.0"). The stress-strain curve for the material behavior of Al2024-O is provided in Figure 4.1.

In order to study the effects of chemical milling, four sets of chemical milling specifications were prescribed to each set of parts. In the first set, designated as set A, the entire part was chemical milled by one-half of the sheet thickness; in the second set, designated as set B, a 2.54 cm x 2.54 cm (2.5" x 2.5") centered pocket was chemical milled by one-half of the sheet thickness; in the third set, designated as set C, a 2.54 cm x 2.54 cm (2.5" x 2.5") centered pocket was chemical milled by one-quarter of the sheet thickness; and finally in the fourth set, designated as set D, a 2.54 cm x 2.54 cm (2.5" x 2.5") off-centered pocket was chemical milled by one-half of the sheet thickness. The patterns for chemical milling a centered and off-centered pocket are shown in Figure 4.3.

The different chemical milling specifications prescribed to the parts serve several purposes. The main reasons are to study the effects of the geometry of the chemically milled regions, the amount of material removed in terms of the original sheet thickness, and the location of the chemical milled regions on the final part shape. The chemical milling specification for a centered pocket versus an off-centered pocket, for instance, introduced a variation in the location of chemical milling regions, which can be used to study the effect of chemical milling in different regions in the part.

As explained in Chapter 3, the simulation of the entire process consisted of the forming simulation and the chemical milling simulation. The forming simulation is required simply for ensuring accurate residual stress distributions in the part. In this forming simu-

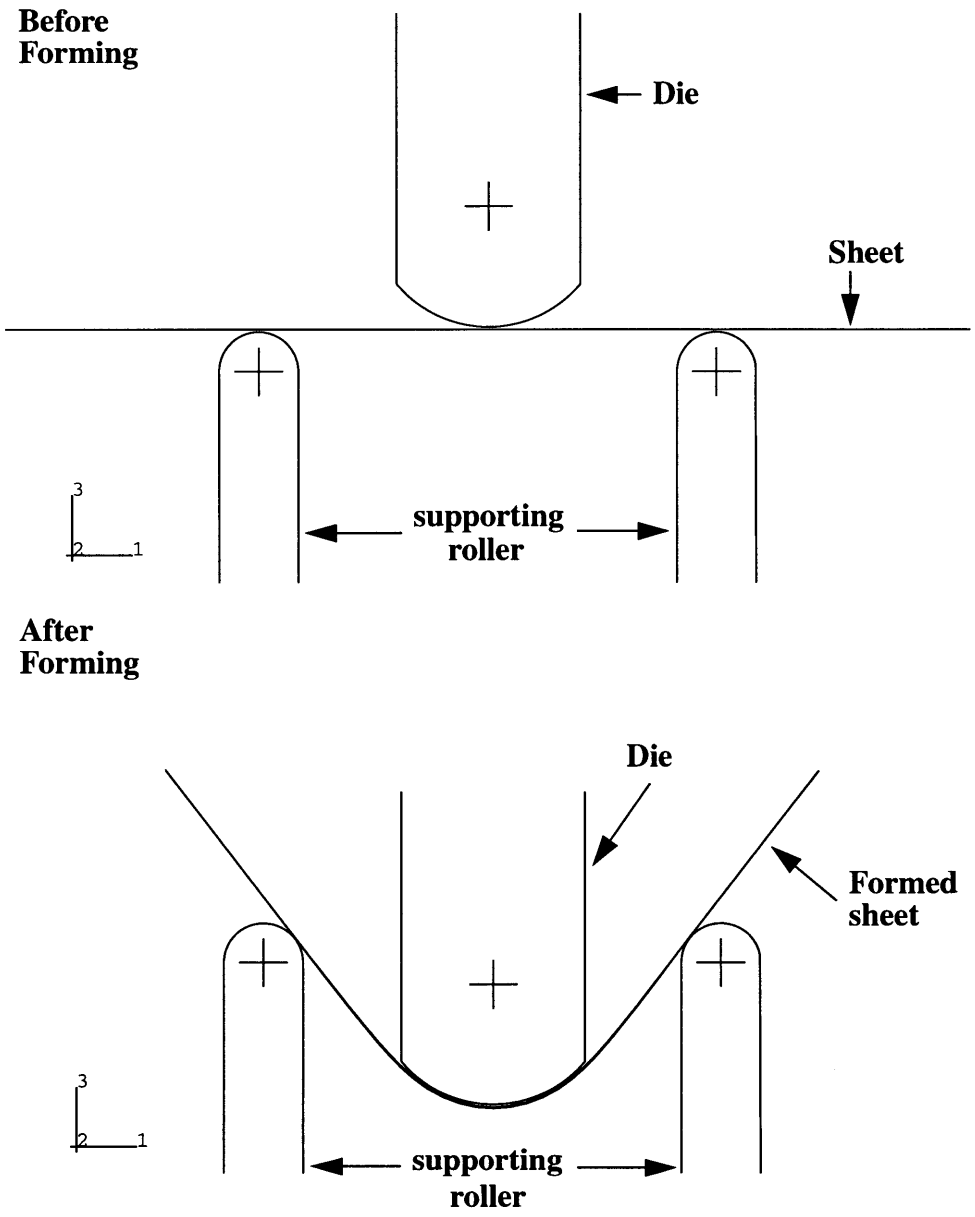

Figure 4.2: Forming setups of parts with simple geometry.

lation, the sheet, modeled with shell elements (ABAQUS type S4R) is initially supported by a pair of rollers, which is modeled as a rigid surface. Then, a die, also modeled as a rigid surface, moves downward to bend the sheet. During the unloading stage, the contact pairs between the die and the sheet and between the sheet and the supporting rollers are removed, after which the sheet is allowed to re-equilibrate to an unloaded configuration. The chemical milling simulation is the same as outlined in Chapter 3, where the chemi-

cally milled sheet is regenerated and the residual stresses before chemical milling are imposed to the sheet using a SIGINI user subroutine. The SIGINI subroutine reads these residual stress data file for all elements and element section points. For each chemical milled element, the residual stress distribution is modified to account the removal of material thickness, using the linear interpolation method. When the imposition of the residual stress state is completed, the sheet is then allowed to "unload" to an equilibrium shape.

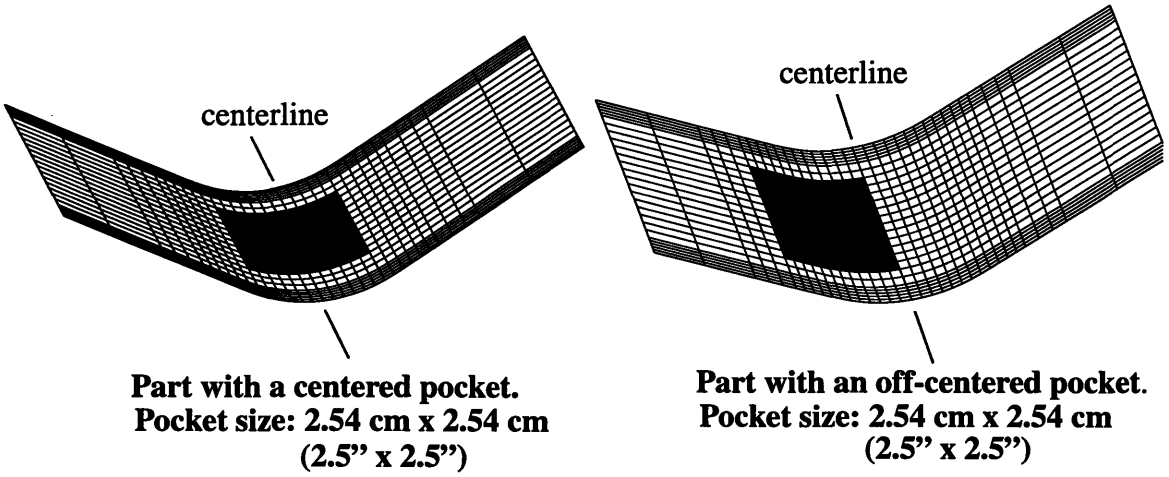

Figure 4.3: Chemical milling patterns: centered pocket (left), off-centered pocket (right).

4.2 Simulation Results and Analysis

One effect of the chemical milling process is the distortion of the part. In order to quantify part distortion, the shape must be measured and quantified by some means. For the simple shapes of this study, the part angle can be monitored. The part angle is depicted in Figure 4.4 and is defined to be the bend angle of the straight section of the part. The change of the part angle after the chemical milling process, $\Delta\Phi$, is defined to be the difference between the part angle before and after the chemical milling process. (See equation 4.1)

$$\Delta\Phi = \Phi_{after} - \Phi_{before} \tag{4.1}$$

It quantifies the effect of the chemical milling process on the part shape. This measurement and quantification of the part distortion in terms of the change in part angle, however,

can be used for the study of these simple shapes only since the forming of the sheet did not involve any pre-stretching or post-stretching of the sheet. Assuming that there is zero stress in the sheet prior to forming, the stresses in the straight section of the sheet would not be affected by the forming and the chemical milling process. This section will remain straight throughout the forming and the chemical milling process. The part distortion can then be quantified in terms of part angle, which measures how much this straight section moves as a result of the change in the curvature of the part.

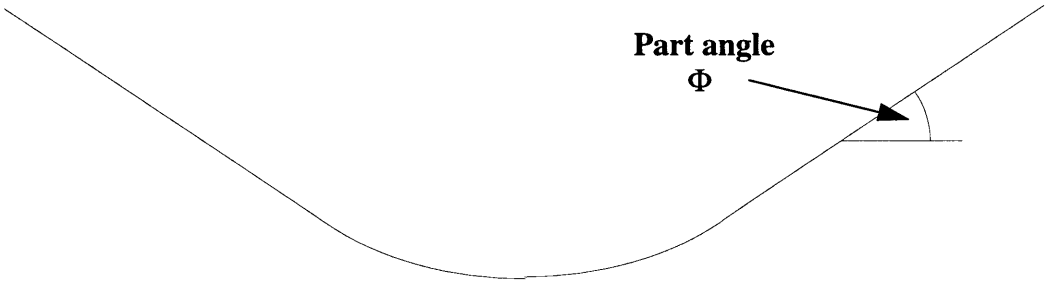

Figure 4.4: Illustration of definition for the part angle.

A positive value of $\Delta\Phi$ indicates that the part sprang inward or closed in after it was chemically milled; a negative value signifies the opposite, which is the springing outward or opening up of the part. Figures 4.5 (a) and (b) illustrate the effect of the chemical milling process as defined by the change in part angle $\Delta\Phi$.

Eight simulations which comprise the forming of two distinct radii of curvature and four different chemical milling specifications for each radius of curvature, were undertaken. Results obtained from the forming simulations illustrate that, for the first part which was formed with a 5.8 cm-radius die, the springback was found to be approximately 10 degrees. The springback of the second part, which was formed with a 3.8 cm-radius die, was found to be about 11 degrees. The comparison between the experimental and simulation results, in the next section, showed that the forming simulations can accurately predict the change of part curvature in the actual process. The changes of part shape due to springback of the sheet for both 5.8 cm-radius die and 3.8 cm-radius die are depicted in Figures 4.6 (a) and (b), respectively.

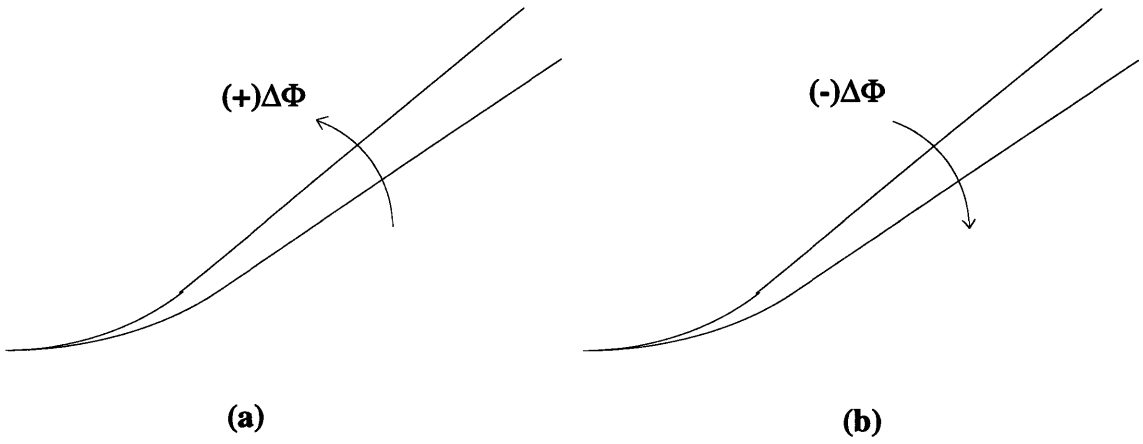

Figure 4.5: Change of the part angle showing the effect of the chemical milling process on the part shape: (a) a positive value of the part angle; (b) a negative value of the part angle.

The results of all the different cases of chemical milling simulations are tabulated in the table 4.1. The results, as seen in table 4.1, are in terms of the change in part angle $\Delta\Phi$ after chemical milling. Using these simulation results, we will first investigate how the part shape is affected by different chemical milling specifications and whether there is a logical explanation or a correlation between the part distortion and the chemical milling specification. The next section will be devoted to looking at the comparison between the simulation and experimental results to see how well the actual process can be modeled by the simulation.

Part number/radius of curvature of the die	Chemical milling specification	$\Delta\Phi$
Part 1/r_{die1} = 5.8 cm	remove 1/2 t of the entire part	3.64°
Part 1/r_{die1} = 5.8 cm	remove 1/2 t of the centered pocket	0.69°
Part 1/r_{die1} = 5.8 cm	remove 1/4 t of the centered pocket	-0.27°
Part 1/r_{die1} = 5.8 cm	remove 1/2 t of the off-centered pocket	(side with pocket) 0.93° (side without pocket) 0.13°
Part 2/r_{die2} = 3.8 cm	remove 1/2 t of the entire part	3.62°
Part 2/r_{die2} = 3.8 cm	remove 1/2 t of the centered pocket	0.62°

Table 4.1: A summary of simulation results on the change in part angle after chemical milling.

Part number/radius of curvature of the die	Chemical milling specification	$\Delta\Phi$
Part 2/r_{die2} = 3.8 cm	remove 1/4 t of the centered pocket	-0.29°
Part 2/r_{die2} = 3.8 cm	remove 1/2 t of the off-centered pocket	(side with pocket) 0.70° (side without pocket) -0.05°

Table 4.1: A summary of simulation results on the change in part angle after chemical milling.

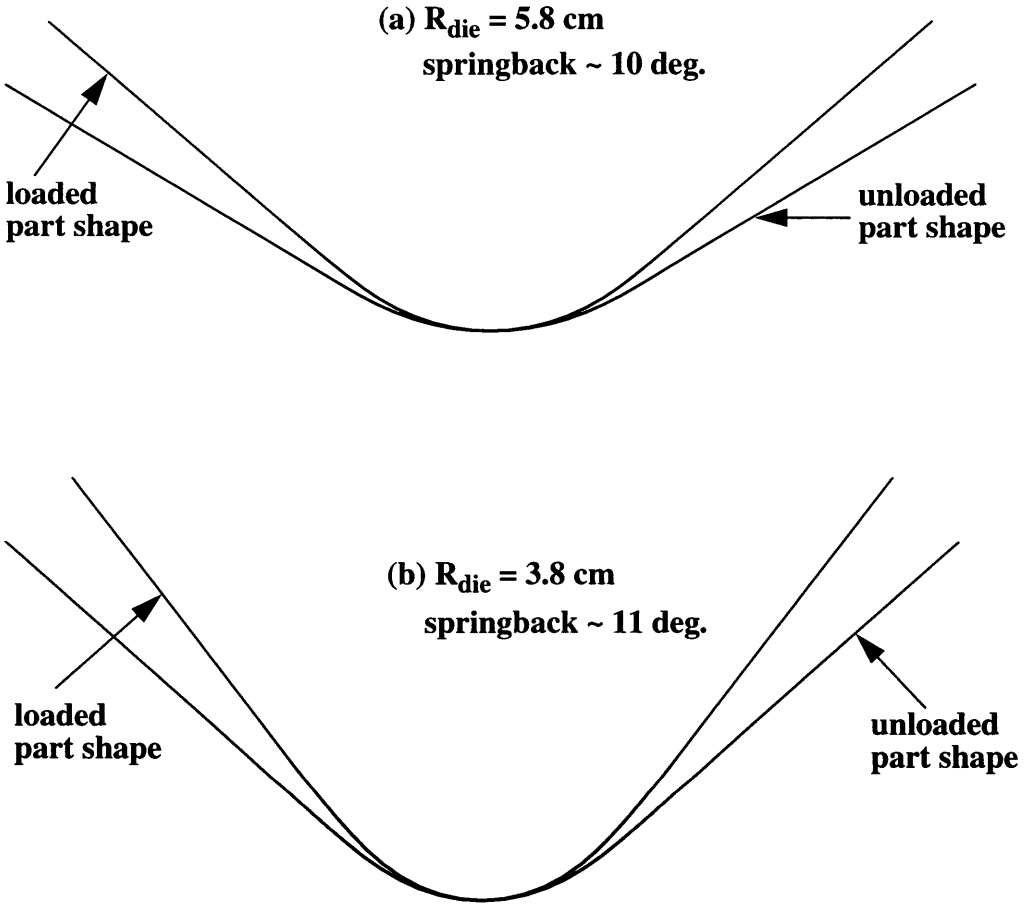

Figure 4.6: Illustration of springback after the sheet is unloaded from forming: (a) die radius = 5.8 cm; (b) die radius = 3.8 cm.

When the entire part was chemically milled by one-half of the sheet thickness, the simulation results showed that the change of the part angle is approximately four degrees. This result subsequently suggests that the part sprang inward after chemical milling, according to the sign of $\Delta\Phi$. This first set of chemical milling specification, which is to

remove one-half of the sheet thickness on the entire part, was intended to be one extreme case where the greatest amount of material is removed from the sheet. The reason for this is twofold: first, chemical milling the entire part exhibits the largest amount of part distortion since an entire layer of material is removed; and second, the analytical solution of a similar type of problem was previously discussed in details, hence, the fundamental physics of the process is well understood. The simulation results further support the first argument. The results from table 4.1 show the largest amount of part distortion is found when chemical milling the entire part. Moreover, this case might represent a limiting case of the effect due to chemical milling. Figure 4.7 is an example that illustrates the dependency of part distortion on the amount of material removed. The part drawings shown in Figure 4.7 were obtained from the simulations and they showed the difference in part shape before and after chemical milling.

Further comparison between the cases of chemical milling the centered pocket of different thickness proves the suspected relationship between the part distortion and the amounts of material removed. (See also Figure 4.8) Even though a small change in part angle $\Delta\Phi$ was observed in both chemical milling one-half and one-quarter of the sheet thickness on the centered pocket, it is apparent that the amount of material removed certainly has an effect on the part distortion and, hence, the final configuration of the part. It is very interesting, however, to notice that the first case of chemical milling the centered pocket to one-half the sheet thickness (Figure 4.8 (a)) resulted in the springing inward of the part, while the second case of chemical milling the same geometry to one-quarter the sheet thickness produced the part distortion in the opposite direction, which is the springing outward of the part (Figure 4.8 (b)). The numerical results in table 4.1 also confirmed this subtle difference.

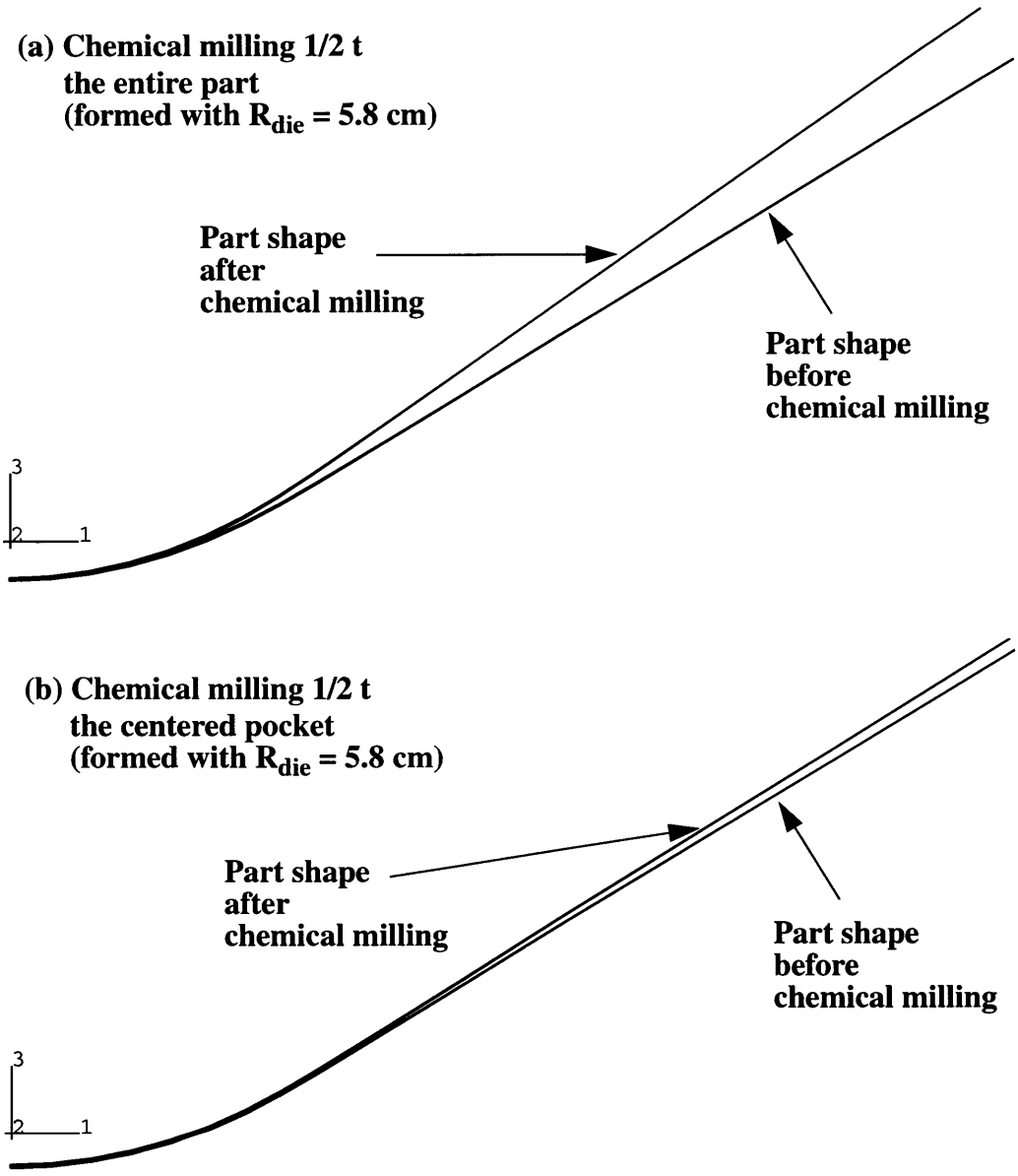

Figure 4.7: Effect of the amount of material removed: (a) chemical milling the entire part by 1/2 t; (b) chemical milling the centered pocket by 1/2 t.

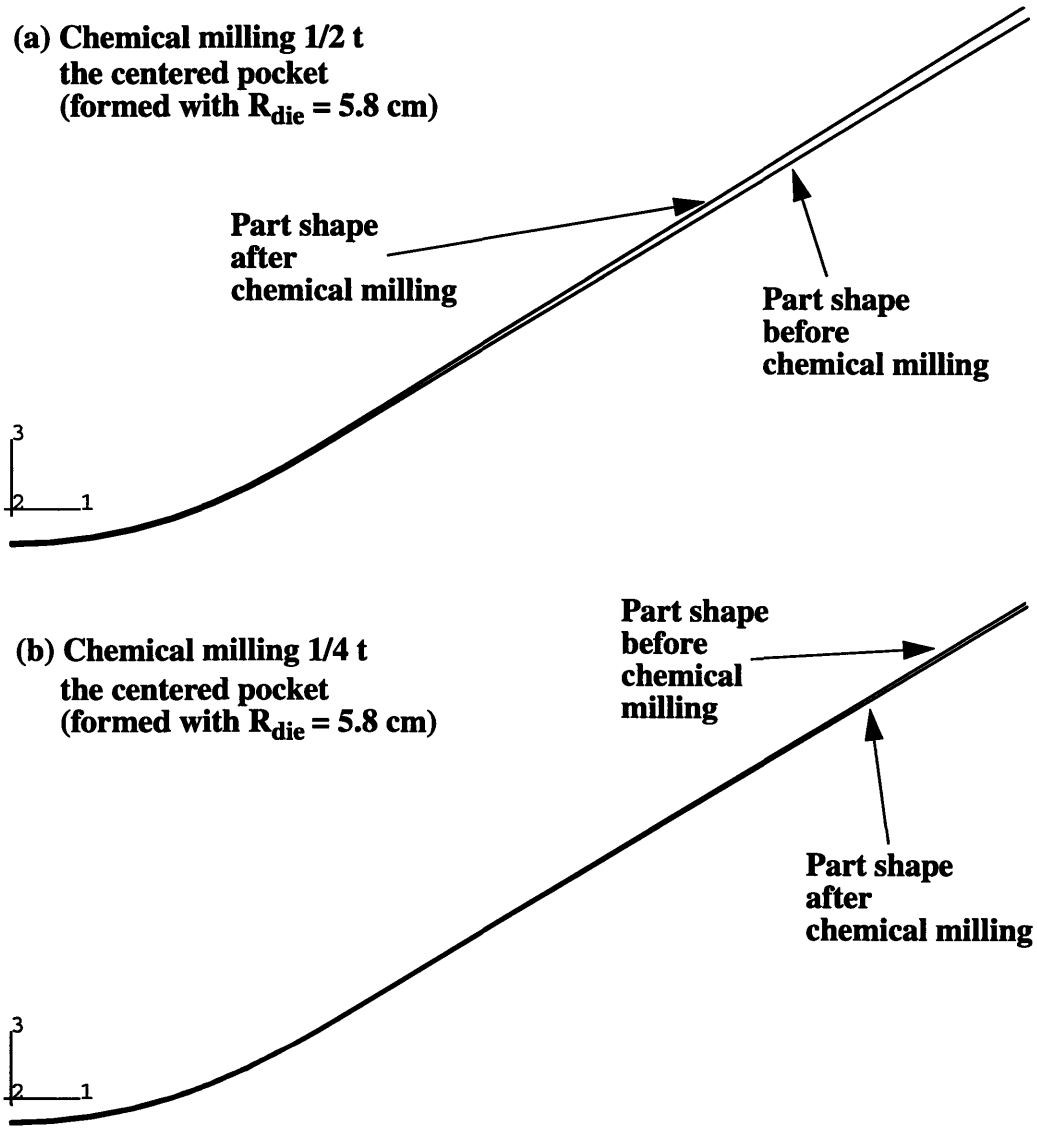

Figure 4.8: Effect of chemical milling different thickness in the sheet: (a) chemical milling 1/2 t of the centered pocket; (b) chemical milling 1/4 t of the centered pocket.

By examining the basic mechanics of the chemical milling process (See Section 1.3.2 and Appendix A), one could infer that this subtle difference in the direction of part distortion is a simple manifestation of the difference in the effective moment removed when different amounts of material (and thus residual stresses) are removed. In other words, in chemical milling one-half the sheet thickness, the stress distribution after the material is removed and before the sheet is allowed to re-equilibrate corresponds to the graph in Figure 4.9 (a). From Section 1.3.2, it was shown that this stress distribution requires an effective moment of $M_{chem} = -\frac{1}{8}\sigma_y h^2$ to be removed in order for the sheet to be in moment equilibrium. The stress distribution in Figure 4.9 (b), on the other hand, corresponds to the residual stress distribution before re-equilibration during the chemical milling process for the case of chemical milling one-quarter of the sheet thickness. Integrating this stress distribution, as illustrated in Appendix A, would result in an effective moment $M_{chem'} = -\frac{5}{144}\sigma_y h^2$ which is different than M_{chem}. Even though, in both cases, the residual stresses in the part are the same before the material is removed, but, by removing different thicknesses of the material, the resulting stress distributions before the sheet is re-equilibrated are essentially different, thus inducing different effective moments to be removed. The differences in the effective moment could cause the part to distort or springback differently, as exemplified by Figure 4.8.

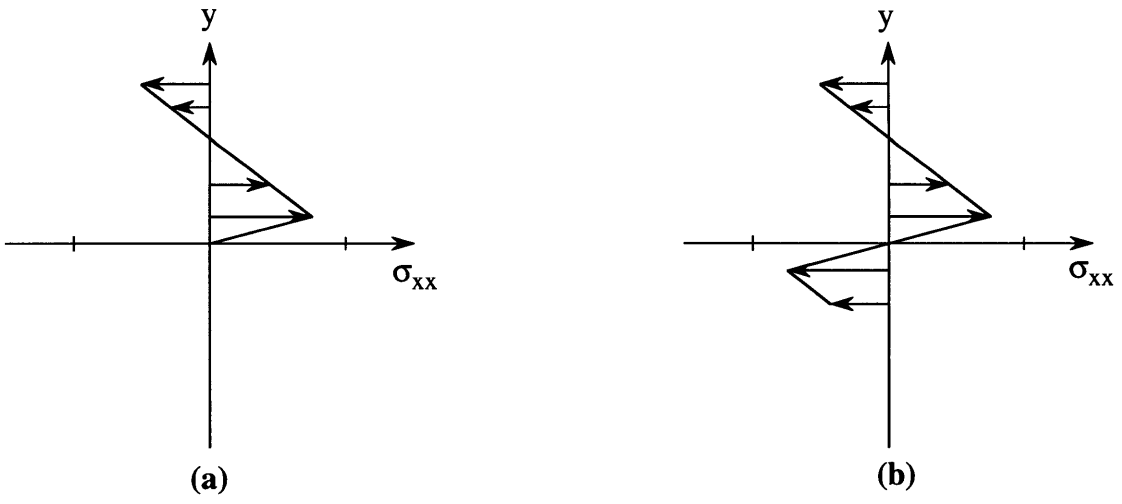

Figure 4.9: Illustration of the difference in residual stress distribution, after material removal and before re-equilibration, in the case of (a) chemical milling 1/2 t and (b) chemical milling 1/4 t.

Moreover, the comparison between the simulation results between chemical milling a centered versus an off-centered pocket of the same geometry illustrates the effect of the position of the chemically milled regions on the part distortion. An off-centered pocket introduces non-symmetry to the problem, which was observed in the difference in change in part angle $\Delta\Phi$ between the side containing the chemically milled pocket and the other side without any chemical milling. As expected, the side with the chemically milled pocket exhibits more springback than the other side because most of the changes in the residual stresses are in the region close to the chemical milled pocket. The effect of the location of chemical milling in the part is depicted in Figure 4.10.

The simulation results further support our earlier hypothesis that the residual stress in the part before chemical milling is critical to the distortion of the part. Removing different amounts of material could affect both the magnitude and the direction of the part distortion, as illustrated in Figures 4.8 and 4.9. The positioning of the chemical milled regions also determine what the final configuration of the part would be. Therefore, it is important that the forming simulations can accurately predict the unloading part configuration and the residual stresses before chemical milling if one is to obtain excellent predictive capability for the chemical milling simulation. In other words, a good forming simulation is a pre-requisite for a good chemical milling simulation. In the next section, we will verify the predictive capability of the forming and chemical milling simulations by comparing the simulation results to the experimental results.

(a) Chemical milling 1/2 t of a centered pocket (formed with R_{die} = 5.8 cm; modeled one-half the sheet using symmetry)

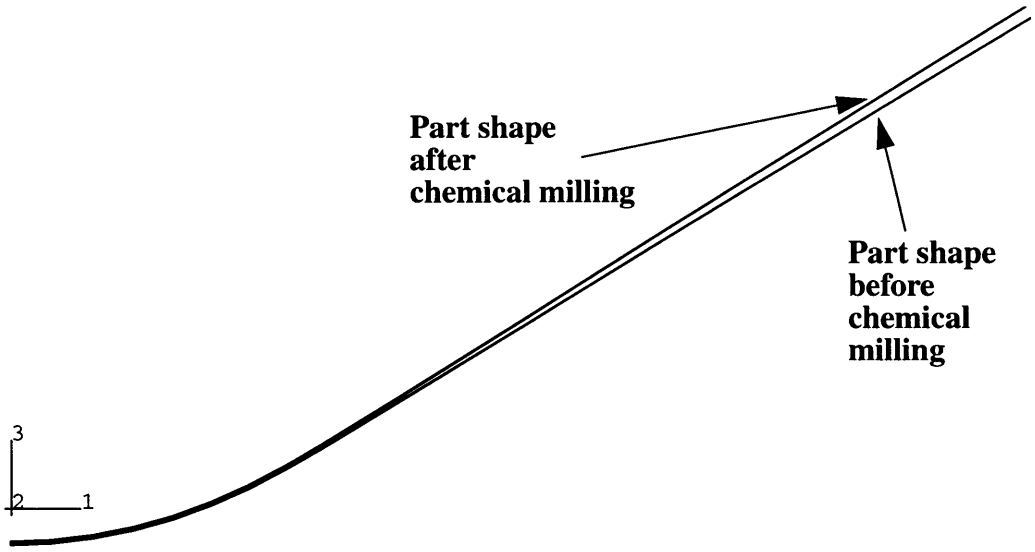

(b) Chemical milling 1/2 t of an off-centered pocket (formed with R_{die} = 5.8 cm)

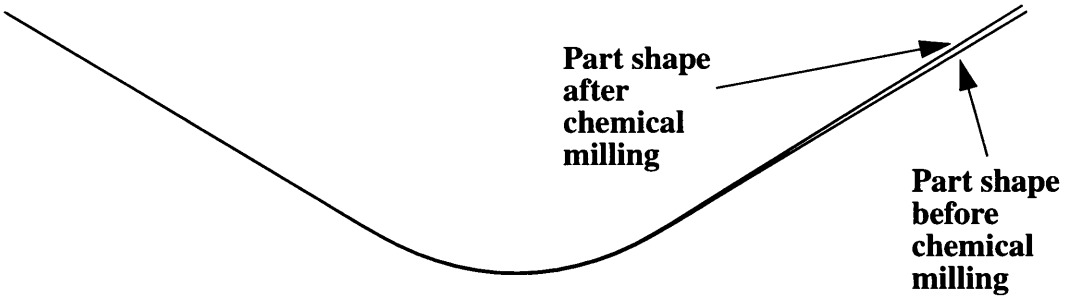

Figure 4.10: Effect of the location of chemical milling regions.

4.3 Comparison Between Experimental and Simulation Results

Experimentally, a set of sixteen parts was formed and chemical milled. A total of eight specifications, consisted of two radii of curvature and four chemical milling specifications, was subjected to the forming and chemical milling of these parts. For each specification, two parts were made to examine the initial repeatability of the results. The data of part configurations was obtained from these experimental parts and was then compared with the simulation results. The objective is to determine how well simulation results match those of experiments by plotting the experimental data against the simulation data. These plots show comparisons of the part configurations as determined by experiments and simulations. A complete compilation of these comparisons is documented in Appendix D.

Overall, the forming simulations appear to produce results that very accurately match the experimental results. These results are showing the part configuration of an unloaded sheet after it was formed. The solid line in Figure 4.11 represents the data obtained from experiments. The simulation data is obtained from the nodal coordinates along the edge of the part and, thus, represents the shape of the part. The simulation results are designated by the circles in Figure 4.11. The simulation results show a concentration of circles or data at the center of the part because the mesh is much more refined at the center of the part than at the perimeter. A fine mesh at the center of the part is required to ensure that the simulation can accurately capture the correct part curvature. The comparisons between the simulations and the experiments, exemplified by the plots in Figure 4.11, show excellent predictions by the forming simulations.

The comparison in part (a) of Figure 4.11 displays a small discrepancy between the simulation and experimental results, particularly at the perimeter of the part. The source of this discrepancy was found to be a result from a number of possible variations made during the forming experiments. The cause of these experimental variations was mostly due to the imperfection in the setup of the forming experiments. For instance, the alignment of the sheet on the supporting rollers was set by a rough approximation. It could not guarantee a perfect alignment with the die or the exact same setup throughout the experiments. In other words, the position of the sheet could be offset with the die by a few millimeters or a few degrees and the forming of the sheet would be a little bit skew and unsymmetric. Since the manufacturing of the dies used a belt-sander to grind and polish the die to a

(a)

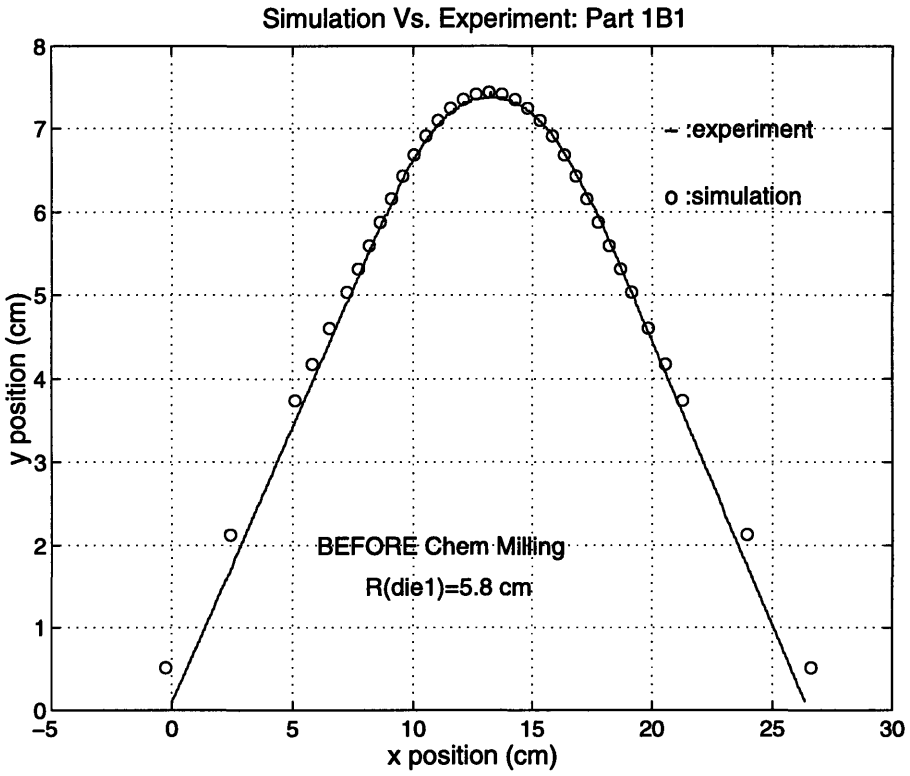

(b)

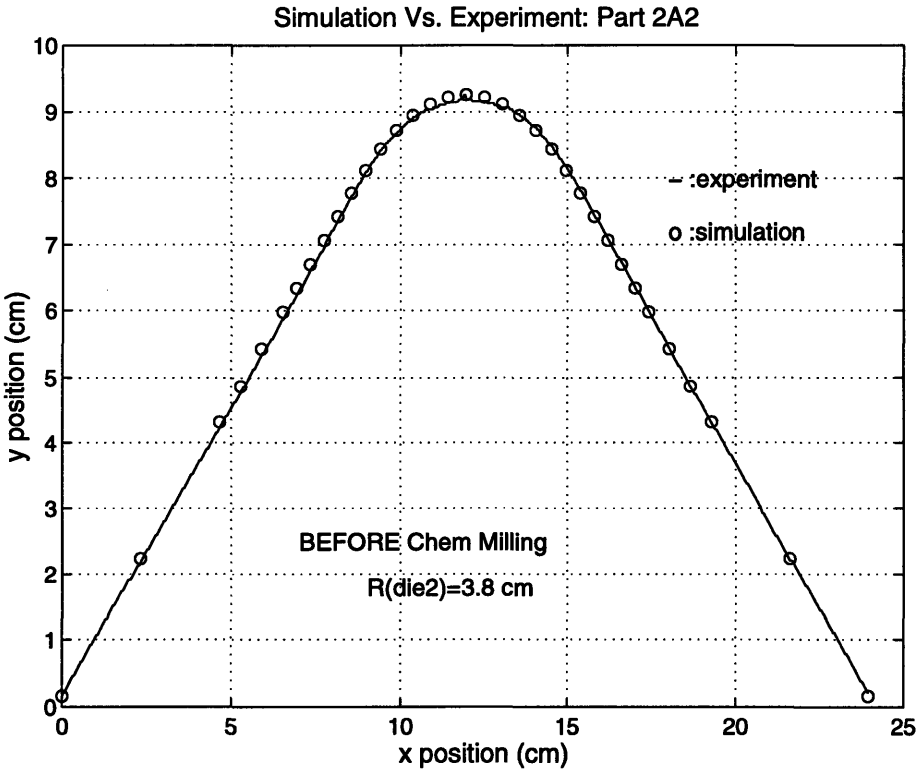

Figure 4.11: Comparison of simulation and experimental results in forming. (a) Part 1: die radius = 5.8 cm. (b) Part 2: die radius = 3.8 cm.

desired radius, the accuracy and precision of the die shape were quite limited. As a result, the two dies made did not have a perfect constant radius of curvature. The variation in the die itself contributed to the imprecise forming experiments. In addition, the observations during forming experiments indicated that slippage occurred between the sheet and the supporting rollers. This slippage could reduce the bending moment applied to the sheet, which, again, causes an error in the forming experiments. Even though the forming experiments included a number of possible variations and undesirable factors, the results such as the ones shown in Figure 4.11 simply illustrate powerful capabilities of our forming simulations.

A few examples of the comparisons between part shapes produced by experiments and simulations after they were subjected to the chemical milling process are shown in Figure 4.12. The results from all four cases of chemical milling specifications: (1) chemical milling 1/2 the thickness of the entire part, (2) chemical milling 1/2 the thickness of the centered pocket, (3) chemical milling 1/4 the thickness of the centered part, and (4) chemical milling 1/2 the thickness of the off-centered pocket are shown in Figure 4.12. And similar to the forming simulations, the chemical milling simulations appear to show excellent predictions of the experimental results, according to the plots of comparisons illustrated in Figure 4.12.

There are, however, some disagreements between simulation and experimental results in the chemical milling experiments in which a part is partially chemical milled. (See Figure 4.12 (b)) The cause of this discrepancy could, again, be traced back to the uncontrolled environment of the experiments and their setup. As already mentioned in Chapter 1 about the chemical milling process, most parts became very thin and flimsy after chemically milling. (The final thickness of the thinnest chemical milled part, for this set of experiments, is 0.8 mm (0.032").) They were easily deformed, as a result. For the partially chemical milled parts, the maskant has to be applied on both sides of the parts as opposed to the case of chemical milling the entire part, which requires only one coating of maskant on the outside. When the maskant is applied to both sides, the part is basically subjected to further deformation due to a removal of the maskant, twice as many times as the other case. Further inspection on the comparison results (See Appendix C) also indicated this trend in discrepancy.

(a)

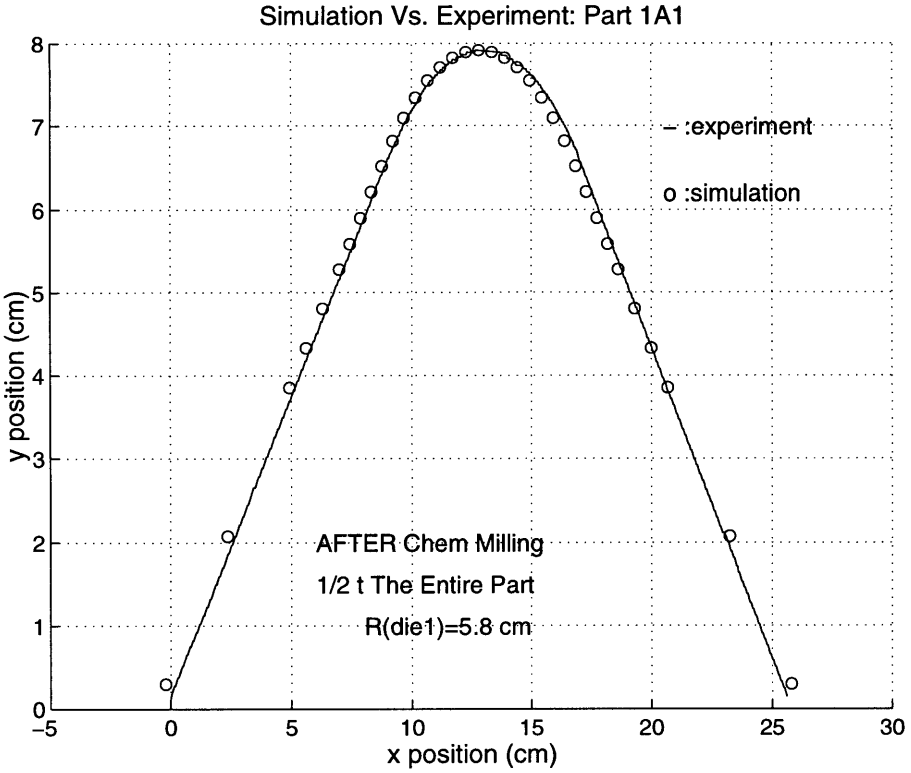
Simulation Vs. Experiment: Part 1A1
– :experiment
o :simulation
AFTER Chem Milling
1/2 t The Entire Part
R(die1)=5.8 cm
y position (cm)
x position (cm)
0
1
2
3
4
5
6
7
8
–5
0
5
10
15
20
25
30

(b)

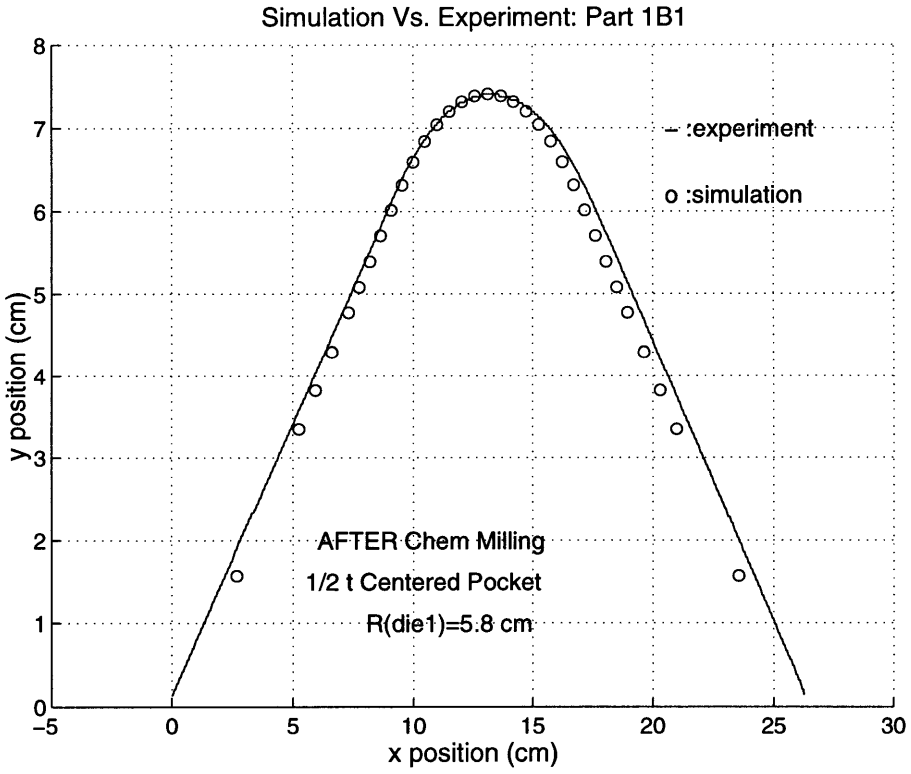
Simulation Vs. Experiment: Part 1B1
– :experiment
o :simulation
AFTER Chem Milling
1/2 t Centered Pocket
R(die1)=5.8 cm
y position (cm)
x position (cm)
0
1
2
3
4
5
6
7
8
–5
0
5
10
15
20
25
30

(c)

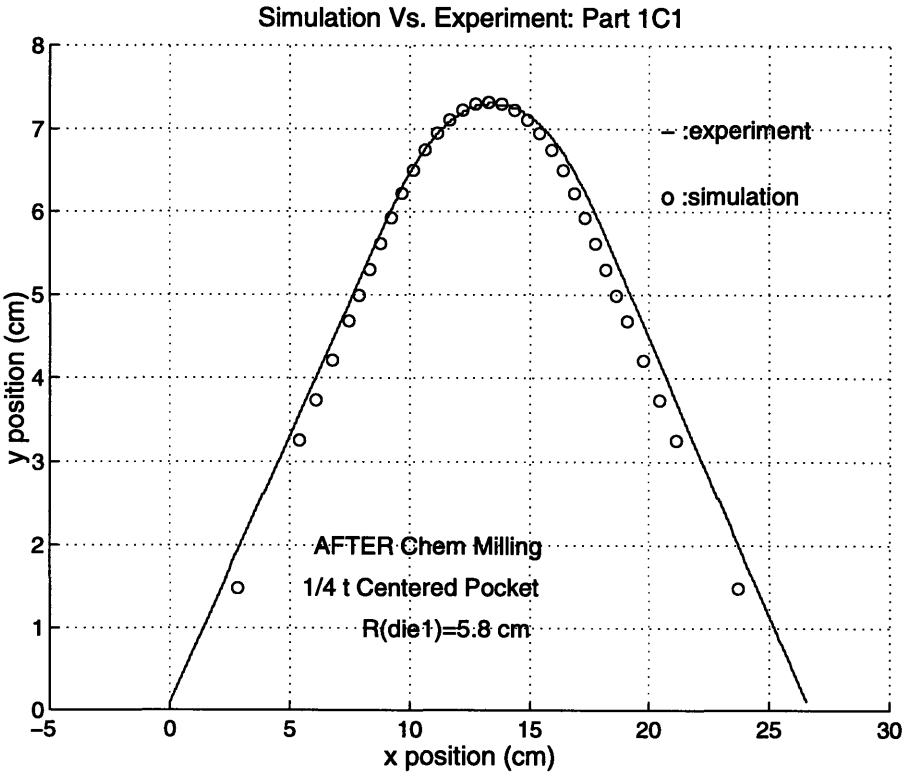

(d)

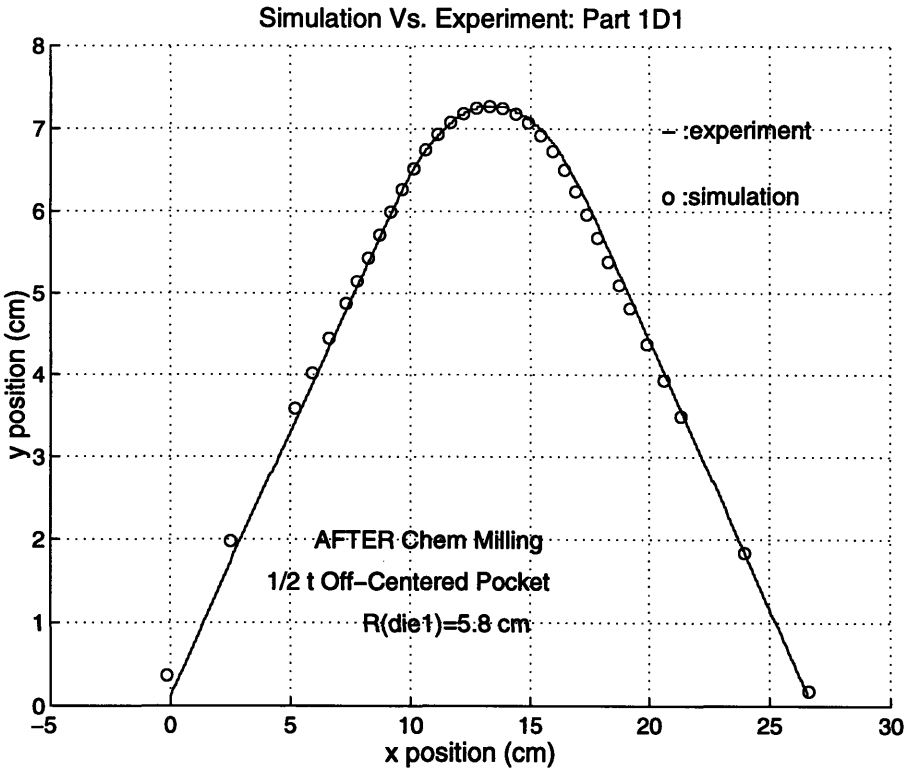

Figure 4.12: Comparison of simulation and experimental results in chemical milling: (a) Chemical milling 1/2 t of the entire part, (b) Chemical milling 1/2 t of the centered pocket, (c) Chemical milling 1/4 t of the centered pocket, and (d) Chemical milling 1/2 t of the off-centered pocket.

From the comparison results, it was found that the discrepancy in part shape is the greatest at the perimeter. However, the curvature at the center of the part after chemical milling was still accurately captured by the simulations. Being able to predict the curvatures at the center of the part after these processes is the most critical component in the simulations. And the center of the part is the most important region because, for most parts, the edges and perimeters of the part would be trimmed and cut after it was formed and before it was chemical milled. Therefore, it can be concluded that our chemical milling simulations can still provide excellent predictions of the part distortion introduced by the chemical milling process.

Chapter 5

Simulations of Chemical Milling Process on A Saddle-Shaped Part

In the previous chapter, each part in consideration had a single radius of curvature. The forming of these parts were simply bending the sheets over a die. It is, in effect, a forming process by bending. There was no pre-stretching or post-stretching involved in the process as it would be in the actual stretch forming process. The stretching of the sheet during forming essentially reduces the effects of the change in residual stresses on the springback of the part. In fact, the amount of springback of the parts considered in the previous chapter would be significantly reduced if they were subjected to the actual stretch forming process. And the effect on part distortion from chemical milling these parts would also be greatly decreased. Therefore, for the parts with simple geometry like the ones used in the previous chapter, the effect of springback of the part can be considerably reduced by imposing a post-stretch to the sheet after it was formed.

With the part of complex geometry, on the other hand, it is more difficult to control the change in residual stresses within the part and the effects such as the one on part distortion from chemical milling. The complexity in part geometry introduces additional constraints on the part and the process. The effect of springback of the sheet is not easily eliminated by a post-stretch imparted to the sheet, which means that the level of residual stresses in the sheet before chemical milling would be quite complicated. Any changes on the residual stress caused by the chemical milling process could possibly augment the magnitude of part distortion. In order to investigate further the effects of the chemical milling process on part distortion, another set of chemical milling simulations was completed on a part with more complex geometry. A chosen geometry is that of a saddle shape. An example of a saddle shape is depicted in Figure 5.1. The saddle shape is one of the most complex geometry for the parts made in the manufacturing of aircraft components. It has a double curvature and an inflection point at the center of the part. A few examples of the saddle-shaped objects are Pringles™ potato chips and a taco shell.

Another part, of which its shape is greatly affected by the chemical milling process or any material removal process, is the I-beam structure used as airframes supporting the fuselage of an aircraft. The manufacturing of this particular part involved extruding the part from a solid aluminum block and, then, drape forming the part over a die. After the I-beam airframe is formed to a desired radius and configuration, it is subjected to an extensive chemical milling process, in which large amounts of material are removed in order to reduce the weight of the structure. In this process, it is occasionally found that the I-beam airframe yields an unpredictable and exceedingly large amount of springback after chemical milling. The simulation of this shape would, however, require a simulation of the extrusion process and a slightly different method in simulating the chemical milling process. Therefore, it will not be pursued any further. This chapter focuses on the simulations of the chemical milling of a saddle-shaped part.

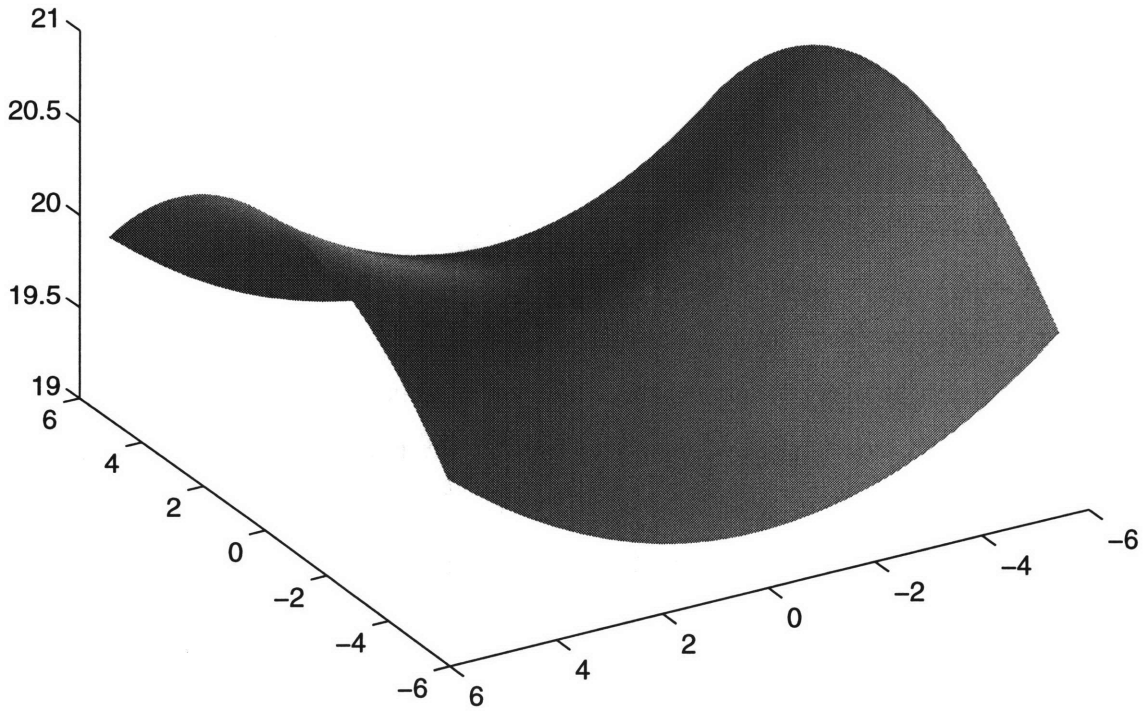

Figure 5.1: An example of a saddle shape.

5.1 Setup Parameters and Chemical Milling Geometries

For this set of analyses, forming of a saddle-shaped part was simulated. The dimension of the formed sheet is 38.1 cm (15") in length by 30.48 cm (12") in width, and has the thickness of 1.6 mm (0.063"). The material of the formed sheet is Al-2024O, which has the Young's Modulus E of 68.9 GPa and the yield stress σ_y of 76.1 MPa.The shape of the die is a torus shape with a 76.2 cm (30") radius of curvature. The sheet is first pre-stretched to about 0.8% plastic strain and then wrapped linearly, in the clockwise direction, by 21 degrees while gradually increasing the stretch load on the sheet from a pre-load of 13,000 klb to about 13,500 klb.

The sheet was modeled with shell elements of ABAQUS type S4R having five section points through the thickness. Taking advantage of the symmetry of the problem, one quarter symmetry of the sheet was modeled, simulated, and analyzed. Figure 5.2 depicts the one-quarter model of the sheet and the die used in this forming simulation. The contact condition between the sheet and the die used the softened contact scheme with the clearance distance of 0.8 mm, which corresponds to one-half the sheet thickness, and the pressure at zero clearance of 5.0 MPa. The contact between the sheet and the die is also modeled as having zero friction.[10]

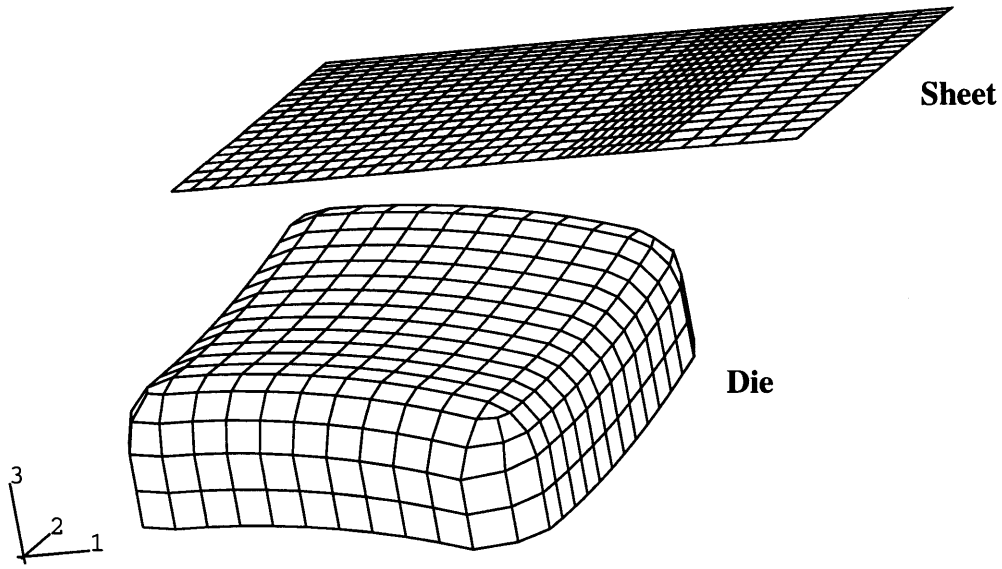

Figure 5.2: Model of a saddle-shaped die and the sheet (1/4 symmetry model).

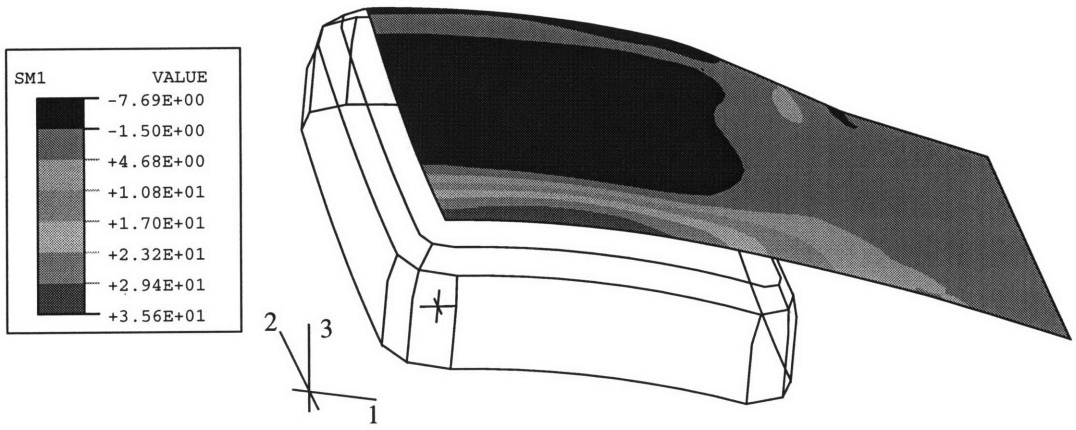

(a) Contour plot of bending moment about local 2-axis.

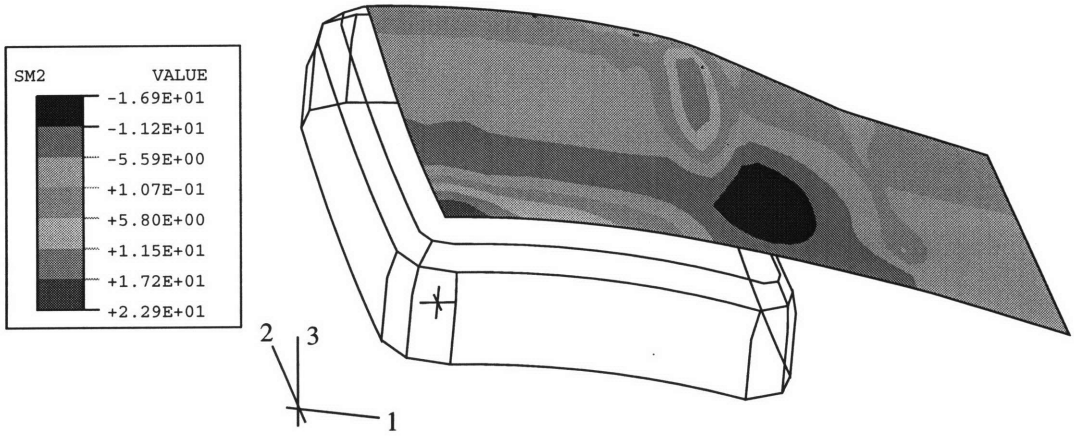

(b) Contour plot of bending moment about local 1-axis.

Figure 5.3: Contour plots showing the section moments in the formed part: (a) Bending moment per unit width about the local 2-axis, (b) Bending moment per unit width about the 1-axis.

As for the chemical milling specifications, the geometry and the location of the chemical milled pocket were chosen in accordance with the stresses and the section moment in the formed part. In other words, the simulation results on the formed sheet were first examined. Specifically the section moments in the formed part were carefully studied. The contour plots of the section moments with respect to the 2-axis (the axis along the width or traverse direction of the sheet) and the 1-axis (the axis along the length or longitudinal direction of the sheet) are shown in Figures 5.3 (a) and (b), respectively. With a prior

knowledge of the residual stresses in the part and the section moments they induced, it is possible to determine the regions which are most affected by the chemical milling process.

Our proposed chemical milling specifications on the saddle-shaped part are shown in Figures 5.4 and 5.5. In selecting these regions, the objective is to study the effect of the chemical milling process by maximizing the part distortion. From the basic mechanics of the chemical milling process, it was shown that the magnitude of the part distortion is proportional to the effective moment to be removed from the part necessary to balance the moment equilibrium condition. Before chemical milling, the part is in equilibrium; the total moment in the part is zero. In order to maximize the part distortion, the idea is to remove the material, hence the residual stress, in the area where there is the highest concentration of section moment so that the moment equilibrium in the part after the material removal and before re-equilibration of the sheet is the most unbalanced. Therefore, the part would have to distort the most in order to compensate for the out-of-balance in the

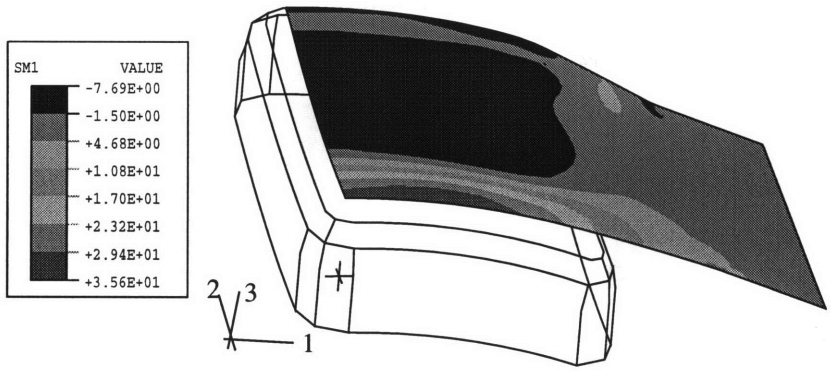

Contour plot of bending moment force about local 2-axis

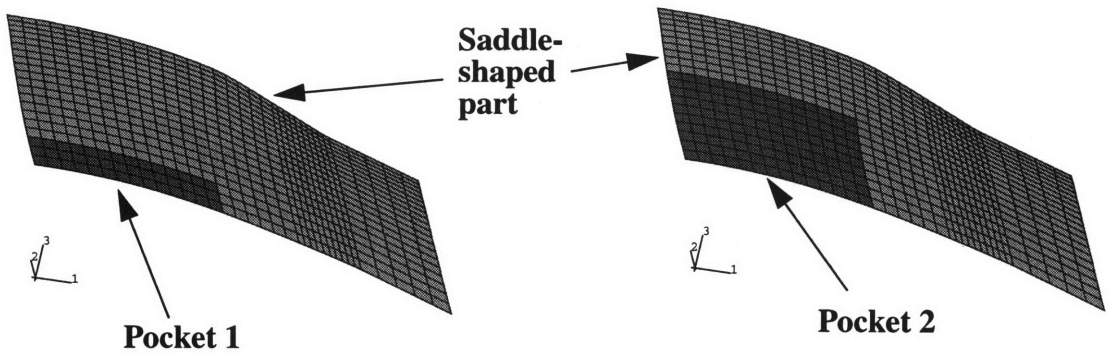

Figure 5.4: Chemical milling specifications 1 and 2 as determined by the contour plot of the bending moment force per unit width about the local 2-axis.

moment equilibrium. The selection of the chemical milled regions was then based upon the contour plots of the section bending moments about both the 1-axis and the 2-axis. The four chemical milling pockets, shown in Figures 5.4 and 5.5, were chosen because they exhibited the highest concentration of the section moments in the part. In addition, for all four chemical milling simulations, the sheet thickness to be removed from the part is specified as one-half the original sheet thickness, which corresponds to 0.8 mm (0.032").

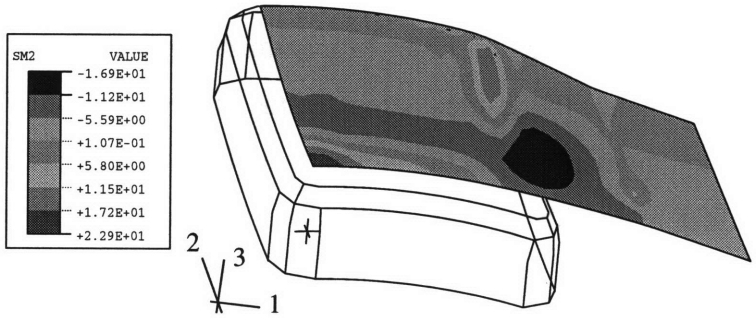

Contour plot of bending moment force about local 1-axis

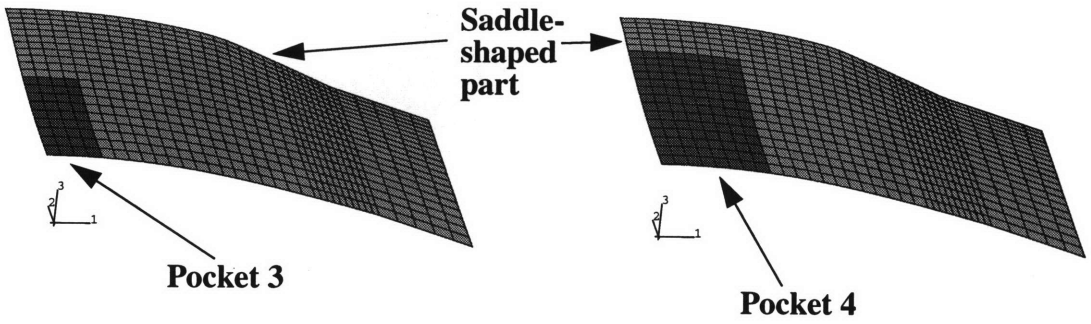

Figure 5.5: Chemical milling specifications 3 and 4 as determined by the contour plot of the bending moment force per unit width about the local 1-axis.

5.2 Simulation Results and Analysis

The analysis of the saddle-shaped part will mainly consider the results from the chemical milling simulations of the four regions or "pockets" specified in the previous section. In the last chapter, a measurement of the part angle was used to quantify the part distortion because of the simplicity of the formed parts. With a more complex part shape such as the saddle shape, this mean of quantifying the chemical milling effect is not accurate enough

to measure the part distortion in the saddle-shaped part. An alternative method must be developed. It was found that the most effective way to quantify the part distortion is to measure directly the displacement of the part in the z-direction. The displacement in the z-direction effectively measures the differences of the part shape before and after chemical milling. It is then defined as the difference in the z coordinates of the same point on a part measured before and after chemical milling. A positive value of the z displacement is an indication of the upward movement of the part. On the contrary, a negative z displacement corresponds to the downward movement of the part. The definition of the z displacement is illustrated in Figure 5.6.

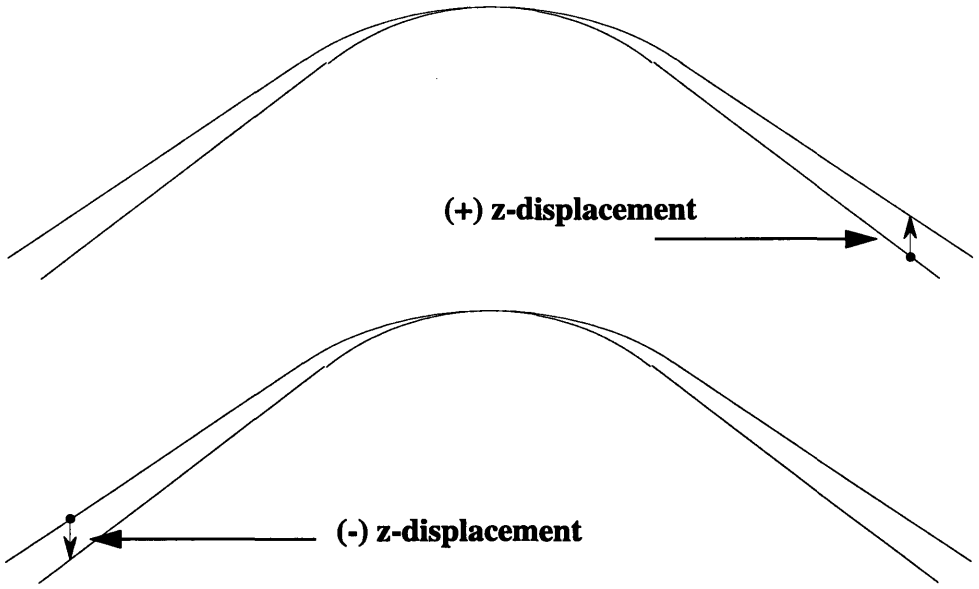

Figure 5.6: Measurement of part distortion with z displacement.

To analyze the results from the chemical milling simulations, the z coordinates of each node in the part were obtained before and after the part is subjected to the chemical milling process. Using MATLAB, the z displacement is found by simply calculating the difference between the values of the z coordinate before and after chemical milling for each node in the part. Subsequently, for each x and y coordinates of a node, a corresponding z displacement is computed. The plot of the z displacement of the entire part is then generated. The next four figures will show the part distortion in terms of the z displacement for each case of chemical milling specifications.

In the first case of chemical milling, a strip made up of 42 elements at the center of the one-quarter symmetry part was chemical milled. (see Figure 5.4) The z displacement of the part subjected to pocket 1 chemical milling specification is shown in Figure 5.7. It shows both the side view of the plot and the three-dimensional view for a better look at the entire part. With this plot, one could see that the maximum distortion of the part is at the edge of the gripper ends, where the z displacement is found to be approximately 2 mm. The distortion at the center of the part is also observed; the magnitude of the z displacement is about 1 mm. However, the distortion at the center of the part is in the opposite direction to the distortion at the perimeter, as indicated by the sign.

The results from the second chemical milling simulation is shown in Figure 5.8. In this simulation, a pocket of larger size (140 elements) than the first pocket, illustrated in Figure 5.4, was chemical milled. Figure 5.8 shows the distortion after chemical milling of this particular part. Similar to the first case, the part distortion is found to occur at the perimeter and at the center of the part. The distortion at the perimeter also has an opposite sign from the distortion at the center of the part. However, the magnitude of the part distortion in this second case is less than the first case by about 0.5 mm to 1.0 mm. It is interesting to note that the profiles of the z displacement of the first two cases of chemical milling are very similar to each other. A possible explanation for this is from the geometry of the two chemical milled pockets, which essentially showed approximately the same amount of section moments removed by the chemical milling process. The area differences between the first and the second pockets do not actually contain a large amount of section moment, which is the reason why the part distortion of the first case of chemical milling is not very different from the second case.

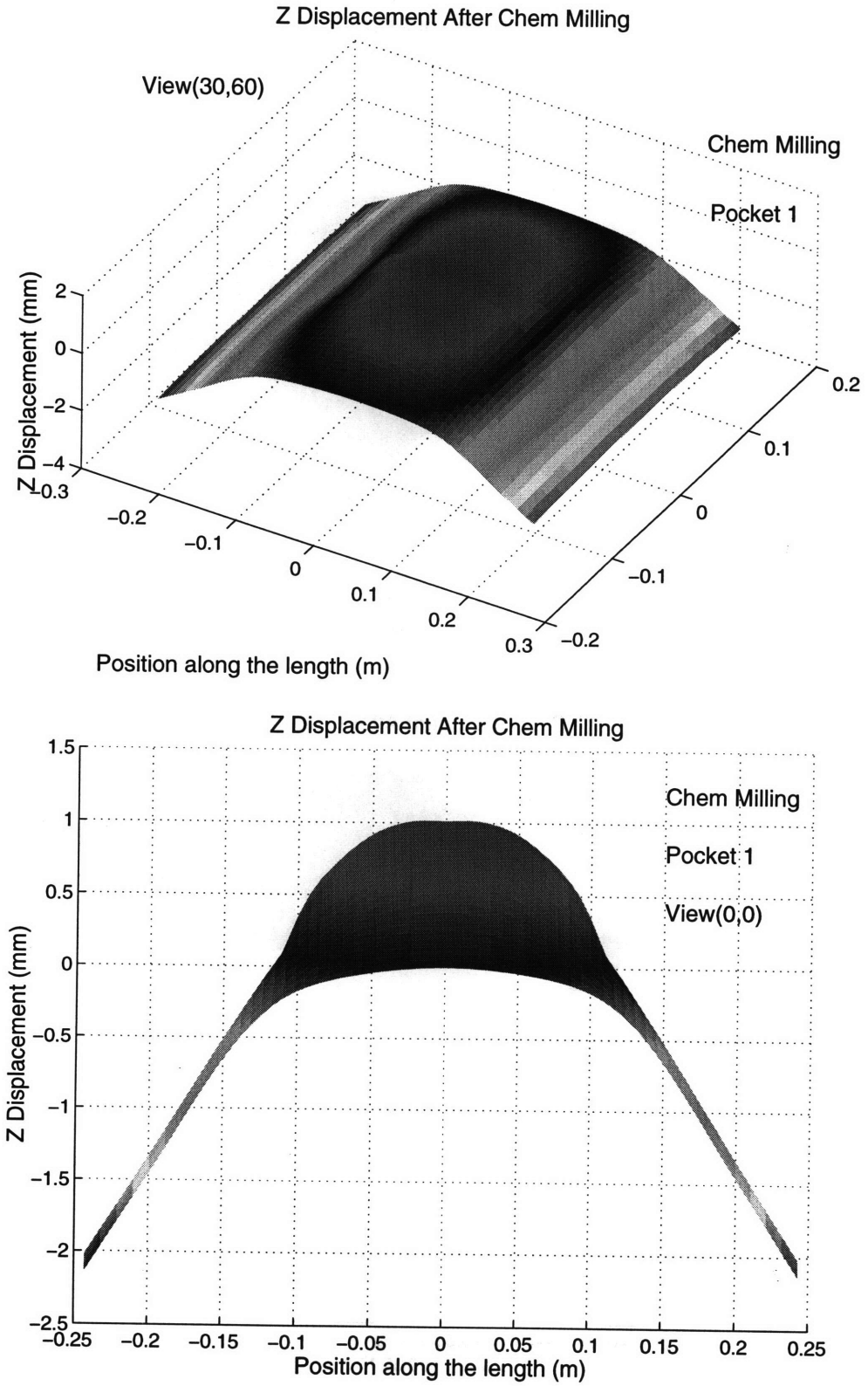

Figure 5.7: Distortion of the saddle-shaped part subjected to pocket 1 chemical milling.

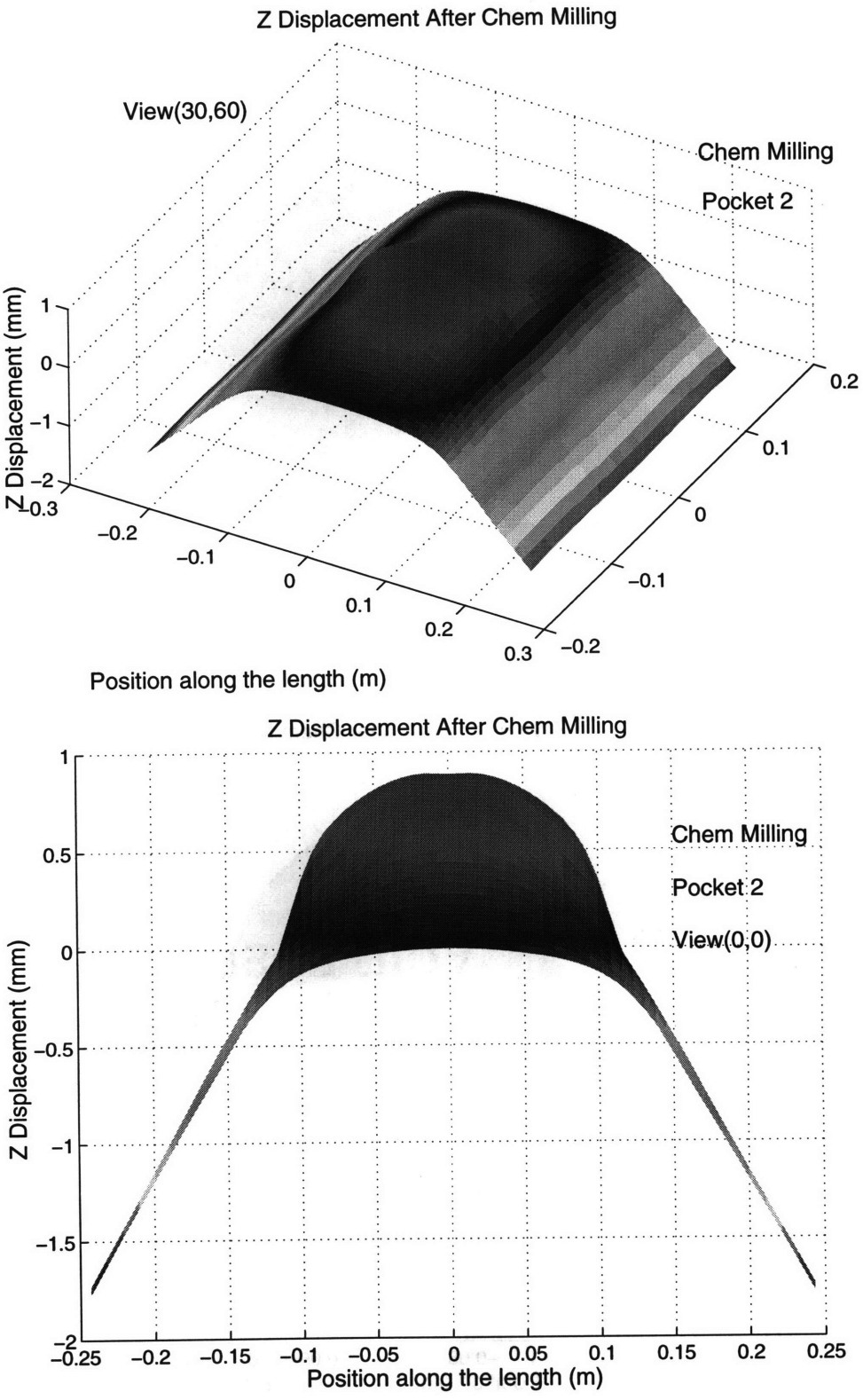

Figure 5.8: Distortion of the saddle-shaped part subjected to pocket 2 chemical milling.

As a matter of fact, the simulation results from the third and fourth cases of chemical milling, as shown in Figures 5.9 and 5.10 respectively, display a similar trend in part distortion as the first and second chemical milling simulations. The geometry and size of the third and fourth pockets are also similar to the first and second pockets; pocket 3 is made up of 36 elements at the center of the part and pocket 4 is made up of 112 elements, also, at the center of the part. (See Figure 5.5) The difference would only be from the fact that pocket 3 and 4 were selected from using the section moment with respect to the 1-axis (the axis along the length of the sheet), rather than the 2-axis (the axis along the width of the sheet) which was used to select the regions for pocket 1 and 2.

The results on the part distortions in the third and fourth chemical milling simulations again indicate that the range of z displacement for the whole part is from -1.2 mm to +0.9 mm from the perimeter of the part to the center. The profiles of the part distortion, however, are a little different than what was observed in the first and second cases of the simulations. Overall, the simulation results demonstrate that the magnitude of the part distortion in the saddle-shaped part is on the order of 2.0 to 3.0 mm. This is very small compared to the size of the part. Physically, this amount of change in part shape is not very conspicuous, especially when the part is on the actual production floor. In addition, one should recognize that this part was formed without any post-stretching, which acts to reduce the amount of springback in the part shape. Therefore, it is reasonable to say that the results from these simulations represent one of the extreme cases in part distortion that would be observed in this type of parts.

However, one of the important goals for the Reconfigurable Tooling for Flexible Fabrication project is to be able to design a die that contains a built-in flexibility capability and also forms a part with a superb accuracy such that the formed part is perfectly fit with others during the assembly. Such high level of accuracy was agreed to be at the part tolerance of plus or minus ten-thousandth of an inch or 0.25 mm. Then, the part distortion in the order of 2.0 mm to 3.0 mm is considered to be significant and the design of the die, as a result, must be corrected to take into account the effect of this part distortion. Another argument is from comparing this part distortion to the sheet thickness. The thickness of the sheet used in these simulations is 1.6 mm and the thickness of the chemical milled regions is 0.8 mm after chemical milling. This comparison shows that the magnitude of the part

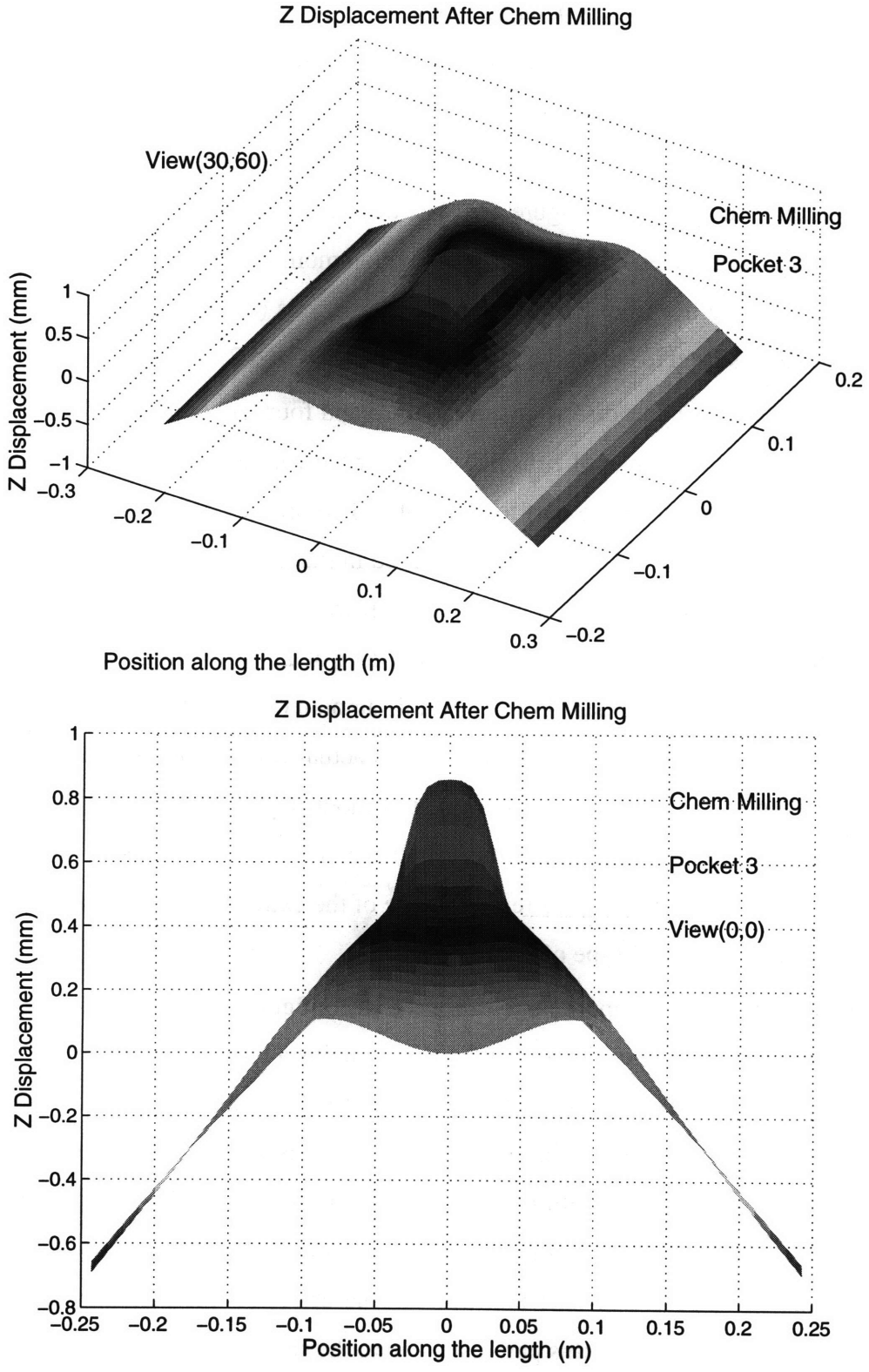

Figure 5.9: Distortion of the saddle-shaped part subjected to pocket 3 chemical milling.

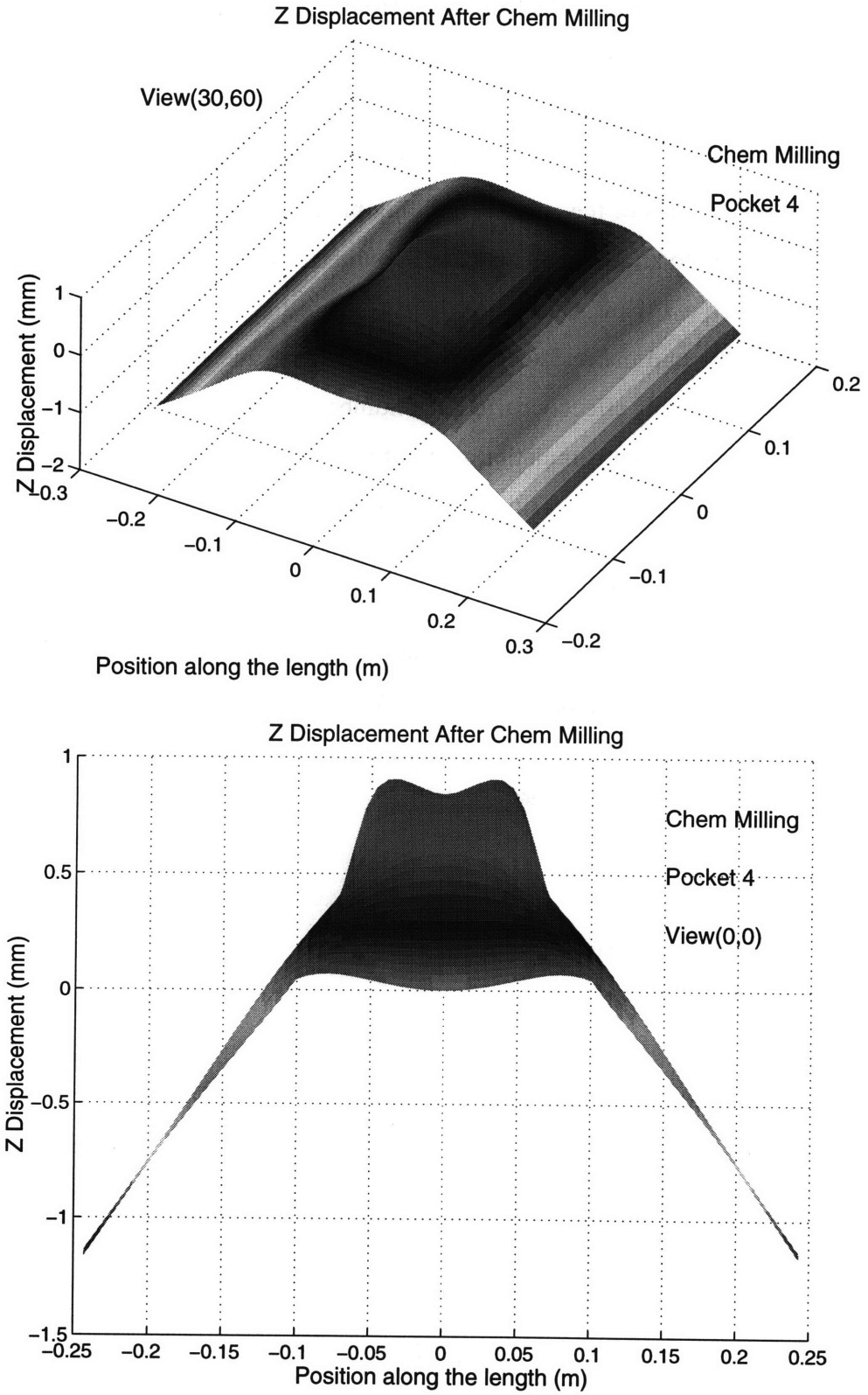

Figure 5.10: Distortion of the saddle-shaped part subjected to pocket 4 chemical milling.

distortion is on the order of the sheet thickness before chemical milling and about twice the sheet thickness after chemical milling. Therefore, we conclude that the effects of chemical milling on the part configuration can be significant and the manufacturing of the aircraft components would be more effective and more accurate if it incorporates the effects of part distortion which resulted from the chemical milling process.

Now that the effects of the chemical milling process and its magnitudes were demonstrated, it is desired to know and understand about the sensitivity of the process. One could ask questions such as, "How sensitive is the part distortion to any variations in the chemical milling process and the residual stresses in the part? and How often and how severe can we expect to see this effect occurred in a number of forming and chemical milling trials?" From a finite element simulation point of view, the results, thus far, seemed to indicate that the part shape is sensitive to the chemical milling process. However, this conclusion is made based on the simulations of only two parts, one of which has a very simple geometry and rough forming and chemical milling specifications while the other is a fictitious part. The amount of data collected thus far is inadequate for us to make any comments on the sensitivity of the process. Additional investigations, simulations, and experimentations should be pursued further if one is to completely understand about the effects of the chemical milling process.

Chapter 6

Incorporating Effects of The Chemical Milling Process To The Die Design

In the previous two chapters, the effects of the chemical milling process were studied through the simulations of the chemical milling of two different part shapes. The simulation results from chemical milling a set of parts of simple geometry and of complex shape indicate a reasonably significant part distortion due to the chemical milling process. The effect of part distortion from chemical milling could reduce the level of accuracy of the final part configuration and, therefore, the precision of the manufacturing process of aircraft components. The overall manufacturing of aircraft components can be greatly improved if the effects of the chemical milling process and other post-forming processes such as the trimming process are incorporated into the initial die design so that the final part shape after forming, trimming, and chemical milling is within the design tolerances and specifications of that particular part. This chapter outlines the methodology which can be used to incorporate these effects from the chemical milling process to determine a better die design. We will analytically describe the concept of this particular methodology in general before focusing on how it could be implemented to the die design that takes into account the effect of the chemical milling process.

6.1 Concept of The Springforward Die Design Algorithm

The technique used in determining the initial die shape in the Reconfigurable Tooling for Flexible Fabrication (RTFF) Project is called the Springforward Algorithm for tooling design, which was developed by Karafillis and Boyce [1] and [2] in 1994. This tooling design algorithm is based on the calculations of an inverse springback. In other words, the main concept of this springforward design algorithm is to reverse the springback phenomenon and to use the information of the unloading moment and the applied load to predict the desired die shape. Figure 6.1 illustrates the fundamental concept underlying the development of this springforward die design algorithm. Essentially, it shows the basic mechanics of the forming and unloading of the sheet.

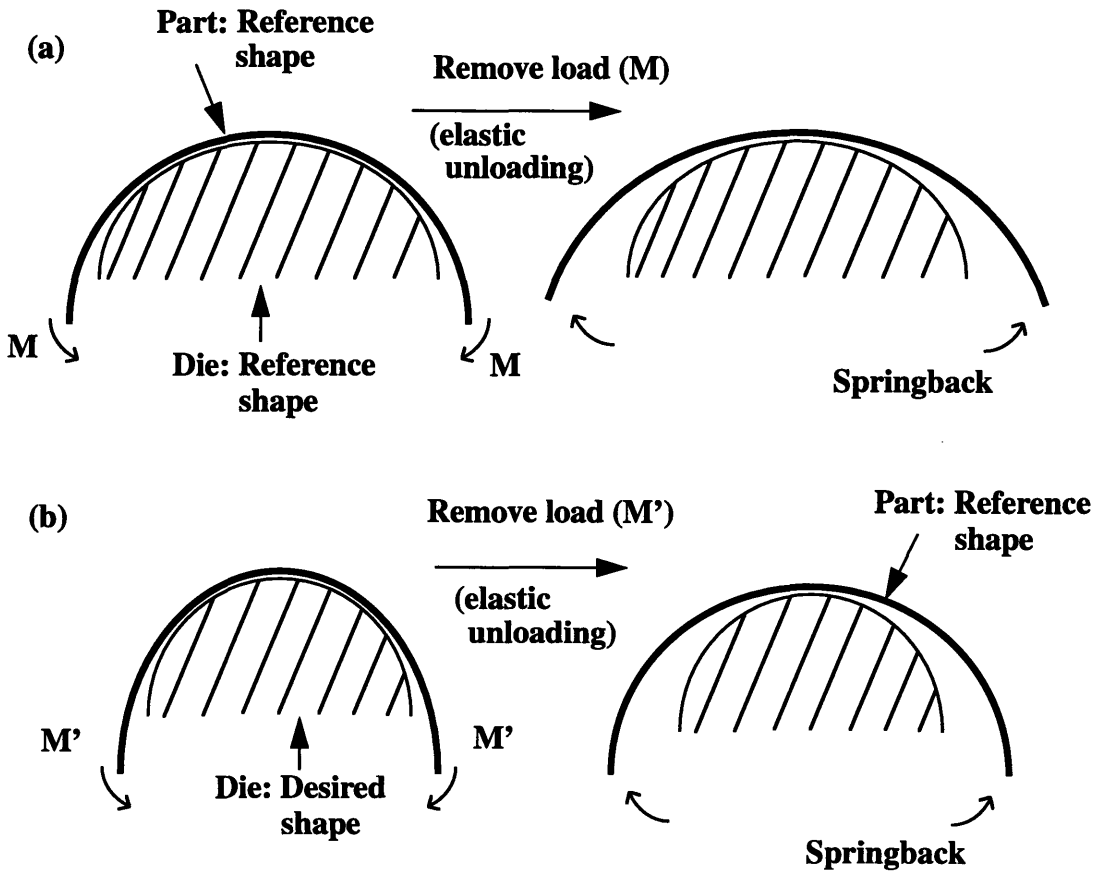

Figure 6.1: Underlying concept of the springforward algorithm.

In figure 6.1 (a), the starting die geometry corresponds to the reference shape or the desired part shape. When the load M is applied to the part to form over the reference die shape. The part conforms to the die and the resulting shape, when the sheet is in the fully loaded state, is the reference part shape. When the load M is removed and the part is subjected to an elastic unloading, the part springs back to a certain curvature which is less than the loaded curvature. Figure 6.1 (b), on the other hand, starts with the die of a desired shape, over which the part is loaded by the moment M'. Upon the elastic unloading of the part, the moment M' is removed and the resulting part curvature after unloading is the reference part shape.

In the springforward algorithm, the idea is to reverse the springback in order to predict the initial desired die shape. This technique is illustrated in Figure 6.2, in which the reference part shape is used as a starting point in the die design. In order to determine the

desired die shape, one can apply the load M', from Figure 6.1, to the reference part shape in an elastic loading manner. Effectively, the reference part shape would "spring forward" to the desired die shape. However, the load M' is not known prior to the die design. Therefore, the method to determine the desired die shape must be achieved iteratively. The process can be summarized as follows. First, the load M, which is applied to the part over the reference die shape, is determined and then applied to the reference part. This first step yields the first die shape, Die_1, to be iterated. This first die shape, Die_1, will not give a desired part shape, but it will produce the part shape which is closer to the desired one. Another part is then formed over the first die shape, Die_1, in order to obtain the load M_1. This load M_1 is then used to apply to the reference shape which would result in the second die shape, Die_2. The second die shape would produce a part shape that is closer to the desired reference part shape. This procedure is iterated for a number of times until the formed part is within the design tolerances and specifications, at which point the desired die shape is comprehended. Convergence is typically obtained in one or two iterations.

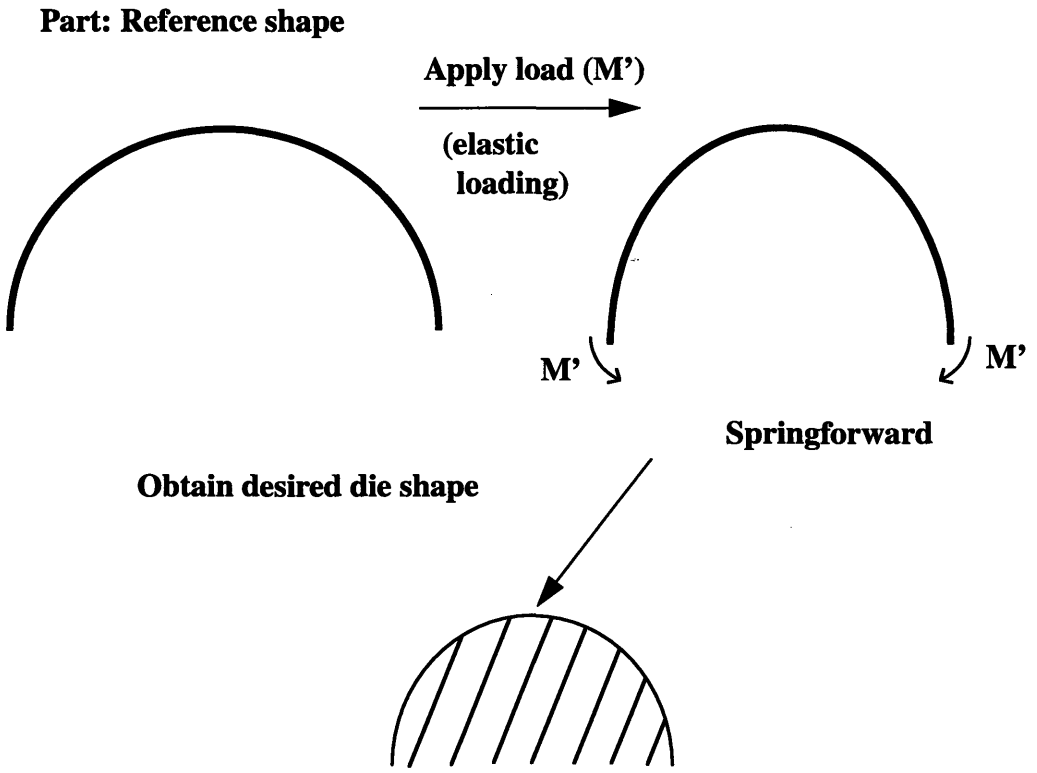

Figure 6.2: Springforward tooling design algorithm.

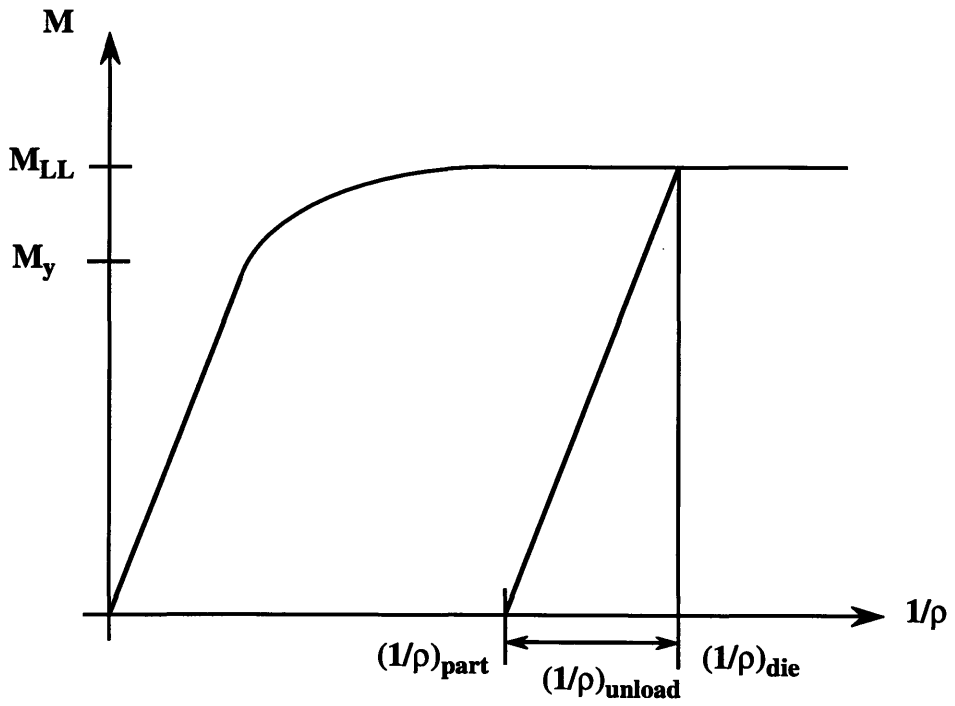

Figure 6.3: Die shape prediction using the moment-curvature diagram.

This concept could also be understood when considering the moment-curvature relationship. The moment-curvature diagram for an *elastic-perfectly plastic* material is shown in Figure 6.3. The part radius or curvature can first be determined from the design specifications. From the basic mechanics of beam bending, as described in details in section 1.3.1, the change of curvature upon unloading can be determined by the relationship between the moment and the curvature.

$$\left(\frac{1}{\rho}\right)_{unload} = \frac{M_{applied}}{EI} \tag{6.1}$$

Furthermore, the springback upon unloading acts to reduce the curvature of the part. Therefore, the curvature (and thus the radius) of the die can be determined by

$$\left(\frac{1}{\rho}\right)_{die} = \left(\frac{1}{\rho}\right)_{part} + \left(\frac{1}{\rho}\right)_{unload} = \left(\frac{1}{\rho}\right)_{part} + \frac{M_{applied}}{EI} \tag{6.2}$$

where $(1/\rho)_{die}$ is the curvature of the die, $(1/\rho)_{part}$ is the desired part curvature, and $(1/\rho)_{unload}$ is the springback of the part. Note that $M_{applied}$ for an elastic-perfectly plastic material is given by

$$M_{applied} = \sigma_y\left[\frac{t^2}{4} - \frac{1}{3}\left(\frac{\sigma_y \rho_{die}}{E}\right)^2\right] \tag{6.3}$$

However, ρ_{die} is unknown. Therefore $M_{applied}$ cannot be found from equation (6.3), and, thus, is an unknown in equation (6.2). In order to obtain ρ_{die}, an iterative process between equation (6.2) and (6.3) must be adopted. To analytically demonstrate the process, a particular example is shown here where a single curvature part of radius ρ_P = 20 cm is to be made from a sheet having the width b = 1 m and the thickness t = 1.6 mm, of which the area moment of inertia is found to be equal to 3.413×10^{-10} m^4. The material behavior of the sheet material is assumed to be elastic-perfectly plastic with the material properties E = 70 GPa and σ_y = 300 MPa. In order to obtain the die shape for manufacturing this particular part, one can begin the iterative process by taking the first die shape to be the shape of the reference part. This yields

$$\frac{1}{\rho_{die(1)}} = \frac{1}{\rho_P} = \frac{1}{0.2\ m} = 5\ \frac{1}{m}$$

The first iteration of the applied moment can be calculated using equation (6.1), since the curvature is still within the linear elastic region of the moment-curvature diagram.

$$M^{(1)}{}_{applied} = \frac{EI}{\rho_{die(1)}} = 120\ N \cdot m \tag{6.4}$$

Then, use equation (6.2) to compute the first iteration on the die shape, which yields

$$\frac{1}{\rho_{die(2)}} = \frac{1}{\rho_P} + \frac{M^{(1)}{}_{applied}}{EI} = 10\ \frac{1}{m} \qquad \therefore \rho_{die(2)} = 0.1\ m = 10cm \tag{6.5}$$

Once the first die shape is obtained, one can return to equation (6.4) to compute the second iteration of the applied moment. Since the curvature is now in the plastic region, equation (6.3) will be used. This is calculated to be

$$M^{(2)}{}_{applied} = \sigma_y\left[\frac{t^2}{4} - \frac{1}{3}\left(\frac{\sigma_y \rho_{die(2)}}{E}\right)^2\right] = 174N \cdot m \tag{6.6}$$

The second iteration on the die shape using equation 6.2 yields

$$\frac{1}{\rho_{die(3)}} = \frac{1}{\rho_P} + \frac{M^{(2)}{}_{applied}}{EI} = 12\ \frac{1}{m} \qquad \therefore \rho_{die(2)} = 0.0815\ m = 8.15cm \tag{6.7}$$

The difference between the first and the second die shape is still significant. Therefore,

another iteration of the die shape is necessary. The third iteration results in

$$M_{applied(3)} = 180\ N \cdot m$$
$$\text{and} \qquad \frac{1}{\rho_{die(4)}} = 13\,\frac{1}{m} \qquad \therefore \rho_{die(4)} = 8cm \tag{6.8}$$

Still, the fourth iteration is necessary. The calculations yield

$$M_{applied(4)} = 180\ N \cdot m$$
$$\text{and} \qquad \frac{1}{\rho_{die(5)}} = 13\,\frac{1}{m} \qquad \therefore \rho_{die(5)} = 8cm \tag{6.9}$$

Equivalence between the third and the fourth die shape signifies the convergence of the calculations for the required die shape. Therefore, in order to form the part having a radius of curvature of 20 cm, the die shape of 8 cm-radius is required.

6.2 Application of The Springforward Algorithm To The Die Design With The Effects of Chemical Milling

As mentioned earlier at the beginning of this chapter, the level of accuracy of the final part shape can be significantly improved when the effects of the chemical milling process are incorporated into the die design. The goal is to be able to account for any part distortions due to chemical milling in the die design such that the resulting die produces a desired part shape after both the stretch forming and the chemical milling process. A similar method as the springforward tooling design algorithm described in the previous section could be used as a tool to incorporate these effects from the post-forming operations into the die design. In this section, a general approach in analytical forms will be presented. The work in numerical simulations is left to be completed in the future.

The schematic of the technique used in implementing the springforward algorithm to incorporate the effects of the chemical milling process in the die design is depicted in Figure 6.4. Clearly, the underlying concept illustrated in Figure 6.4 is the same as that of the springforward algorithm. The main objective is essentially to design the die that compensates for the effective moment removed as a result of the material removal in the chemical milling process. The basic mechanics of the chemical milling process in section 1.3.2 illustrate that the re-equilibration of the residual stress in the sheet could result in the change of part shape. The part distortion is, in essence, equivalent to removing the effec-

tive load M_{cm} from the part. This "springback" from chemical milling is shown in Figure 6.4.

Since the residual stress in the sheet before chemical milling and the chemical milling specifications for the particular part are known, the effective load removed M_{cm} can be readily determined. Therefore, in order to evaluate the final die shape which takes into account the effects from the chemical milling process, the effective load M_{cm} is applied to the first die shape that was obtained from figure 6.2. The elastic loading of M_{cm} would result in the desired die shape, which produces the reference part shape after the forming and the chemical milling process. With this die design methodology, the effectiveness of the manufacturing process of aircraft components can be significantly improved.

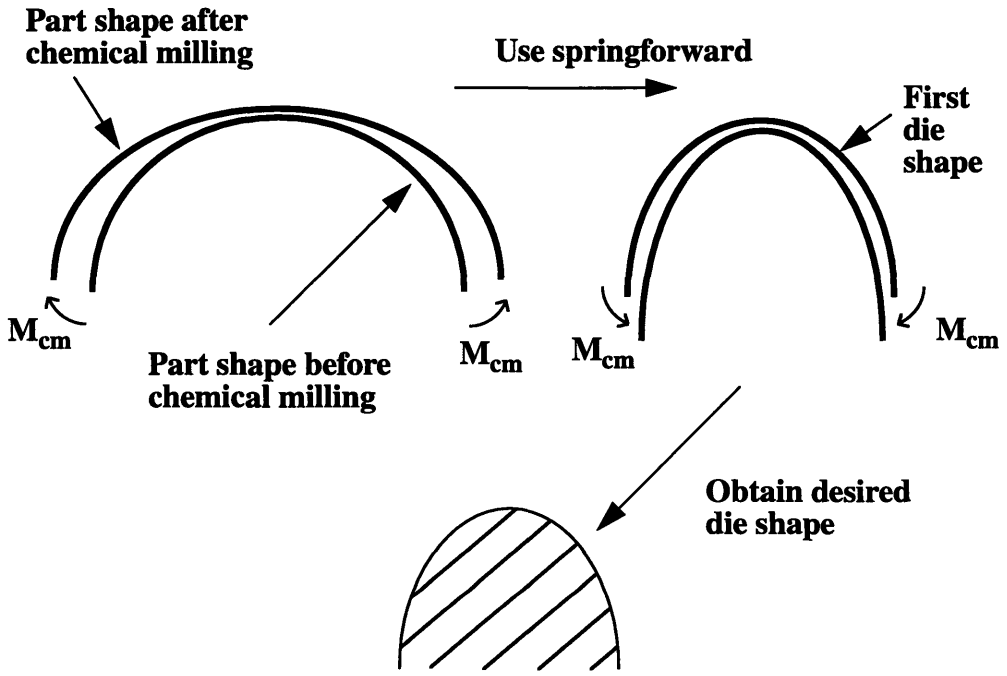

Figure 6.4: The integration of the effects of the chemical milling process in the final die design through the implementation of the Springforward algorithm.

Analytically, it can be shown that, by incorporating the effects of the chemical milling process to the die design, the accuracy of the final part shape produced is greatly increased. According to the derivation in Section 1.3.1, the change in curvature $\frac{1}{\rho_{ul1}}$ recovered from the unloading of the sheet was found to be equal to $\frac{M_{bend}}{EI}$. Similarly, the change of curvature $\frac{1}{\rho_{ul2}}$ recovered from the chemical milling is equivalent to $\frac{M_{cm}}{EI_{new}}$, where M_{cm} is

the effective moment to be removed from the chemical milled sheet and I_{new} is the area moment of inertia of the chemical milled sheet. After the sheet is chemically milled, the final part shape deviates from the reference part shape. Therefore, the die shape needs to be modified in order to compensate for the part distortion from chemical milling.

The shape of the new die incorporates the effect of the chemical milling process by including the change of part curvature $\frac{1}{\rho_{ul2}}$ into the final die design such that

$$\frac{1}{\rho_{die2}} = \frac{1}{\rho_{die1}} + \frac{1}{\rho_{ul2}} \tag{6.10}$$

With the new die shape retaining a curvature of $\frac{1}{\rho_{die2}}$, the sheet is initially unloaded to a curvature $\frac{1}{\rho_{P'}}$, which does not correspond to the reference part shape. However, when the part is chemically milled, the effects of chemical milling cause the part to distort. Since the die already takes into account the effect of part distortion from chemical milling, the final part shape after chemical milling is essentially the reference part shape.

To analytically demonstrate this concept, the part from the example described in section 6.1 is chemical milled. The chemical milling specification is such that a quarter of the sheet thickness of the entire part is removed. This results in a new sheet thickness of 1.2 mm, which yields the new area moment of inertia to be equal to 1.44×10^{-10} m^4. From the Appendix A, the effective moment removed due to chemical milling M_{cm} is found to be

$$M_{cm} = \frac{5}{144}\sigma_y h^2 = 15\,\frac{1}{m} \tag{6.11}$$

The change of curvature recovered from chemical milling $\frac{1}{\rho_{ul2}}$ is computed using equation (6.1), which yields

$$\frac{1}{\rho_{ul2}} = \frac{M_{cm}}{EI_{new}} = 1.5\,\frac{1}{m} \tag{6.12}$$

Then, using equation (6.10) to calculate the new die shape:

$$\frac{1}{\rho_{die2}} = \frac{1}{\rho_{die1}} + \frac{1}{\rho_{ul2}} = 14.04\,\frac{1}{m} \qquad \therefore \rho_{die2} = 7.1cm \tag{6.13}$$

When the forming process begins with this die shape ρ_{die2}, the applied moment in the loaded configuration can be calculated using equation (6.3).

$$M_{loaded} = \sigma_y\left[\frac{t^2}{4} - \frac{1}{3}\left(\frac{\sigma_y \rho_{die2}}{E}\right)^2\right] = 183\ N \cdot m \tag{6.14}$$

The change of curvature during unloading of the sheet is found to be

$$\frac{1}{\rho_{ul}} = -\frac{M_{loaded}}{EI} = -7.6\,\frac{1}{m} \tag{6.15}$$

Therefore, the part shape obtained from bending the sheet over this die shape is

$$\frac{1}{\rho_{P1}} = \frac{1}{\rho_L} + \frac{1}{\rho_{ul}} = \frac{1}{\rho_{die2}} + \frac{1}{\rho_{ul}} = 6.4\,\frac{1}{m}$$
$$\therefore \rho_{P1} = 15.7cm \tag{6.16}$$

As expected, this first part shape does not correspond to the desired part shape. It is then chemical milled with the chemical milling specification of removing one-quarter of the sheet-thickness. Using equation (6.11) for the effective moment removed and equation (6.12) for the change of curvature due to chemical milling, the final part shape can be calculated and is found to be

$$\frac{1}{\rho_{P2}} = \frac{1}{\rho_{P1}} - \frac{1}{\rho_{ul2}} = 6.4\frac{1}{m} - 1.5\frac{1}{m} = 4.9\,\frac{1}{m}$$
$$\therefore \rho_{P2} = 20.2cm \tag{6.17}$$

As a result, the part shape after chemical milling is within close proximity to the desired part shape. This simple calculations illustrates that the die design that incorporates the effects of the chemical milling process yields an accurate final part shape.

Chapter 7

Conclusion

The manufacturing process of most aircraft sheet metal components consists mainly of the stretch forming process and a number of post-forming operations such as the trimming and the chemical milling process. In the stretch forming process, a sheet metal is stretched over a die such that the sheet metal retains a certain part curvature according to the design specifications. Due to the elastic recovery aspect of the material behavior, the design of the die is required to compensate for any springback of the sheet. And, because of a low production volume of aircraft components, the design and production of these dies become a major part of the overall cost in the manufacturing process of aircraft structures. As a result, MIT, Northrop Grumman Corporation and Cyril Bath partake in a research effort to develop a new and advanced technology which utilizes finite element analysis, a new adaptive tooling design coupled with a feedback control capability, and a rapid 3-D shape measurement in order to improve the productivity and efficiency of the manufacturing process of aircraft components, particularly the stretch forming process. With this technology, the productivity of the manufacturing process can be improved considerably and the manufacturing costs in terms of both time and money are significantly reduced.

After the stretch forming process is completed, the sheet metal has to be processed through a number of post-forming operations, namely the trimming and the chemical milling process, before it is ready to be assembled. The chemical milling process, in particular, appears to affect the productivity of the overall manufacturing process because of its potential in causing part distortion. Therefore, the current research presented in this thesis focuses mainly in studying the effects of the chemical milling process on the final part configuration. The objective is to model the chemical milling process using finite element analysis in order to predict the part distortion due to chemical milling. And, by using a similar technique as the springforward tooling design algorithm developed by Karafillis and Boyce [1] and [2], the effects of the chemical milling process can be incorporated into the die design which would help increase the level of accuracy of the manufacturing process of aircraft sheet metal components.

The chemical milling process is essentially a material removal process through chemical reactions with the sheet material. The primary objective is to reduce the weight of the aircraft components by selectively thinning the sheet material from the areas in which it is not structurally required in the final part, thereby maintaining the structural strength and integrity of the part. When the sheet material is removed from the part during chemical milling, the residual stress in the part is, in essence, changed which, as a result, requires the stress to re-equilibrate. The re-equilibration of the residual stress in the sheet often causes the part to distort to an undesired configuration. Realizing the importance of the state of the residual stress in the sheet before chemical milling, the developed algorithm in simulating the chemical milling process places a substantial emphasis in replicating the residual stress in the chemical milled sheet before re-equilibration.

The model of the chemical milling process includes the simulations of both the stretch forming process and the chemical milling process. From the sensitivity study of different types of element formulations, shell elements are selected to be used in modeling the sheet because of its ability to accurately capture the residual stress distribution and part curvature after chemical milling. In addition, simulations using shell elements prove to be reasonably efficient in terms of required computing time and memory. The simulation of the chemical milling process commences by regenerating the sheet in its unloading configuration as a starting geometry and imposing the residual stress in the sheet. ABAQUS supported "user subroutine" is used to develop an algorithm to simulate the imposition of the residual stress in the sheet. In this algorithm, the residual stress in the part is first obtained from the unloaded state of the sheet, and is then imposed to all elements and element integration points, according to the chemical milling specifications. For each chemical milled element, however, the imposition of residual stress is required to take into account the modification of the stress distribution in the sheet as a result of the removal of material thickness. The modification or mapping of the residual stress distribution in the chemical milled regions is achieved through a curve fitting method of the data of stresses. This algorithm also has a capability to distinguish between chemical milled elements from non-chemical milled elements, thus allowing the user to simulate the actual selective chemical milling process of any parts and components.

After the technique to simulate the chemical milling process is developed, a simple case of simulation is conducted to compare the simulation results to the analytical results. This is the case which involves a simple sheet and die geometry, a linear material behavior such as that of the elastic-perfectly plastic material, and a simple loading condition. The analytical solutions of the forming process and the chemical milling process are derived and the resulting stress distributions through the sheet thickness are plotted against the results obtained from the simulations. The comparison between the analytical solutions and the simulation results showed that the simulation results accurately match the analytical results.

In order to further investigate the predictive capabilities of the simulation methodology, a number of experiments are carried out and the experimental results are compared with the simulation results. In this comparison, parts of simple geometry are formed and chemically milled. Simulations of the forming and the chemical milling process of this particular set of parts are also conducted. The chemical milling specifications of these parts vary such that the effect of removing different material thicknesses and different locations in the part can be studied. The profiles of the part shape after forming and chemical milling as obtained from simulations are compared with the experimental results. Overall, the comparison between the simulation and experimental results showed an excellent predictive capability of the simulations in modeling the forming and the chemical milling process. Both simulation and experimental results also showed the effect of chemical milling different sheet thicknesses and locations in the part. The effect of part distortion is found to be proportional to the amount of material removed, both in terms of the material thickness and the area of the chemical milled region.

In the actual stretch forming process of aircraft sheet metal components, the sheet is often post-stretched after it is formed. The post-stretching of the sheet, when implemented properly, wipes out the stress distribution through the sheet thickness, making the stress through the thickness constant, and thus eliminating any bending moment. This manufacturing scheme using the post-stretch is the most effective when the part shape is simple. For a more complicated part shape, the residual stress associated with moment recovery is not as easily eliminated by the post-stretching of the sheet because of the geometric con-

straints. Therefore, it can be deduced that the effects of part distortion due to chemical milling of a more complex part shape could be significant.

Consequently, the chemical milling of a part with complex geometry is simulated. A saddle shape is selected for this particular case study because of its characteristics in double curvature. Several chemical milling specifications are imposed to the saddle-shaped part in the chemical milling simulations. The results obtained from the simulations showed that the effects of part distortion due to chemical milling are found to be significant, when considering the target design tolerance set by the industry. If the part distortion incurred by the chemical milling process is taken into account early on in the design stage of the die, the overall manufacturing process of aircraft sheet metal components can be significantly improved.

A similar method as the springforward tooling design algorithm can be implemented to the die design in order to incorporate any effects from the post-forming operations, especially the chemical milling process. The fundamental concept of this technique is based on the design of a die shape that compensates the effective load to be removed, thus the change of part curvature, from the chemical milled sheet. With this technique, a convergence of the desired die shape which would produce a correct part reference shape after the forming and the chemical milling process can be obtained after a few number of iterations. The algorithm has been analytically demonstrated on simple curvature parts. The development of this algorithm to incorporate the effects of the chemical milling process into the die design for complex shapes utilizing finite element analysis, however, is not completed. Several matters need to be considered, in terms of examining the issues of mapping the applied load from a final part shape to the formed sheet and the transformation of the meshing of a part to a sheet. Essentially, more research is required to develop this algorithm numerically and to implement it in the closed loop die design.

Appendix A

Analytical Solutions For The Cases of Chemical Milling Different Sheet Thicknesses

In Chapter 1, a closed form solution of the chemical milling process for removing one-half the sheet thickness of the entire part was derived. In addition to the solution presented in Chapter 1, a closed form solution of the case of chemical milling one-quarter of the sheet thickness will be described in this appendix. It will also follow from the analysis of the forming process shown in Section 1.3.1. In other words, the same forming process as the one discussed in Section 1.3.1 is used to obtain the residual stress state in the sheet prior to chemical milling. As one could recall from the discussion of the stretch forming process in Chapter 1, the residual stress distribution in the sheet after forming is expressed by equation (1.9) as

$$\sigma_{r1} = \begin{cases} \left(1 - \frac{3}{t}y\right)\sigma_y & ,0 < y \le \frac{t}{2} \\ \left(-1 - \frac{3}{t}y\right)\sigma_y & ,-\frac{t}{2} \le y < 0 \end{cases}$$

where y is the position through the thickness of the sheet, t is the original sheet thickness, and σ_y is the tensile yield stress of the sheet material. The corresponding plot of the residual stress distribution is depicted in Figure A.1.

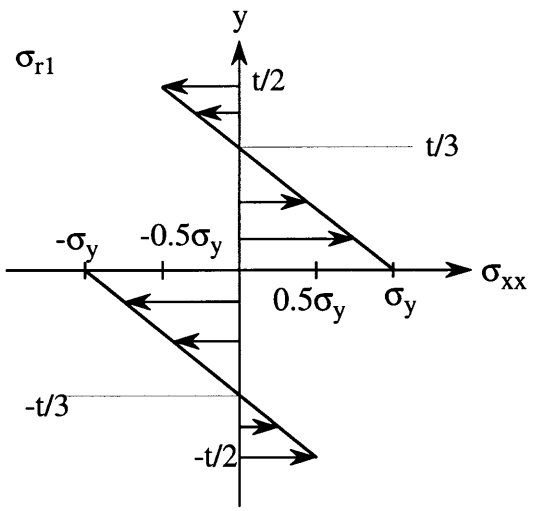

Figure A.1: Normal residual stress distribution, σ_{r1}, in the sheet before chemical milling.

A specific case of chemical milling one-quarter the sheet thickness on the inside of the entire part will be considered. This is corresponding to a removal of the material below the neutral axis; the stress distribution in the sheet after the material is removed and before the sheet is allowed to re-equilibrate is shown in Figure A.2.

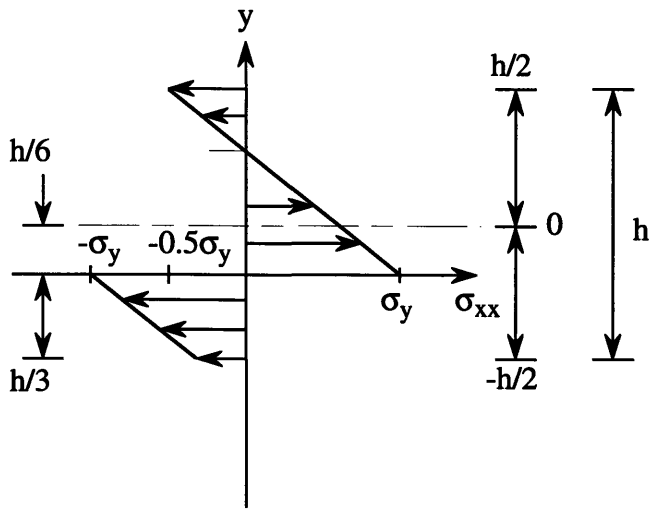

Figure A.2: Normal residual stress distribution before the sheet re-equilibrates from chemical milling. One-quarter of the sheet thickness is removed.

After chemical milling, the new thickness of the sheet h is equal to $\frac{3}{4}t$, where t is the original sheet thickness. The neutral axis of the sheet is also shifted as a result of chemical milling; its new location is assumed to be at $h = 0$, the center of the new sheet thickness. In order to express the stress distribution in Figure A.2 in term of the new sheet thickness h, a simple equation of a straight line is used. Essentially, the stress distribution consists of two straight lines, one above the original neutral axis and one below the original neutral axis. For the line above the original neutral axis $-\frac{h}{6} < y \leq \frac{h}{2}$, using the two data points

$$\sigma_{xx}\left(y = \frac{h}{2}\right) = -\frac{\sigma_y}{2} \text{ and } \sigma_{xx}\left(y = -\frac{h}{6}\right) = \sigma_y$$

to obtain the values for m and b in the line equation $y = m\sigma_x + b$ and the stress distribution above the original neutral axis is found to be

$$y = -\frac{4}{9}\frac{h}{\sigma_y}\sigma_{xx} + \frac{5}{18}h$$

$$\text{or } \sigma_{xx} = -\frac{9\sigma_y}{4h}y + \frac{5}{8}\sigma_y \qquad ,-\frac{h}{6} < y \le \frac{h}{2} \tag{A.1}$$

Similarly, for the line below the neutral axis, the two data points are

$$\sigma_{xx}\left(y = -\frac{h}{6}\right) = -\sigma_y \text{ and } \sigma_{xx}\left(y = -\frac{h}{2}\right) = -\frac{1}{4}\sigma_y$$

which will give the expression for the stress distribution below the neutral axis as

$$y = -\frac{4}{9}\frac{h}{\sigma_y}\sigma_{xx} - \frac{11}{18}h$$

$$\text{or } \sigma_{xx} = -\frac{9\sigma_y}{4h}y - \frac{11}{8}\sigma_y \qquad ,-\frac{h}{2} \le y < -\frac{h}{6} \tag{A.2}$$

The force equilibrium condition needs to be satisfied, hence,

$$\sum F = \left[-\frac{1}{2}\frac{\sigma_y}{2}\left(\frac{2}{9}h\right) + \frac{1}{2}\sigma_y\left(\frac{4}{9}h\right)\right] + \left[-\frac{1}{2}\frac{3\sigma_y}{4}\left(\frac{1}{3}h\right) - \frac{\sigma_y}{4}\left(\frac{1}{3}h\right)\right] + f = 0$$

$$\therefore f = \frac{1}{24}h\sigma_y \tag{A.3}$$

A fictitious force f is required to balance the force equilibrium equation. This force corresponds to a normal stress of

$$\sigma_f = \frac{1}{24}\sigma_y \tag{A.4}$$

For the moment equilibrium condition, first using the expression for the stress distribution in equations A.1 and A.2 and integrate them with respect to y, we obtain

$$M_{chem'} = \int_{-\frac{h}{2}}^{-\frac{h}{6}}\left(-\frac{9\sigma_y}{4h}y - \frac{11}{8}\sigma_y\right)y(1)dy + \int_{-\frac{h}{6}}^{\frac{h}{2}}\left(-\frac{9\sigma_y}{4h}y + \frac{5}{8}\sigma_y\right)y(1)dy$$

$$= -\frac{3\sigma_y}{4h}y^3 - \frac{11}{16}\sigma_y y^2\Big|_{-\frac{h}{2}}^{-\frac{h}{6}} + \left(-\frac{3}{4}\right)\frac{\sigma_y}{h}y^3 + \frac{5}{16}\sigma_y y^2\Big|_{-\frac{h}{6}}^{\frac{h}{2}} = -\frac{5}{144}\sigma_y h^2 \tag{A.5}$$

Then when considering the equation for moment equilibrium, it is apparent that the moment in the sheet is not zero. Hence, an unloading moment is required.

$$\sum M = M_{chem'} + M_{unload3} = 0 \qquad \therefore M_{unload3} = -M_{chem'} = \frac{5}{144}\sigma_y h^2 \tag{A.6}$$

This unloading moment $M_{unload3}$ is equal to a normal stress of

$$\sigma_{unload3} = \frac{M_{unload3}y}{I_{new2}} = \frac{5}{12}\frac{\sigma_y}{h}y \tag{A.7}$$

where I_{new2} is the moment of inertia of the sheet after chemical milling. Finally, the residual stress in the sheet after removing one-quarter of the sheet thickness is calculated by simply superposing the residual stress in the sheet before chemical milling with the stress required to balance the force and moment equilibrium equations.

$$\sigma_{r3} = \begin{cases} -\frac{9\sigma_y}{4h}y + \frac{5}{8}\sigma_y + \frac{5}{12}\frac{\sigma_y}{h}y + \frac{1}{24}\sigma_y & ,-\frac{h}{6} < y \le \frac{h}{2} \\ -\frac{9\sigma_y}{4h}y - \frac{11}{8}\sigma_y + \frac{5}{12}\frac{\sigma_y}{h}y + \frac{1}{24}\sigma_y & ,-\frac{h}{2} \le y < -\frac{h}{6} \end{cases}$$

$$= \begin{cases} -\frac{11\sigma_y}{6h}y + \frac{2}{3}\sigma_y & ,-\frac{h}{6} < y \le \frac{h}{2} \\ -\frac{11\sigma_y}{6h}y - \frac{4}{3}\sigma_y & ,-\frac{h}{2} \le y < -\frac{h}{6} \end{cases} \qquad \text{(A.8)}$$

This final residual stress distribution is depicted in Figure A.3

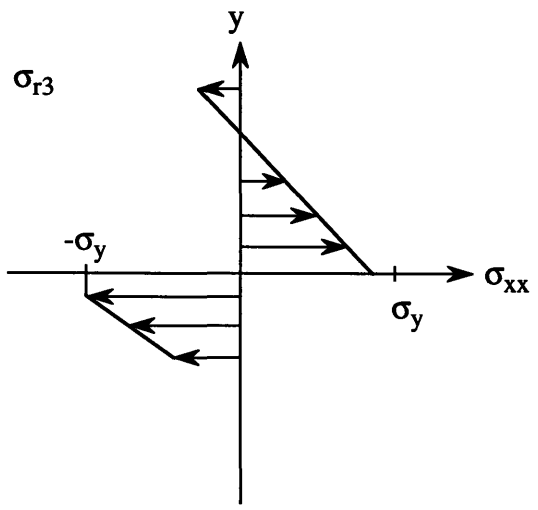

Figure A.3: Final residual stress distribution after chemical one-quarter of the sheet thickness on the inside of the part.

Appendix B

Simulations of Chemical Milling Using Continuum Elements and The Effects of Element Aspect Ratio on Results

B.1 Motivation

From the study of the capabilities of different finite element formulations in Chapter 2, it appears that both continuum elements and shell elements are suitable for the modeling of the stretch forming process. Shell elements appear to be more suitable for modeling complex three-dimensional shapes and problems of high bending stress such as that of the stretch forming process. Because of the nature of the stretch forming process, it is then possible that shell elements might produce more accurate results than continuum elements. For the simulation of the chemical milling process, however, the use of continuum elements, at a first glance, seems to be more appropriate. With continuum elements, the chemical milling process is easily simulated using ABAQUS Element Removal option, which allows the user to remove selected elements in the mesh. Since the nature of the chemical milling process is the removal of material, this option provides a perfect scheme in the modeling of the process.

The use of continuum elements also has several additional advantages over the use of shell elements in the simulation of the chemical milling process. With continuum elements, contour plots of stress and strain distribution through the sheet thickness are readily available. Furthermore, a complex etched geometry can be modeled with relative ease. The modeling of a fillet radius at the corners of an etched pocket is achieved by simply refining the mesh in that region and selectively removing elements as to create a rounding effect of a corner. This modeling concept of mesh refinement is depicted in Figure B.1. Because of the aforementioned arguments, a study to investigate the possibility of modeling the chemical milling process utilizing continuum elements is first conducted and presented in this appendix.

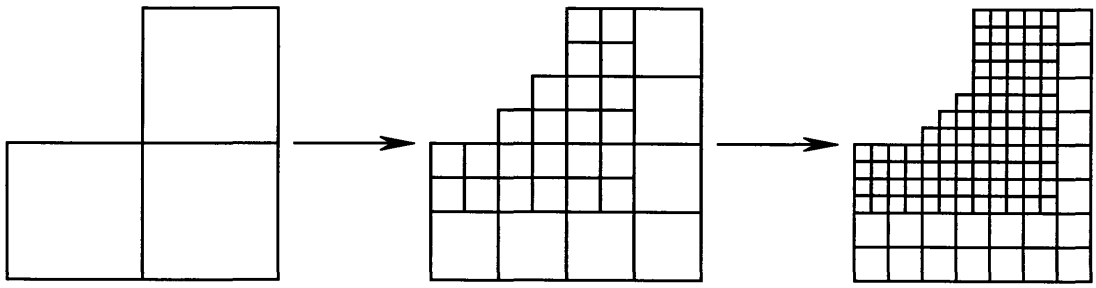

Figure B.1: Modeling of a fillet radius at the corners of an etched pocket through mesh refinement.

B.2 Sensitivity Study

Here, a sensitivity study aimed at investigating the mesh configuration and density required to effectively predict the effect of the chemical milling process is presented. First, a study which shows that the aspect ratio of continuum elements plays an important role in the level of accuracy of the simulation results is described.

B.2.1 Setup Conditions and Modeling Parameters

In the sensitivity study of element aspect ratio, the basic approach is to simulate the problem where the part is small and the chemical milling geometry is simple. The simulation of interest is the one for which a strip of sheet, having a dimension of 0.1 m x 6.35 mm (4.0" x 0.25") and 1.6 mm (0.063") thickness, is wrapped (without stretching) over a 5.1 cm (2.0") smooth, rigid, cylindrical die. This strip of sheet is modeled so that it has an elastic-perfectly plastic material property, with a Young's modulus E of 68.9 GPa and a yield strength σ_y of 76.1 MPa. In doing so, the simulation results can be easily compared with the analytical solution of the problem to evaluate the level of accuracy of the chosen algorithm. The loading condition on this strip is such that the region of the strip in contact with the die has fully yielded. In this particular case, the strip is wrapped to approximately 36 degrees in the clockwise direction. The simulation conditions are summarized and depicted in Figure B.2.

The strip is modeled with the first-order plane strain continuum elements (ABAQUS type CPE4). The varying parameter of this sensitivity study is the aspect ratio of the continuum elements used in the modeling of the strip; the number of elements through the

thickness of the sheet is fixed to ten elements while the number of elements along the length of the strip is varied so that the aspect ratio alters from 1:10 to 1:1. The varying element aspect ratios and their corresponding element density and configuration are summarized in table B.1. Other modeling parameters associated with the contact between the strip and the die are the same as those previously used in the study of effect of friction at the sheet-die interface in Chapter 2. Readers are referred to Section 2.3.1 and the ABAQUS/Standard User's Manual for more detailed discussion on the modeling of the contact problem. In this particular study, however, the contact between the strip and the die is modeled as having zero friction.

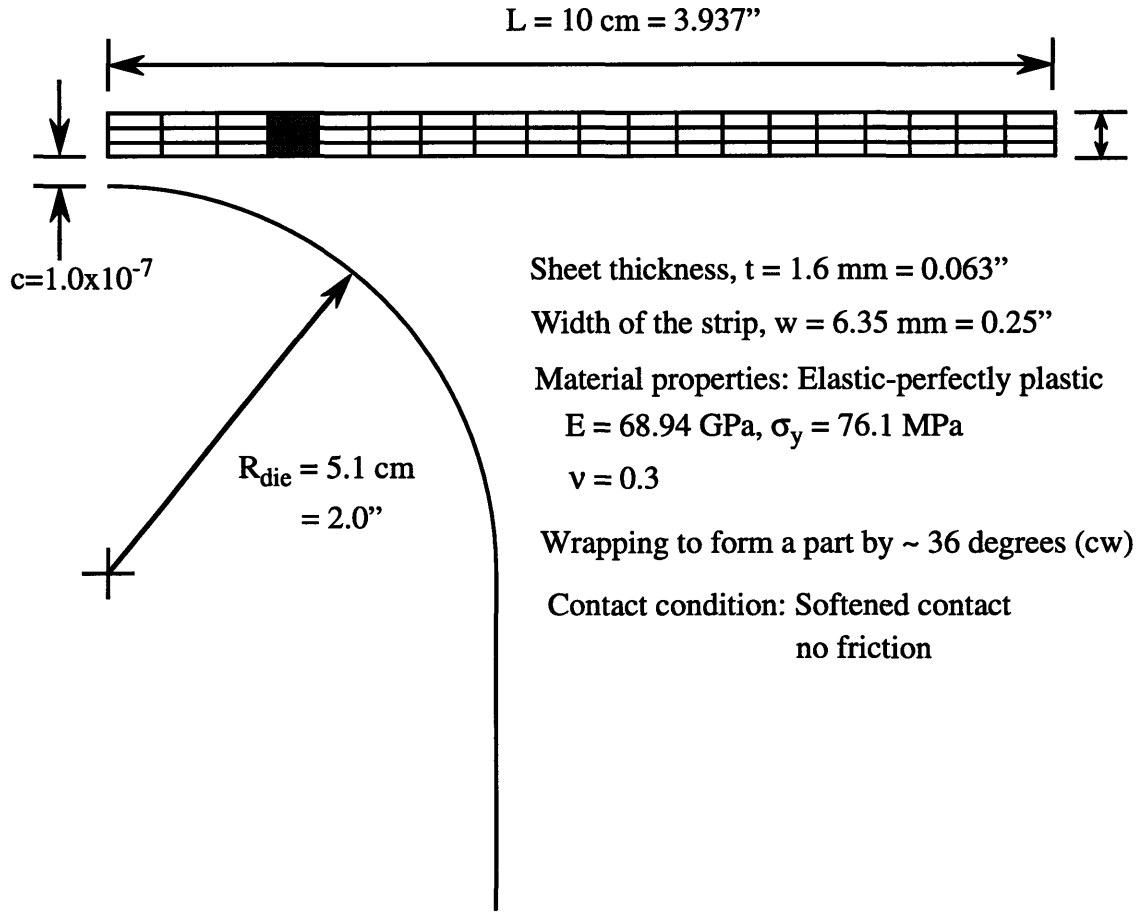

Figure B.2: Setup conditions used in the sensitivity study of CPE4 aspect ratio.

Element Aspect Ratio	Number of elements along the length of the strip	Number of elements through the thickness of the strip	Total number of elements used in modeling the strip
1:1	625	10	6250
1:3	208	10	2080
1:6	104	10	1040
1:10	63	10	630

Table B.1: Varying element aspect ratio and corresponding mesh configuration.

After the strip is formed and unloaded to its final equilibrium state, the chemical milling process of the strip is then simulated. The chemical milling specification is such that the entire one-half of the strip original thickness, 0.8 mm (0.32"), is to be removed. The main reason for selecting this chemical milling specification is that the analytical solution can be easily compared with the simulation results. As mentioned earlier, the modeling technique used in simulating the chemical milling process, when continuum elements are used to model the sheet, is through the use of ABAQUS Element Removal option. In this set of simulations, a set of selected elements, forming the bottom portion of the entire strip, is removed, while all the nodes in the model are constrained from all displacements and rotations. Essentially, the remaining part of the strip is prevented from re-equilibrating at the step of element removal. After the elements are removed, the constraints are removed and the strip is then allowed to re-equilibrate to compensate for the change in the residual stresses in the part.

B.2.2. Results From Element Sensitivity Study

The finite element simulations provide a tremendous amount of information in terms of stress and strain distribution in the part, and the change of a part shape. In this sensitivity study, the profiles of bending stress distribution through the sheet thickness will be considered. The information pertaining to the stresses in the strip will be taken from the shaded region depicted in Figure B.2. This is the region in which the strip is in full contact with the die and is fully yielded during the forming step of the simulation.

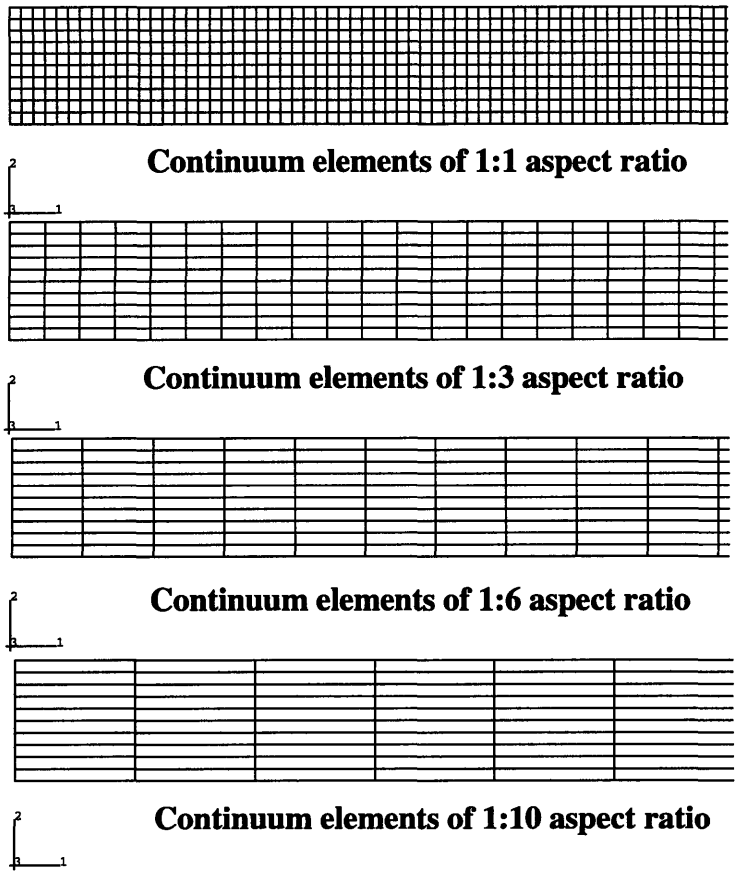

Figure B.3: Elements with different aspect ratios used in this sensitivity study.

The comparison of the through-thickness stress distributions between simulations of elements with different aspect ratios will be analyzed. Particularly, the simulations with continuum elements of 1:10, 1:6, 1:3, and, finally, 1:1 aspect ratio, constitute this sensitivity study. The drawings of continuum elements of different aspect ratios used in this case study are shown in Figure B.3. These results will also be plotted against the stress profiles as predicted by the analytical solutions derived in Section 1.3.1 and 1.3.2. Figure B.4 shows the loading stress distribution through the sheet thickness during forming. The solid line represents the stress distribution in the sheet according to the analytical solution, while different symbols identify stress data points as obtained from Gaussian integration points of continuum elements with different aspect ratios. The stress distribution in Figure B.4 indicates a fully plastic bending in the sheet during forming. The results show that when aspect ratio of the continuum elements is 1:1, the sheet has yielded at about the

material yield stress of 76.1 MPa. But when the element aspect ratio changes to 1:10, the sheet appears to exhibit plastic flow of a stress level of 60 MPa.

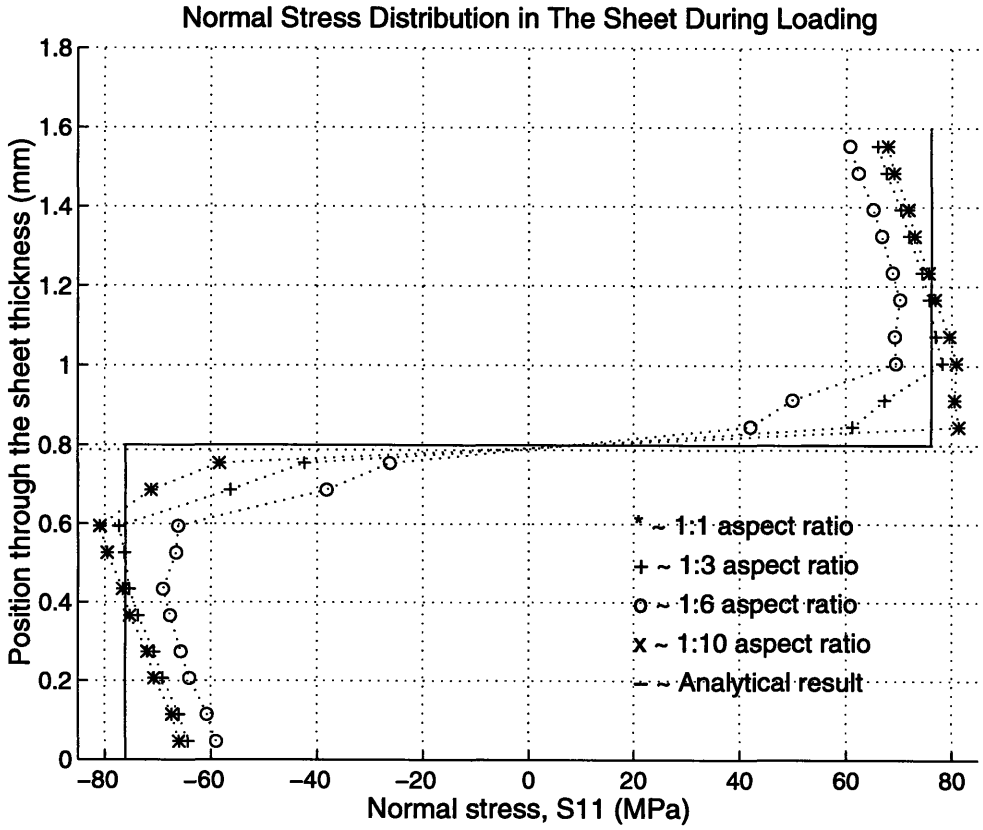

Figure B.4: Stress distribution (σ_{11}) in the sheet during loading.

The unloading stress distribution in the sheet before chemical milling is then considered and is shown in Figure B.5. The evidence of the effect of aspect ratio on the accuracy of simulations can again be seen from these stress profiles. With a relatively high aspect ratio of 1:10 in this particular study, the simulation result deviates significantly from the analytical solution. This unloading stress distribution clearly shows that the aspect ratio of continuum elements need to be of order 1:1 to obtain a solution that accurately matches the analytical result.

Furthermore, when we examined the unloading stress distribution in the sheet after chemical milling as illustrated in Figure B.6, the effect of aspect ratio of continuum elements in the simulations of the chemical milling process became even more apparent. Figure B.6 illustrates that all of the simulations, except the one with a 1:1 aspect ratio, result

in an unloading stress distribution after chemical milling, which satisfies the equilibrium of membrane forces, but does not satisfy the moment equilibrium. In other words, ABAQUS appears to accept a solution in which there is still a moment at any section of the unloaded part.

According to these findings, it is conclusive to say that the aspect ratio of continuum elements in the chemical milling simulations must be of order 1:1 to obtain accurate predictions of part shape after chemical milling. The results of this investigation is quite appalling as they seem to indicate that even with aspect ratios within a range considered to be acceptable by most finite element experts, the simulation results are quite sensitive to the element shape, and they can be truly considered reliable only for very small aspect ratios. Since the sheet used in a forming process is generally long and thin, the simulation would then require an extremely large number of elements to model the sheet; a total of 6,250 elements was used to model a strip when using elements of 1:1 aspect ratio. This is computationally inefficient and unacceptable. Therefore, the use of continuum elements in the chemical milling simulations is eliminated. Instead, the chemical milling process will be modeled and simulated with shell elements (ABAQUS type S4R).

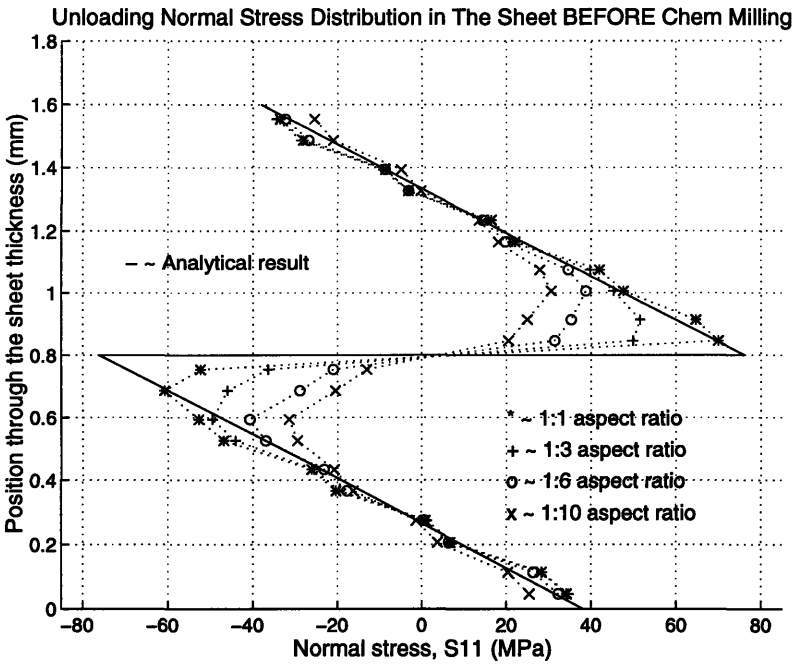

Figure B.5: Unloading stress distribution in the sheet BEFORE chemical milling.

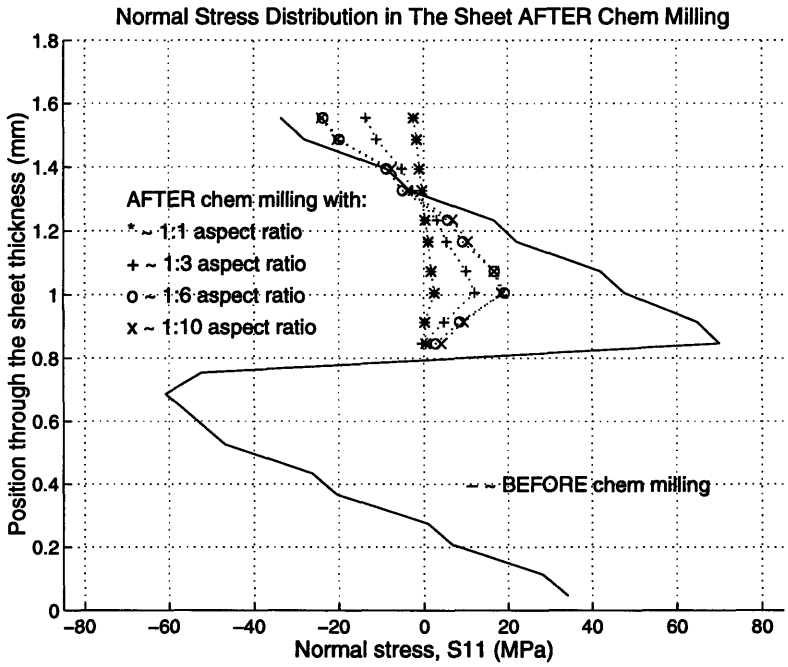

Figure B.6: Unloading stress distribution in the sheet AFTER chemical milling.

Appendix C

Example of The SIGINI User Subroutine for The Chemical Milling Simulations

```
      SUBROUTINE SIGINI(SIGMA,COORDS,NTENS,NCRDS,NOEL,NPT,LAYER,KSPT,
     +   LREBAR,REBARN)
C
      INCLUDE 'ABA_PARAM.INC'
C
      DIMENSION SIGMA(NTENS),COORDS(NCRDS)
      CHARACTER*8 REBARN
C
      COMMON DONE, SDATA(700,15),NWDAT(700,33)
      LOGICAL DONE
      REAL SDATA,NWDAT

      INTEGER SS,RR,ROWNUM,COLS11,COLS22,COLS12

     SS=700
     RR=15
     IF (.NOT.DONE) THEN
      CALL KINIS(SS,RR)
     END IF

     ROWNUM=NOEL-9
     COLS11=(KSPT*3)-2
     COLS22=(KSPT*3)-1
     COLS12=(KSPT*3)

     SIGMA(1) = NWDAT(ROWNUM,COLS11)
     SIGMA(2) = NWDAT(ROWNUM,COLS22)
     SIGMA(3) = NWDAT(ROWNUM,COLS12)

     RETURN
     END

**********************************************************************

     SUBROUTINE KINIS(SS,RR)
C
     INCLUDE 'ABA_PARAM.INC'

C    ARGUMENT DECLARATION
     INTEGER SS,RR
```

```
C   GLOBAL DECLARATION
    COMMON DONE, SDATA(700,15),NWDAT(700,33)
    LOGICAL DONE
    REAL SDATA,NWDAT

C   LOCAL DECLARATION

    INTEGER ELEDUM,INTDUM,START,Z,SECPT,STAR1,STAR2,STAR3,
   +      JUNK1
    REAL SVAL1,SVAL2,SVAL3

    OPEN (UNIT=101,ACCESS='SEQUENTIAL',
   +     FILE='/home/ashby/nick/Saddle/finpost2.dat')

    IF (.NOT.DONE) THEN

     DO 50 Z=1,SS,1
       DO 80 SECPT=1,RR,1
         SDATA(Z,SECPT)=0.0
 80    CONTINUE
 50   CONTINUE

      DO 100 Z=1,SS,1
        START=0
        DO 200 SECPT=1,5,1
          READ (101,*) ELEDUM,INTDUM,JUNK1,SVAL1,SVAL2,SVAL3
          STAR1=START+1
          STAR2=START+2
          STAR3=START+3
          SDATA(Z,STAR1)=SVAL1
          SDATA(Z,STAR2)=SVAL2
          SDATA(Z,STAR3)=SVAL3
          START=STAR3
 200    CONTINUE
 100  CONTINUE

C    DO CURVE FIT FOR THE CHEM MILLED SECTION (LINEAR
C    PIECEWISE INTERPOLATION)
       CALL CURVEFIT(SS)

C    DISCARD STRESSES DUE TO MEMBRANE FORCE IN THE PART
C    TO PREVENT BUCKLING OF THE PART WHEN UNLOADED.
       CALL MEMBRANE(SS)

       DONE=.NOT.DONE

    END IF
    CLOSE (UNIT=101)
    RETURN
    END
```

```
**************************************************************************
C*****THIS CURVE FIT SUBROUTINE PERFORMS A PIECE-WISE LINEAR**********
C*****INTERPOLATION CURVE FIT OF THE STRESS DISTRIBUTION IN THE********
C*****CHEMICAL MILLED ELEMENTS.***************************************

      SUBROUTINE CURVEFIT(SS)

      INCLUDE 'ABA_PARAM.INC'

C     ARGUMENT DECLARATION
      INTEGER SS

C     GLOBAL DECLARATION
      COMMON DONE, SDATA(700,15),NWDAT(700,33)
      LOGICAL DONE
      REAL SDATA,NWDAT

C     LOCAL DECLARATION
      INTEGER NUMSPT,H,M,T1,T2,N,COUNT
      REAL T,NEWT,NEWY0,NEWINC,OLDY0,OLDINC,YOLD1,YOLD2,A,
     +    NEWY(11),OLDY(5),S1TEMP(11),S2TEMP(11),S3TEMP(11)

      PARAMETER (NUMSPT=5,T=1.6002E-3)

C     FIND POSITIONS OF NEW SECTION POINTS
      NEWT=(7*T)/10
      NEWY0=0.0
      NEWINC=NEWT/(11-1)
      DO 250 H=1,11,1
        NEWY(H)=NEWY0+((H-1)*NEWINC)
  250 CONTINUE

C     FIND POSITIONS OF OLD SECTION POINTS
      OLDY0=0.0
      OLDINC=T/(NUMSPT-1)
      DO 275 H=1,5,1
        OLDY(H)=OLDY0+((H-1)*OLDINC)
  275 CONTINUE

C     DO CURVE FIT FOR STRESSES(LINEAR PIECEWISE INTERPOLATION)
      DO 300 M=1,SS,1
        DO 350 H=1,11,1
          IF ( NEWY(H).LE.OLDY(3) ) THEN
            IF (NEWY(H).LE.OLDY(2)) THEN
              YOLD1=OLDY(2)
              YOLD2=OLDY(1)
              T1=(2*3)-2
              T2=(1*3)-2
            ELSE
              YOLD1=OLDY(3)
```

```
            YOLD2=OLDY(2)
             T1=(3*3)-2
             T2=(2*3)-2
           END IF
         ELSE
           IF ( NEWY(H).LE.OLDY(4) ) THEN
             YOLD1=OLDY(4)
             YOLD2=OLDY(3)
             T1=(4*3)-2
             T2=(3*3)-2
           ELSE
             YOLD1=OLDY(5)
             YOLD2=OLDY(4)
             T1=(5*3)-2
             T2=(4*3)-2
           END IF
         END IF
         A=(YOLD1-NEWY(H))/(YOLD1-YOLD2)
         S1TEMP(H)=(SDATA(M,T1)*(1-A))+(SDATA(M,T2)*A)
         T1=T1+1
         T2=T2+1
         S2TEMP(H)=(SDATA(M,T1)*(1-A))+(SDATA(M,T2)*A)
         T1=T1+1
         T2=T2+1
         S3TEMP(H)=(SDATA(M,T1)*(1-A))+(SDATA(M,T2)*A)
 350  CONTINUE

      DO 375 N=1,11,1
        COUNT=(N*3)-2
        NWDAT(M,COUNT)=S1TEMP(N)
        COUNT=COUNT+1
        NWDAT(M,COUNT)=S2TEMP(N)
        COUNT=COUNT+1
        NWDAT(M,COUNT)=S3TEMP(N)
 375 CONTINUE
 300 CONTINUE

   RETURN
   END

**********************************************************************
C** THIS SUBROUTINE CALCULATES THE AVERAGE STRESS IN THE PART ***
C** THEN SUBTRACT IT FROM THE STRESS, THUS ELIMINATING THE   ******
C** STRESS DUE TO MEMBRANE FORCE.  THIS IS TO PREVENT BUCKLING****
C** OF THE PART WHEN IT IS UNLOADED.**********************************

    SUBROUTINE MEMBRANE(SS)

    INCLUDE 'ABA_PARAM.INC'
```

```
C    ARGUMENT DECLARATION
     INTEGER SS

C    GLOBAL DECLARATION
     COMMON DONE,SDATA(700,15),NWDAT(700,33)
     LOGICAL DONE
     REAL SDATA,NWDAT

C    LOCAL DECLARATION
     INTEGER NSP,SDIR,B,SCOMP,CLM,TIMES
     REAL NTH,DT,HDT,TOTS,SADD,AVEST

     PARAMETER (NTH=1.12014E-03,NSP=11,SDIR=3)

     DT=NTH/(NSP-1)
     HDT=DT/2
     DO 700 B=1,SS,1
       DO 800 SCOMP=1,SDIR,1
         CLM=SCOMP
         SADD=0.0
         TOTS=0.0
         DO 900 TIMES=1,NSP,1
           IF (TIMES.EQ.1 .OR. TIMES.EQ.NSP) THEN
              SADD=SDATA(SS,CLM) * HDT
           ELSE
              SADD=SDATA(SS,CLM) * DT
           END IF
          TOTS=TOTS+SADD
          CLM=CLM+3
 900     CONTINUE
         AVEST=TOTS/NTH
         CLM=SCOMP
         DO 1000 TIMES=1,NSP,1
           SDATA(SS,CLM)=SDATA(SS,CLM) - AVEST
           CLM=CLM+3
1000     CONTINUE
 800   CONTINUE
 700 CONTINUE

     RETURN
     END
```

Appendix D

Compilation of Results on The Comparison Between Simulation And Experimental Results of The Parts With Simple Geometry

R_{die1} = 5.8 cm (2.32") / Part Number 1

Chem Milling 1/2 t of The Entire Part.

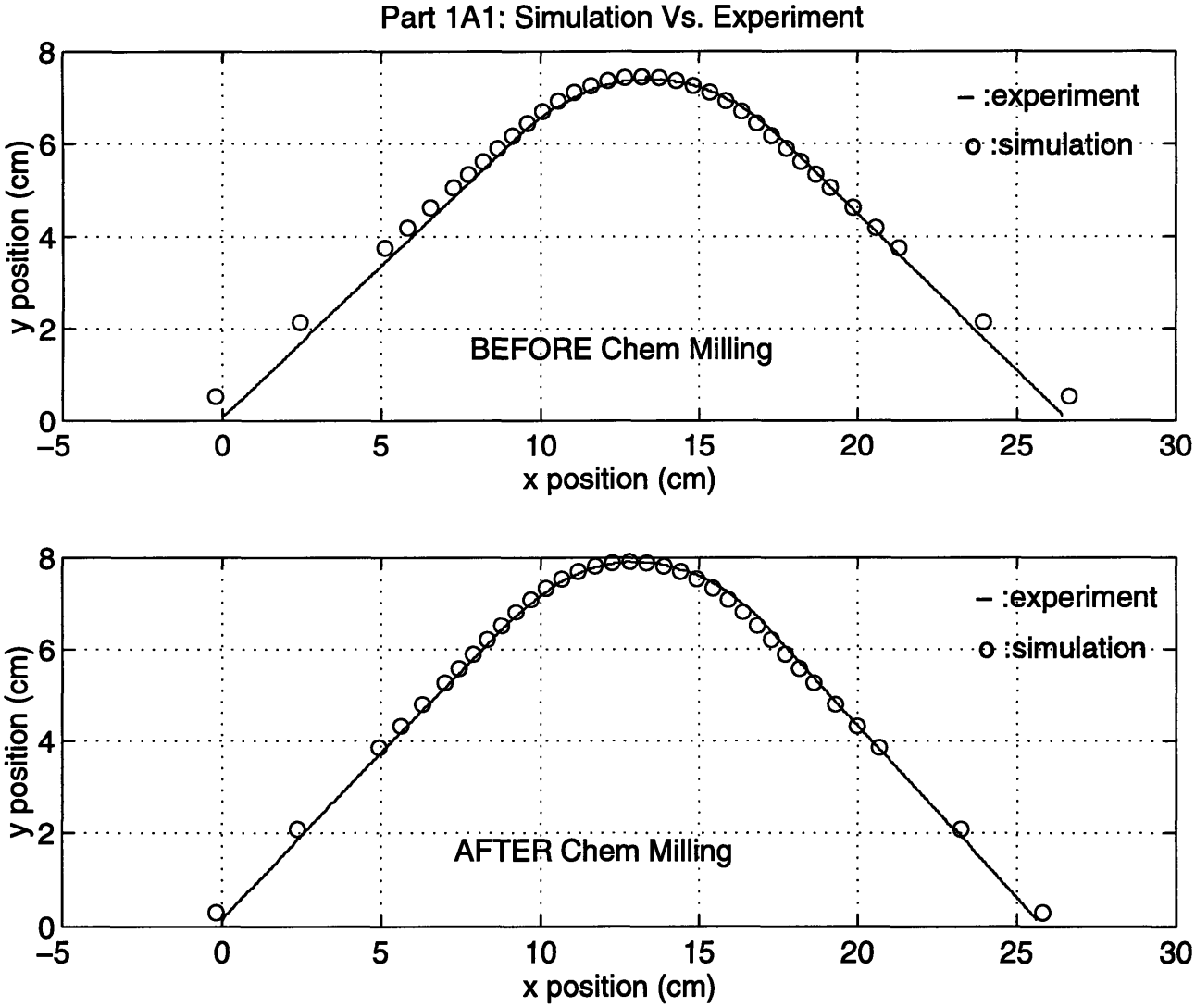

R_{die1} = 5.8 cm (2.32") / Part Number 2

Chem Milling 1/2 t of The Entire Part.

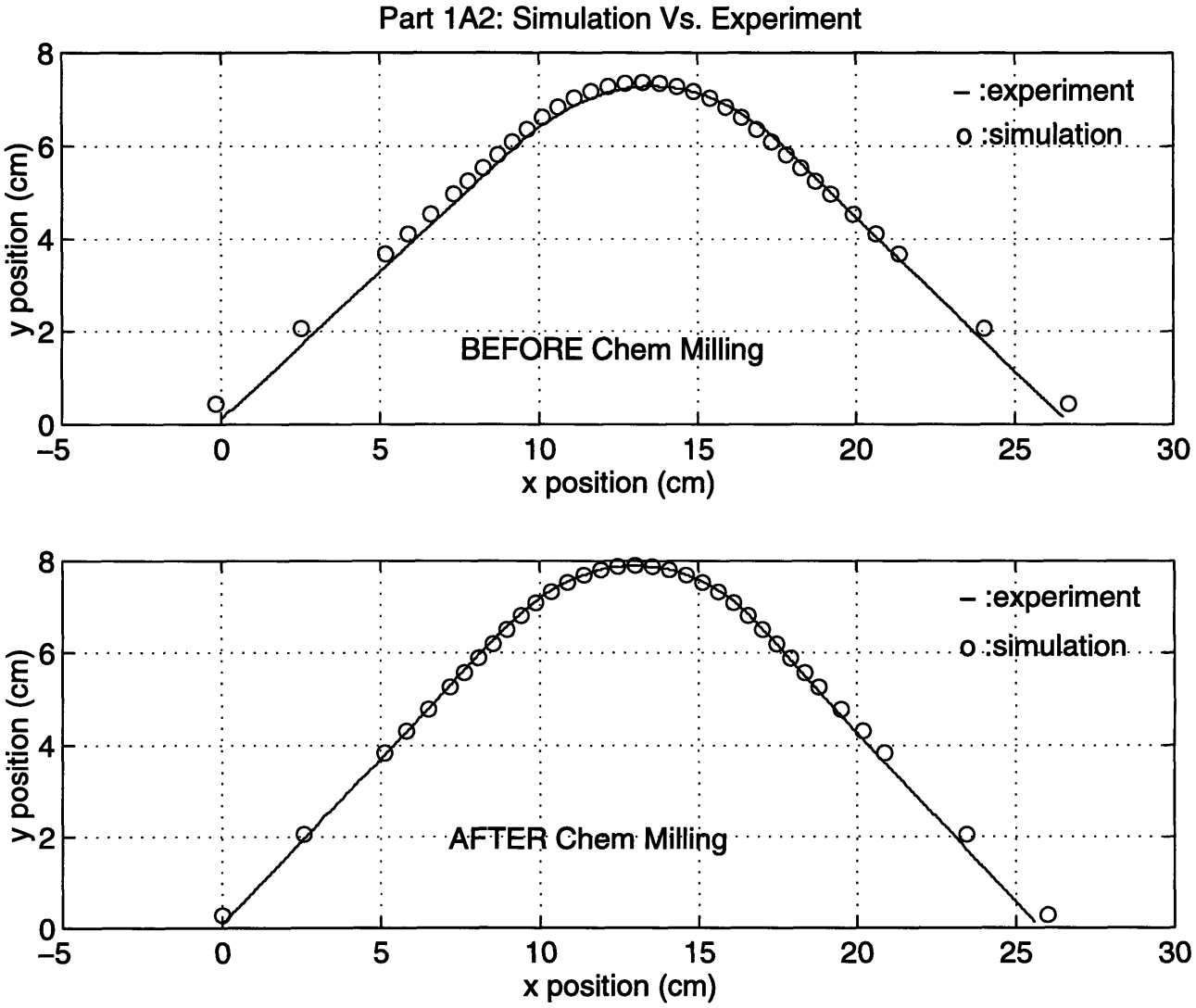

R_{die1} = 5.8 cm (2.32") / Part Number 1

Chem Milling 1/2 t of The Centered Pocket.

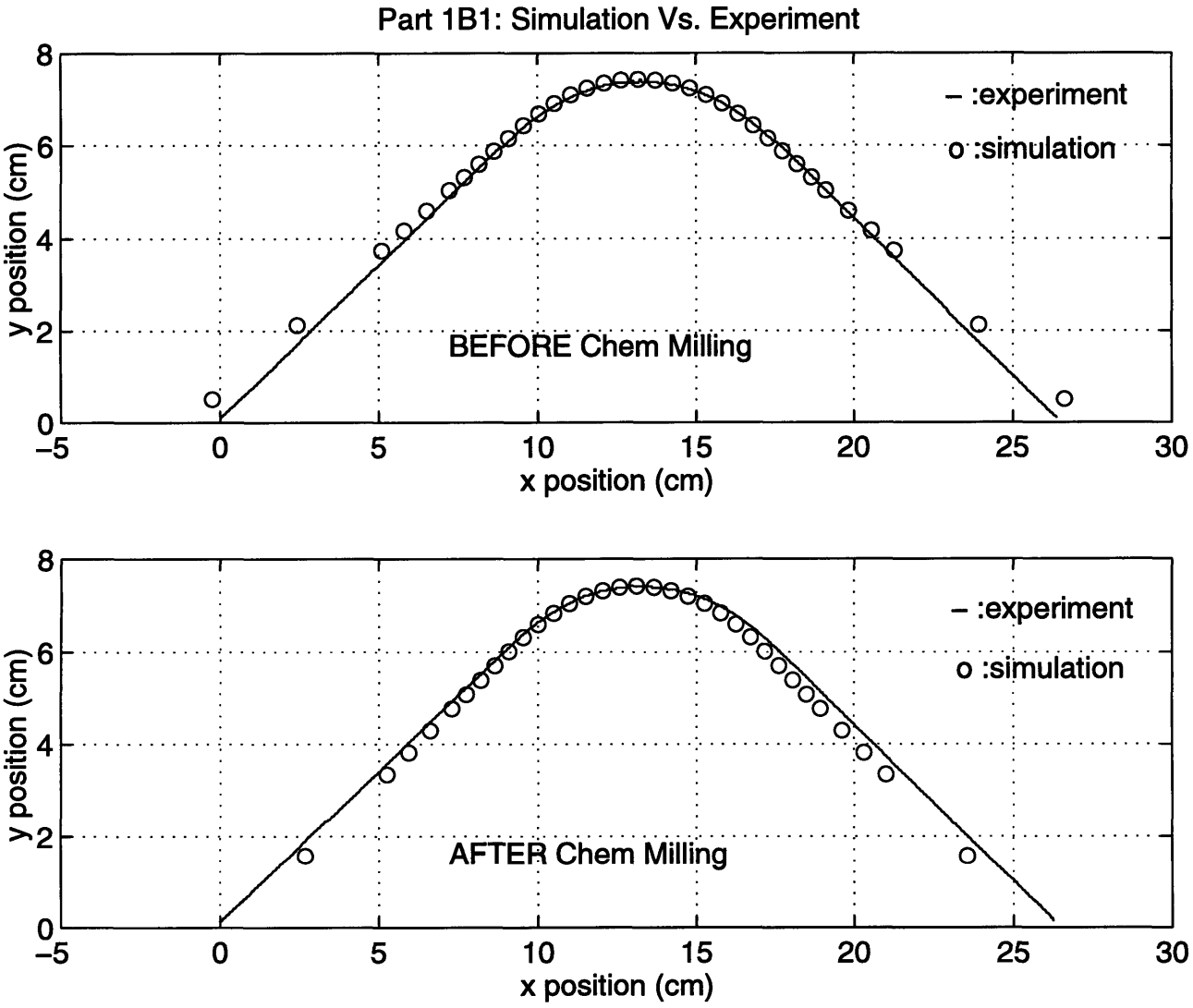

R_{die1} = 5.8 cm (2.32") / Part Number 2

Chem Milling 1/2 t of The Centered Pocket.

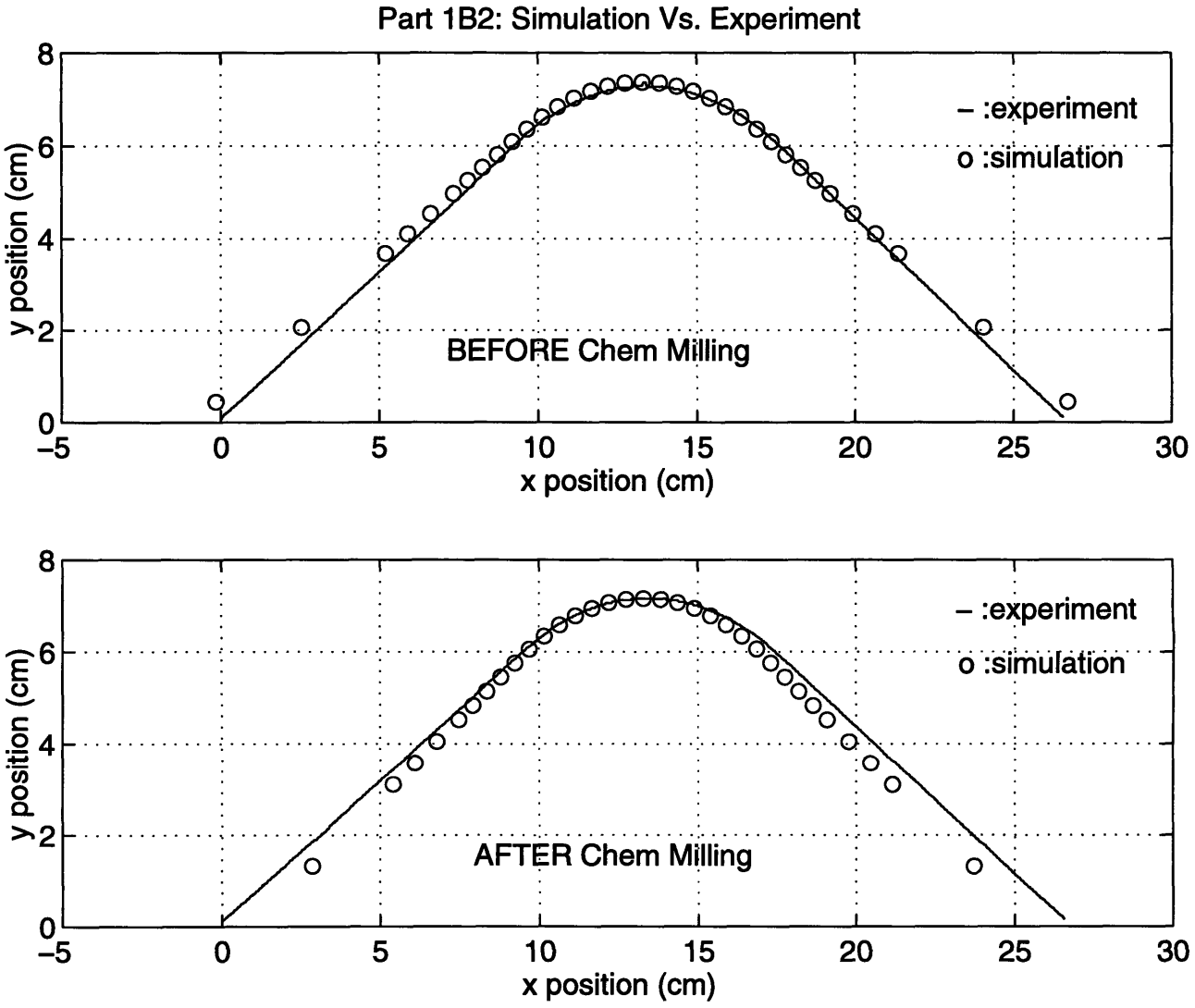

R_{die1} = 5.8 cm (2.32") / Part Number 1

Chem Milling 1/4 t of The Centered Pocket.

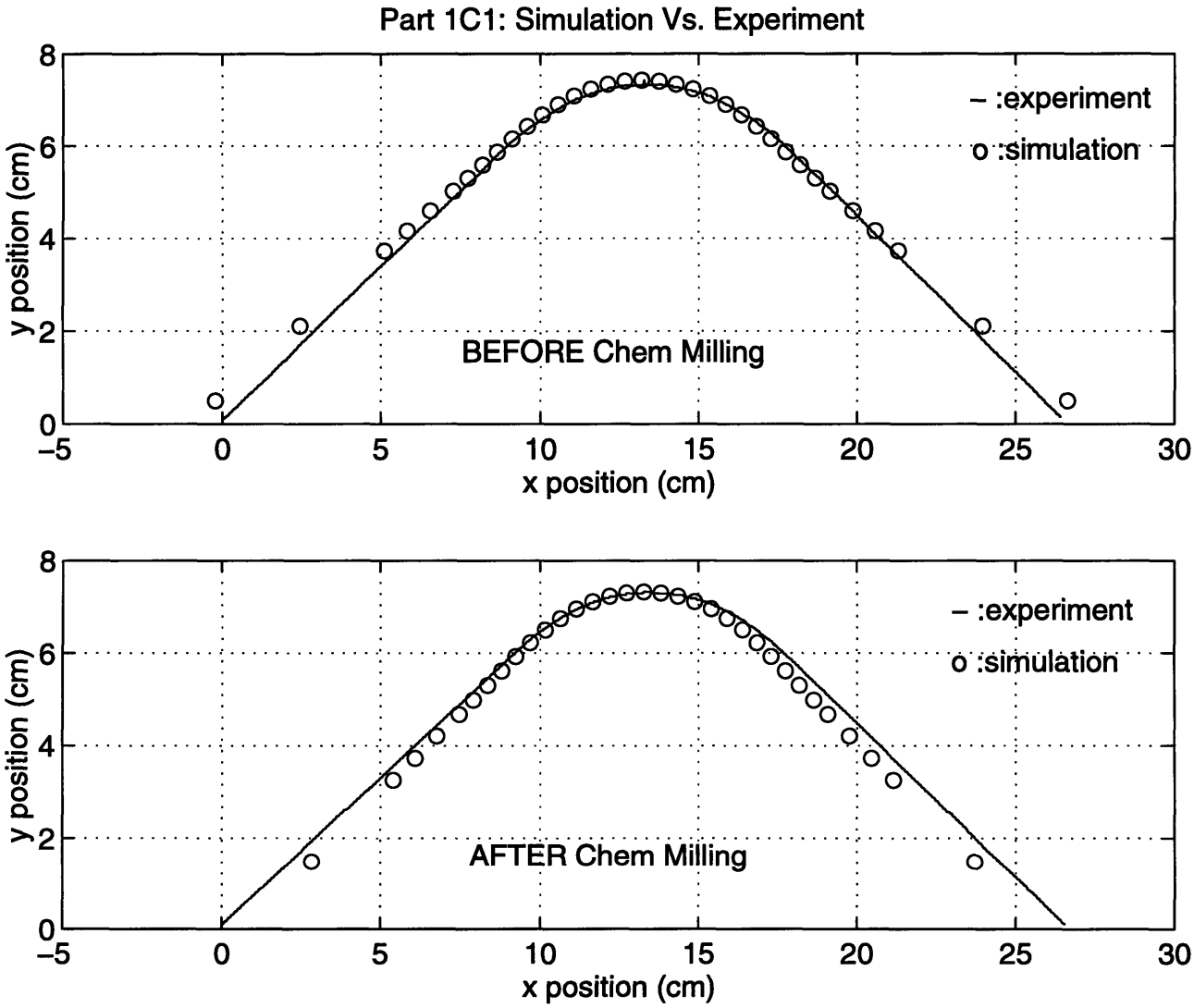

R_{die1} = 5.8 cm (2.32") / Part Number 2

Chem Milling 1/4 t of The Centered Pocket.

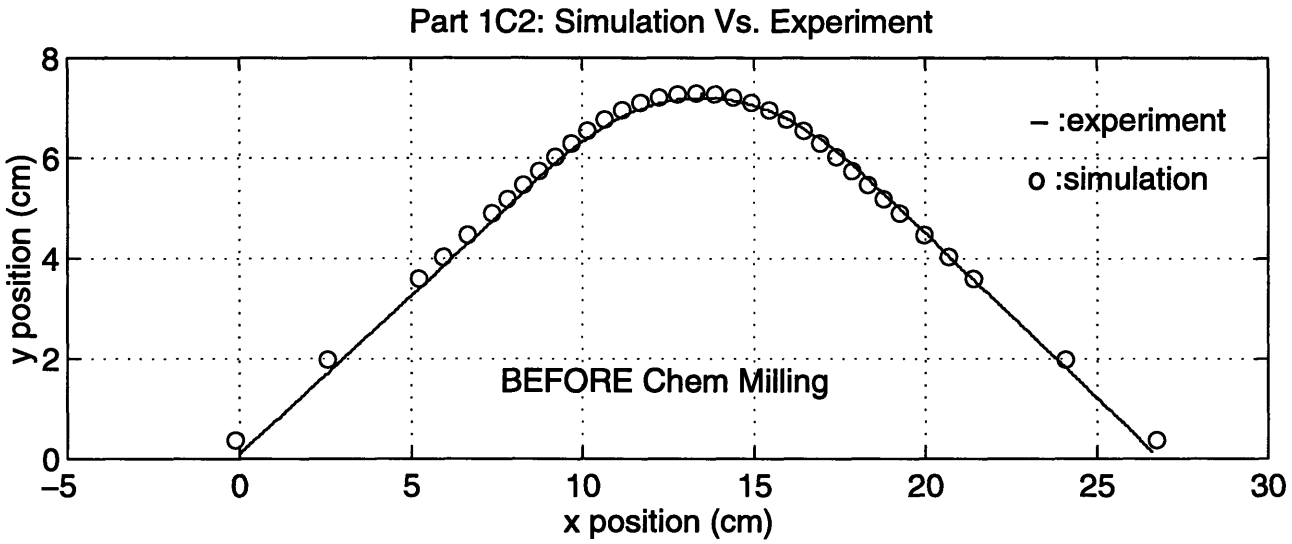

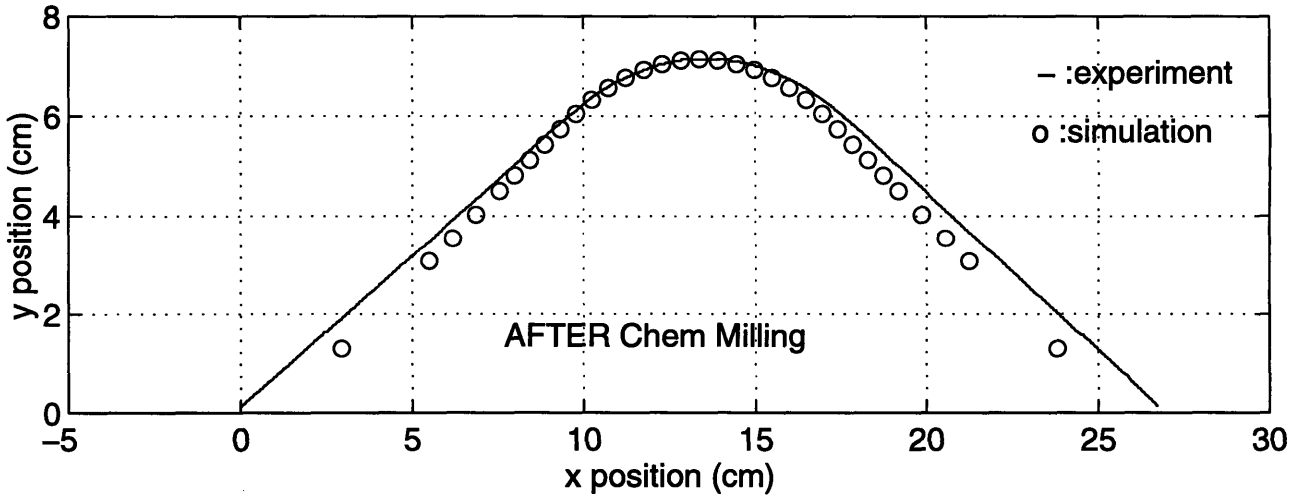

R_{die1} = 5.8 cm (2.32") / Part Number 1

Chem Milling 1/2 t of The Off-Centered Pocket.

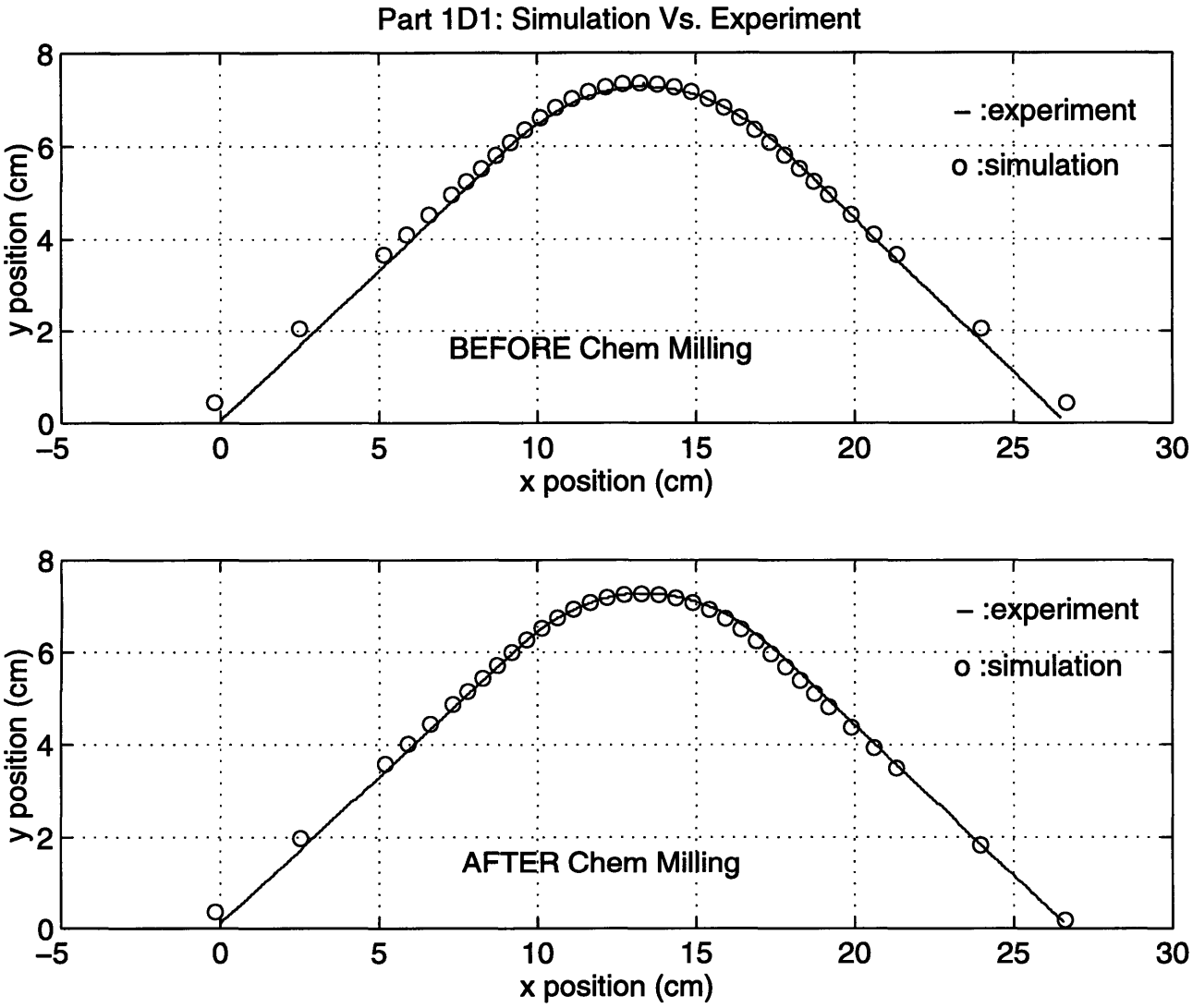

R_{die1} = 5.8 cm (2.32") / Part Number 2

Chem Milling 1/2 t of The Off-Centered Pocket.

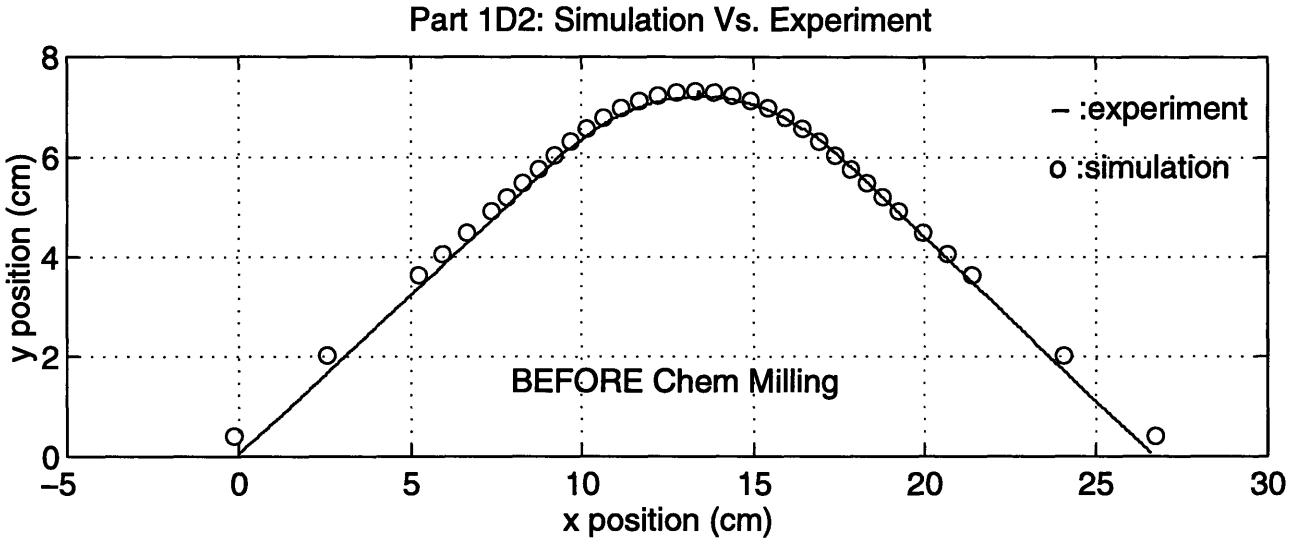

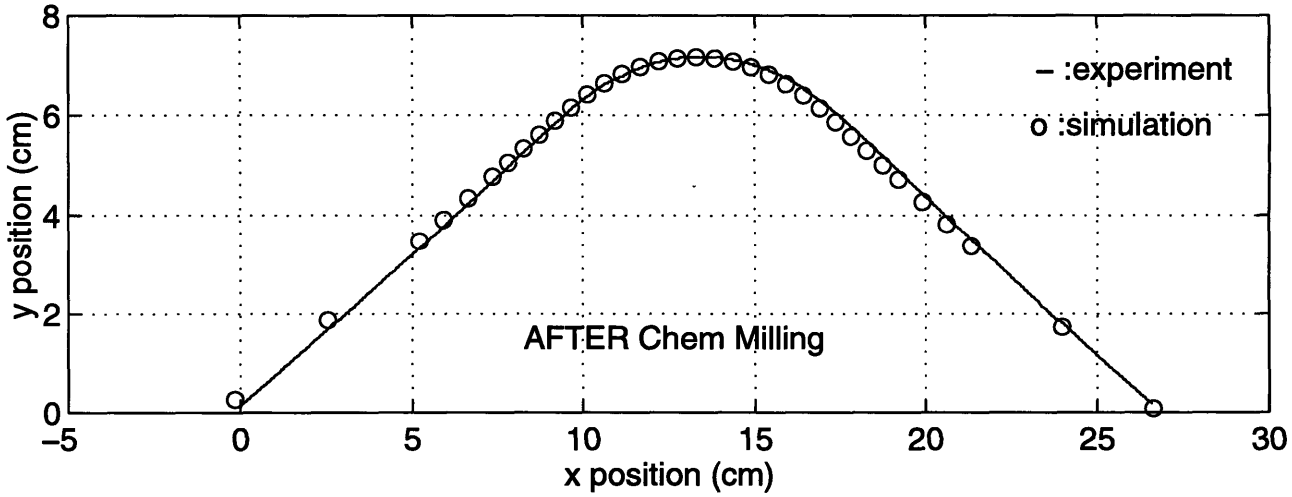

R_{die2} = 3.8 cm (1.52") / Part Number 1

Chem Milling 1/2 t of The Entire Part.

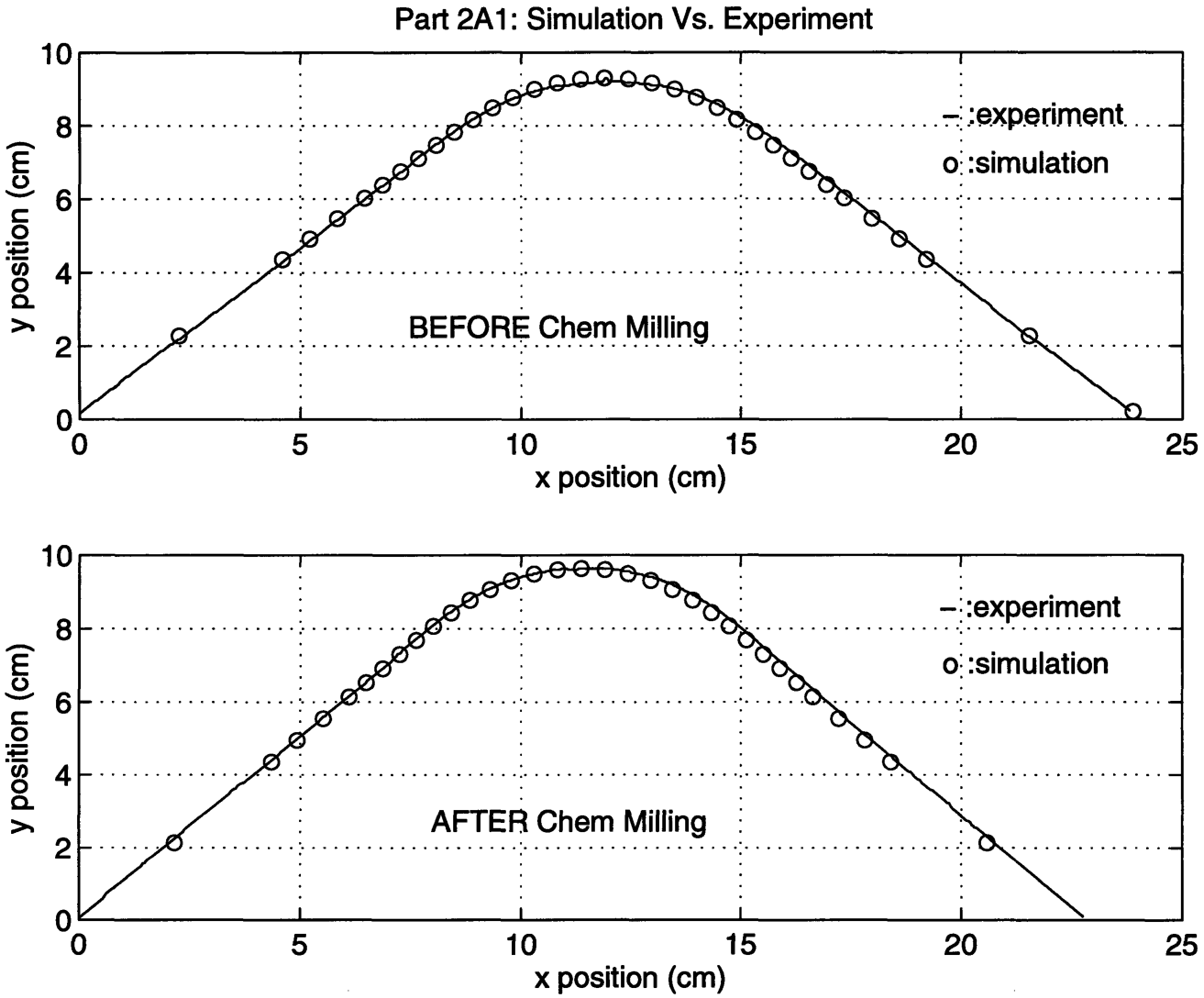

R_{die2} = 3.8 cm (1.52") / Part Number 2

Chem Milling 1/2 t of The Entire Part.

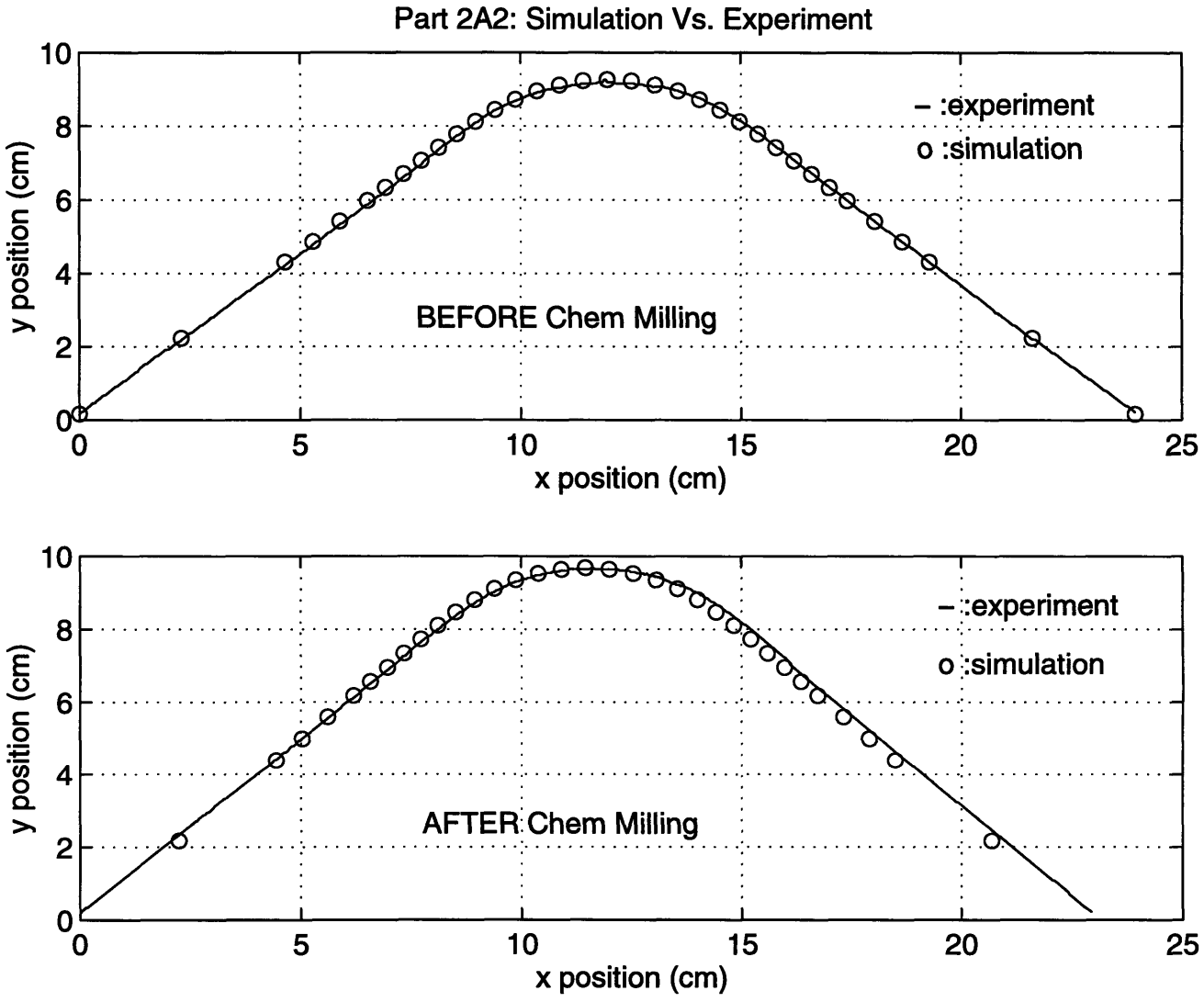

R_{die2} = 3.8 cm (1.52") / Part Number 1

Chem Milling 1/2 t of The Centered Pocket.

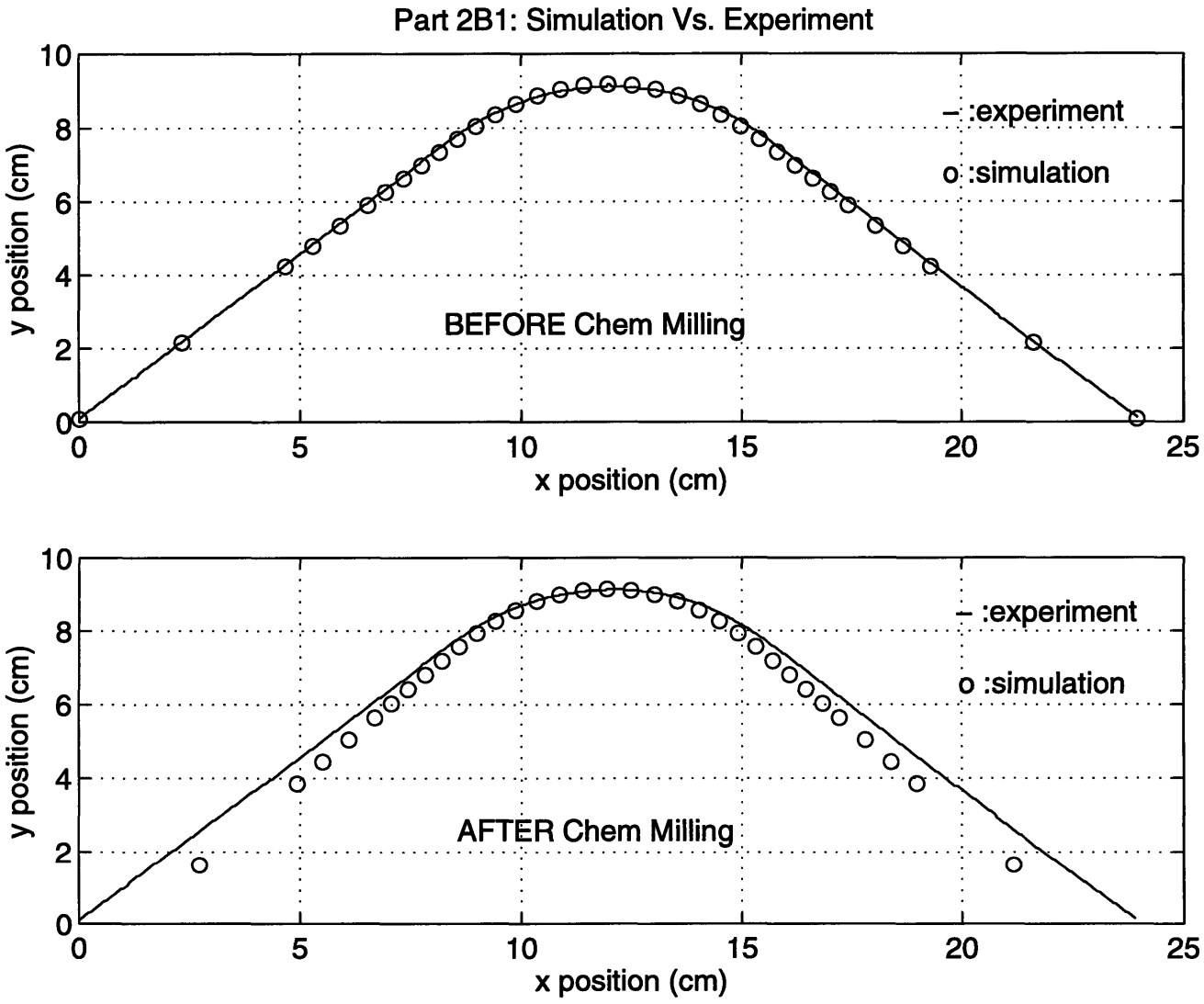

R_{die2} = 3.8 cm (1.52") / Part Number 2

Chem Milling 1/2 t of The Centered Pocket.

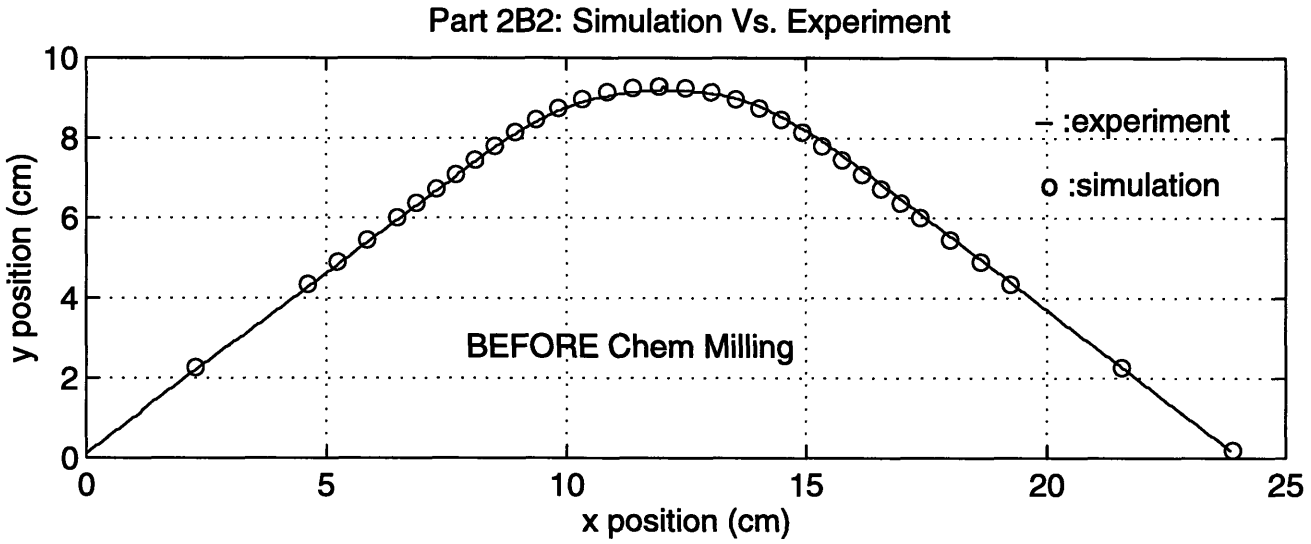

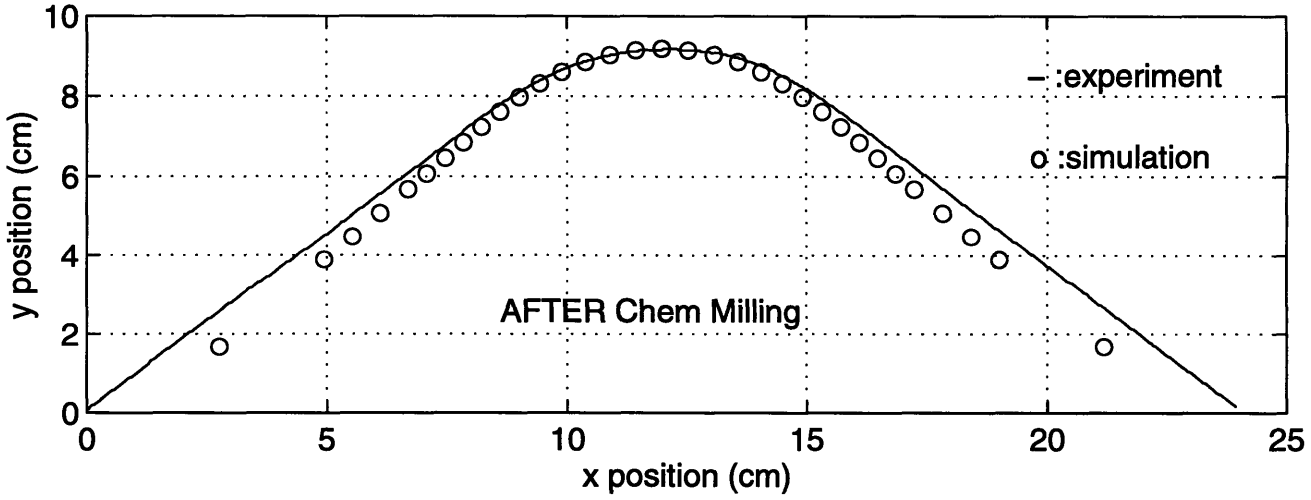

R_{die2} = 3.8 cm (1.52") / Part Number 1

Chem Milling 1/4 t of The Centered Pocket.

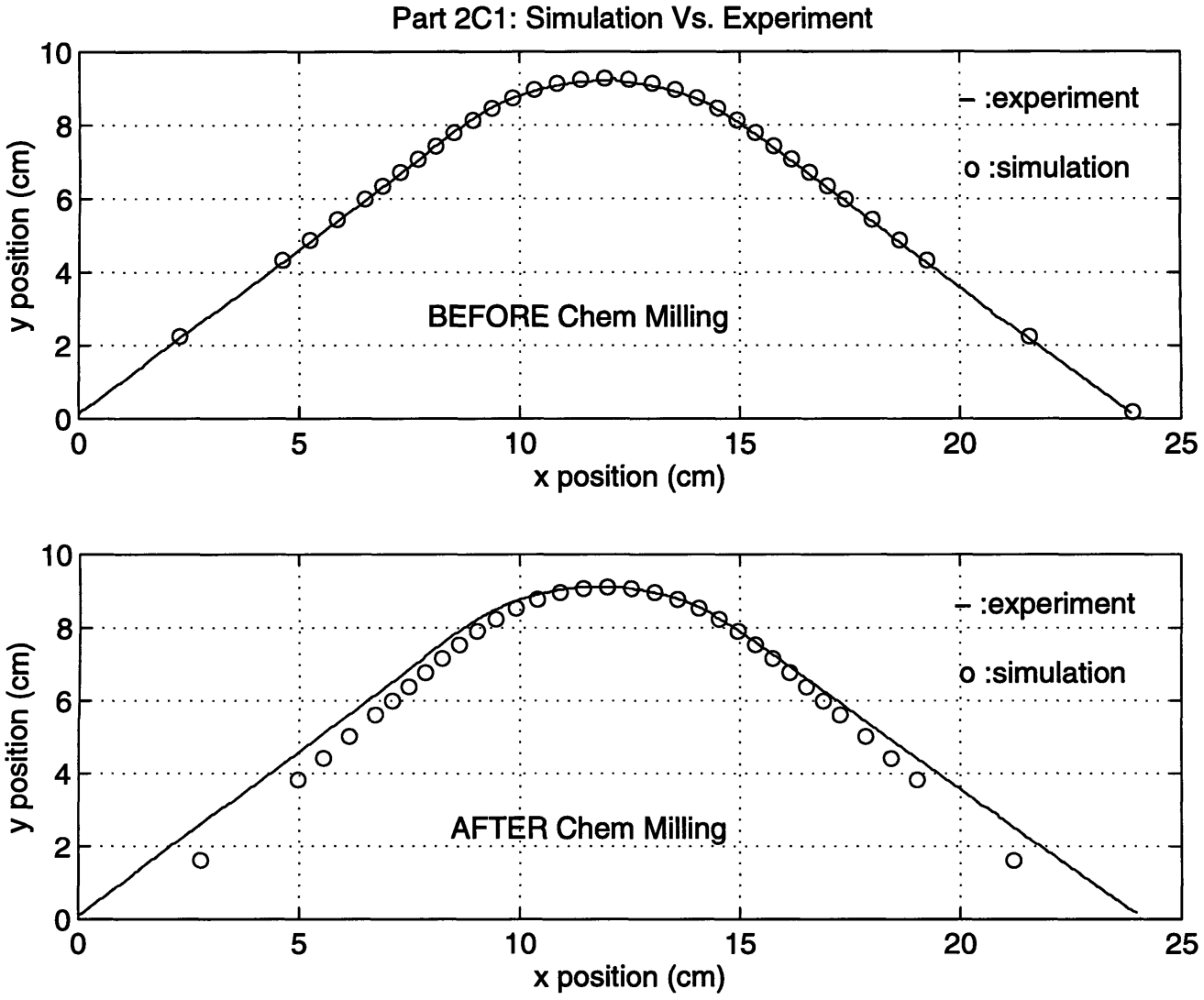

R_{die2} = 3.8 cm (1.52") / Part Number 2

Chem Milling 1/4 t of The Centered Pocket.

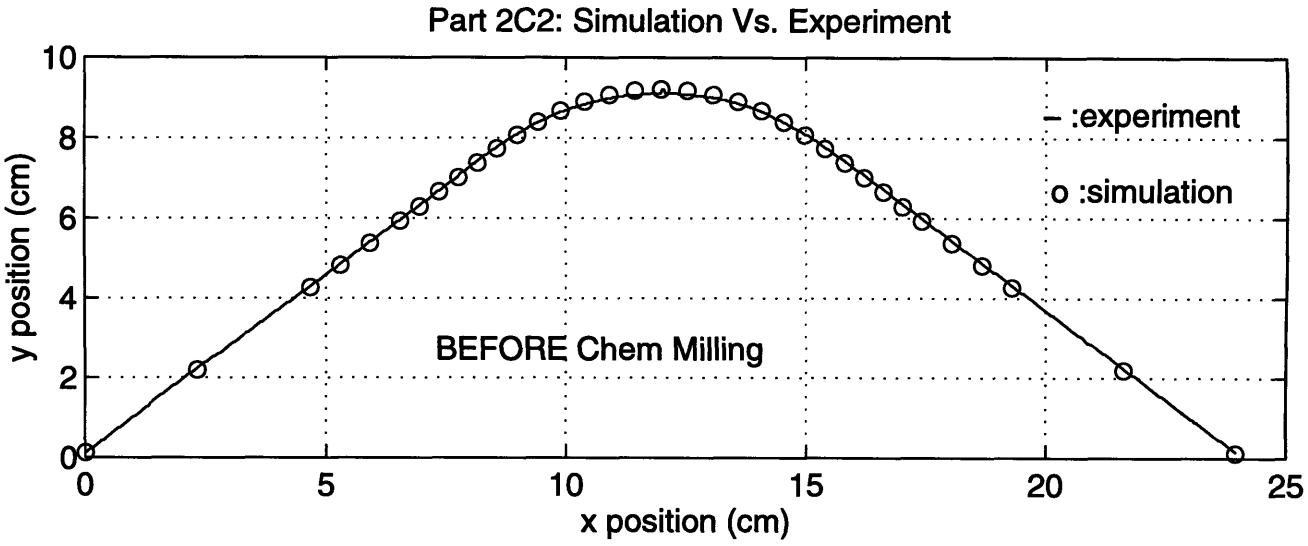

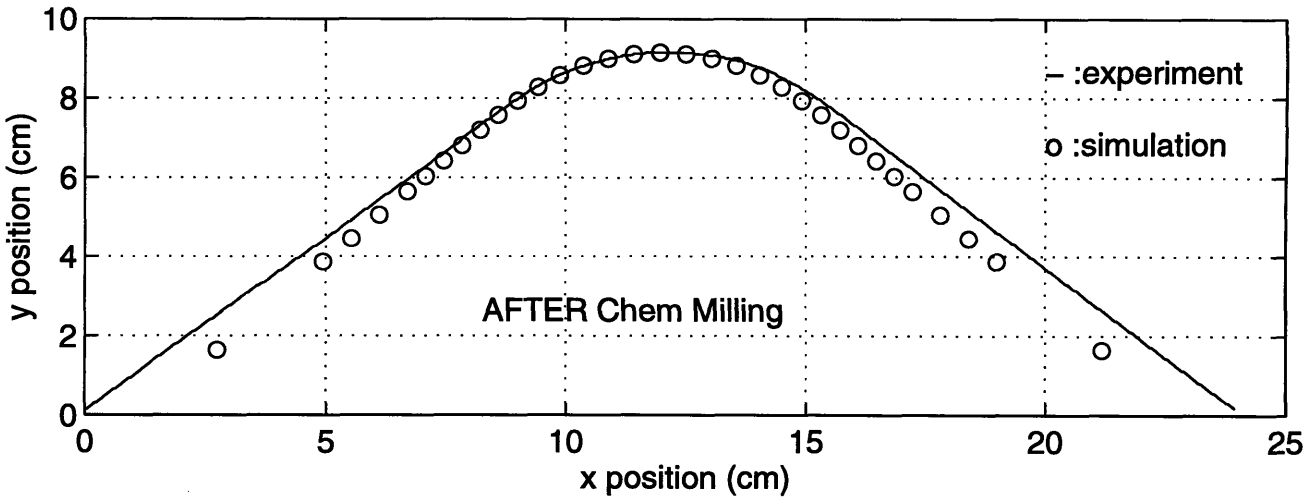

R_{die2} = 3.8 cm (1.52") / Part Number 1

Chem Milling 1/2 t of The Off-Centered Pocket.

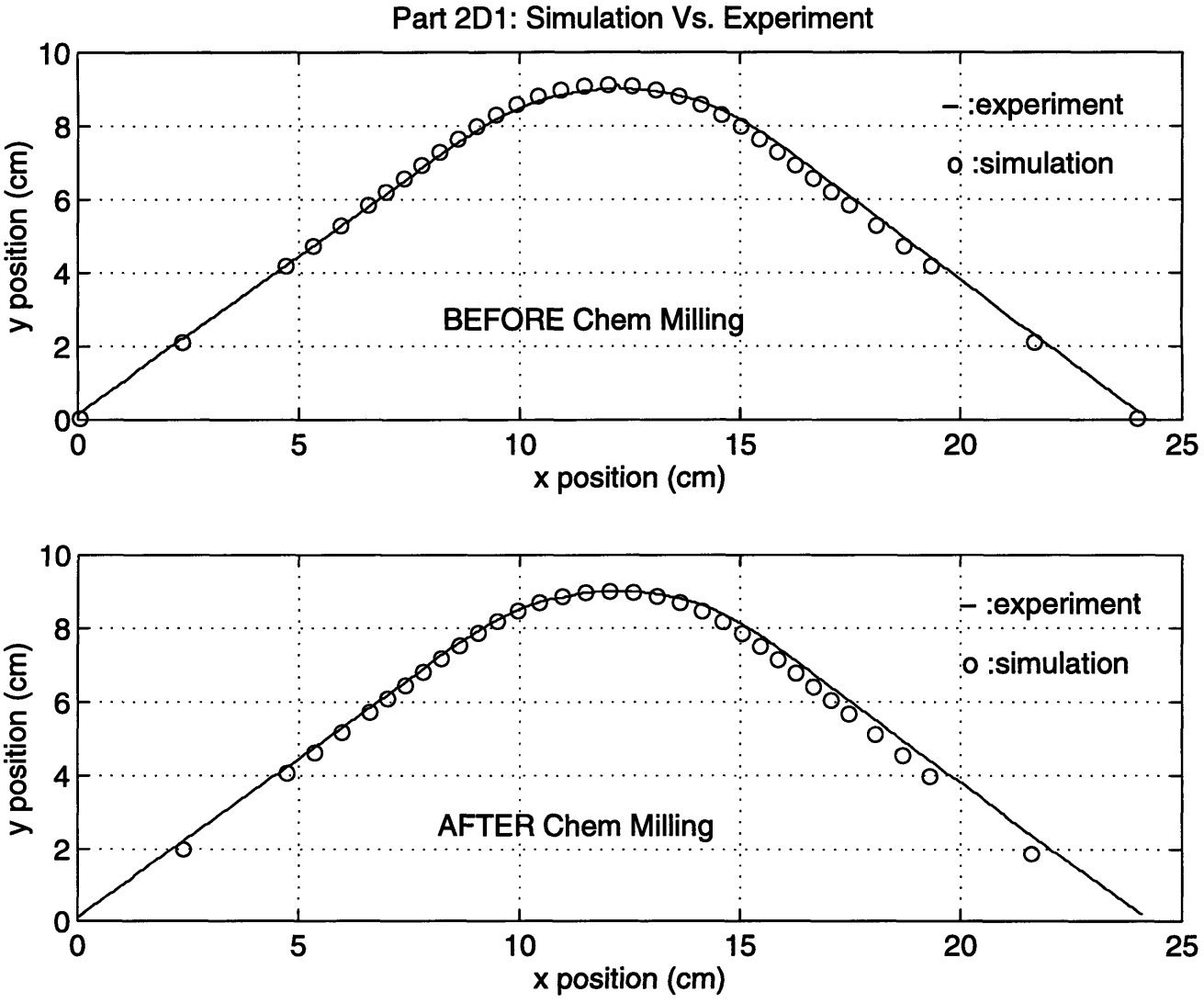

R_{die2} = 3.8 cm (1.52") / Part Number 2

Chem Milling 1/2 t of The Off-Centered Pocket.

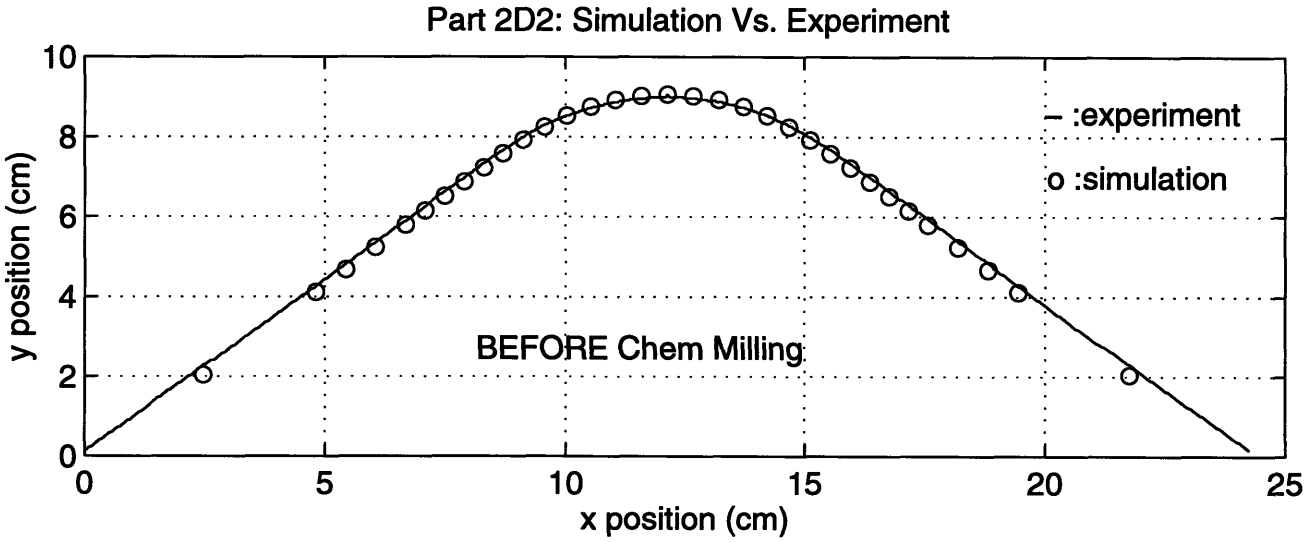

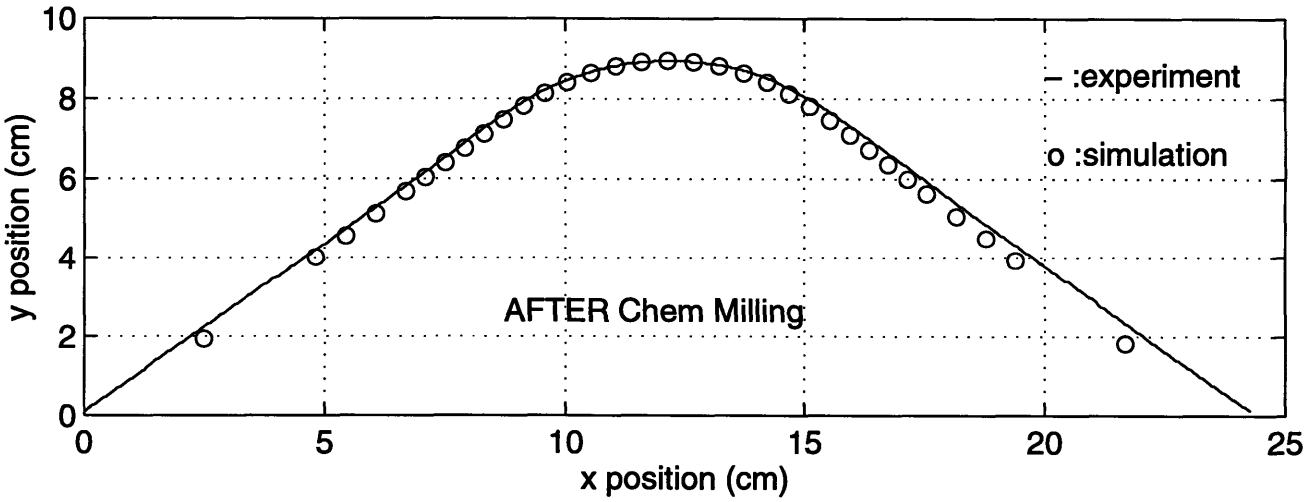

References

[1] Karafillis, A. P., and M. C. Boyce. 1996. Tooling and Binder Design For Sheet Metal Forming Processes Compensating Springback Error. *International Journal of Mechanical Tools In Manufacturing. Vol. 36. No. 4*: pp.503-526.

[2] Taylor, L., J. Cao, A. P. Karafillis, and M. C. Boyce. 1995. Numerical Simulations of Sheet-Metal Forming. *Journal of Materials Processing Technology 50*: pp.168-179.

[3] Harris, W. T. 1976. *Chemical Milling: The Technology of Cutting Materials By Etching.* Oxford: Oxford University Press.

[4] Cook, R. D., D. S. Malkus, and M. E. Plesha. 1989. *Concepts And Applications of Finite Element Analysis Third Edition.* New York: John Wiley & Sons.

[5] Prathap, G. 1993. *The Finite Element Method in Structural Mechanics.* Dordrecht, The Netherlands: Kluwer Academics Publishers.

[6] Bathe, K. J. 1982. *Finite Element Procedures In Engineering Analysis.* Englewood Cliffs, New Jersey: Prentice-Hall, Inc.

[7] Taylor, R. L. 1988. Finite Element Analysis of Linear Shell Problems. *The Mathematics of Finite Elements And Applications VI.* London, England: Academics Press Limited.

[8] Hibbitt, Karlsson & Sorensen, Inc. *ABAQUS Theory Manual, Version 5.5.* Pawtucket, RI. 1995.

[9] Hibbit, Karlsson & Sorensen, Inc. *ABAQUS/Standard User's Manual Volume I & II, Version 5.5.* Pawtucket, RI. 1995.

[10] Socrate, S. *Simulations of The Forming Process On A Saddle-Shaped Part.* 1997.